

# The Impact of Cross-Polarization on RGB Imaging, Color Calibration and Accuracy



Vom Fachbereich Informatik  
der Technischen Universität Darmstadt  
genehmigte

## DISSERTATION

zur Erlangung des akademischen Grades eines  
Doktor-Ingenieurs (Dr.-Ing.)  
von

**M.Sc. Tarek Abu Haila**

geboren in Damaskus, Syrien

Referenten der Arbeit: Prof. Dr. Arjan Kuijper  
Technische Universität Darmstadt

Prof. Dr. techn. Dr. -Ing. eh. Dieter W. Fellner  
Technische Universität Darmstadt

Prof. Dr. Thomas S. A. Wallis  
Technische Universität Darmstadt

Tag der Einreichung: 06/02/2024  
Tag der mündlichen Prüfung: 22/01/2024

Darmstädter Dissertation  
D 17

Tarek Abu Haila, The Impact of Cross-Polarization on RGB Imaging, Color Calibration and Accuracy.  
Dissertationsort: Darmstadt, Technische Universität Darmstadt.  
Veröffentlichungsjahr der Dissertation auf TUpriints: 2024.  
Tag der mündlichen Prüfung: 22.01.2024  
Veröffentlicht unter CC BY-SA 4.0 International.  
<https://creativecommons.org/licenses/>



# Erklärung zur Dissertation

Hiermit versichere ich die vorliegende Dissertation selbständig nur mit den angegebenen Quellen und Hilfsmitteln angefertigt zu haben. Alle Stellen, die aus Quellen entnommen wurden, sind als solche kenntlich gemacht. Diese Arbeit hat in gleicher oder ähnlicher Form noch keiner Prüfungsbehörde vorgelegen.

Darmstadt, den 04.Dez.2023

Tarek Abu Haila

---

# Abstract

Polarization filters are very useful and come very handy in various applications ranging from artifacts digitization to medical imaging where shiny reflective surfaces hinder clear imaging otherwise, and consequently would cause false reading of the data. Usually polarization filters are used so to eliminate any undesirable reflections, specularities and highlights a surface would depict given the surface's material and the lighting setup. In most applications that uses polarization filters, more information of the actual imaged surface are retrieved which would be obscured behind highlights otherwise, so the imaged surface looks rather continuous and complete. However, how polarization filters actually affect and influence the imaged surface color receive too little attention despite its importance in applications such as cultural heritage digitization, faithful product photography or medical skin and tissues imaging among others.

In this thesis we address fundamental issues polarization filters cause to color registration, reproduction and consequently color calibration, so to make people and other researchers aware of the consequences of using polarization filters in their applications especially people whose concern is to have a faithful and accurate color reproduction such in the cultural heritage digitization sector. We propose, as well, a new method of automated mosaic scanning that is, first, overcome the problem of undesirable surface reflections despite the use of cross-polarization due to the highly reflective material's surface finish. Second, paving the way towards color calibration for 3D textures.

The following work demonstrates in details how polarization filters affect color reproducibility and grayscale linearity, it shows as well how polarization filters can be a potential cause of shift in the white-point of a light source which has consequences on how surface colors under such polarized light source would be rendered. Finally, we demonstrate, while using cross-polarization, a new proposed method of color calibration based on a mosaic approach that can be the backbone of standardizing 3D digitization and texture color correction while keeping color accuracy in mind.

With the help of this work, it is possible now to understand the changes that happen to the imaged colors while using cross-polarization and how these changes make color faithful reproduction deviate from the real measurements that are usually measured using a spectrophotometer (the ground-truth; actual perception). This body of research also explains and show how grayscale colors are affected so that grayscale linearity cannot be guaranteed anymore depending on the imaged material, and also why some colors may look washed-out when imaged using cross-polarization. The reader will also be able to understand how cross-polarization contributes to a shift in the light source's white-point and a change in the color-correlated temperature (CCT) which will affect consequently how surface colors would interact with the light source and being mathematically calculated. Finally, a new approach to color calibration with the help of cross-polarization and a moving camera/light source combination for large color target scans and/or highly reflective surfaces is introduced, the new approach is being assessed against the *ISO* standards for color calibration and reproduction in cultural heritage showing that it is viable and passes the highest possible *ISO* level for color accuracy and fidelity.



# Zusammenfassung

Lichtpolarisierung ist ein Phänomen, indem Lichtwellen gezwungen sind, nur in eine bestimmte Richtung zu oszillieren. Dabei existieren zwei verschiedene Formen von Licht, entweder als Wellen oder Quantenpakete. In der vorliegenden Arbeit handelt es sich um Lichtwellen und ihr Verhältnis in Bezug auf Materialien. Die Polarisation von Licht erfolgt durch das Passieren durch einen Polarisationsfilter. Auf der anderen Seite des Filters oszilliert das Licht nur in einer bestimmten Richtung. Dies führt dazu, dass das Licht die Hälfte seiner Intensität verliert. Polarisationsfilter helfen bei der Eliminierung der Spiegelungen/Reflexionen, deshalb sind sie für Menge von verschiedenen Anwendungen und Projekten unerlässlich z.B. Medizinische Fotografie, Forensik, Geologische Mineralien und Felsfotografie, Digitalisierung von Kulturerbe Artefakten usw. Spiegelungen/Reflexionen sind abhängig von den verwendeten Materialien. Zum Beispiel haben glossy Materialien wie polierte Oberfläche, im Gegensatz zu matt Materialien, die Tendenz, bei Lichteinwirkung Reflexionen zu erzeugen. Reflexionen begleiten uns in unserem Alltagsleben, wie zum Beispiel bei Zähnen, Glas, Münzen, Edelstahl usw.

Polarisation, in der Hinsicht der Physik, ist nachvollzogen. Jedoch gibt es nicht ausreichende Recherche, die das Phänomen aus der Perspektive der Anwendung und Nutzung von Polarisationsfiltern behandelt. In der Wissenschaft kommt die Frage vor, wie die fotografierten Farben von den Filtern in der Realität beeinflusst werden?

Das System, das hinter den Forschungsfragen steckt, ist *CultArm3D*, eine entwickelte Technologie stammt aus Fraunhofer IGD, in Darmstadt. Das Ziel des Systems ist Hochqualität und Farbakkurat Digitalisierung zu bieten und zu gewährleisten. Das System besteht aus einem Roboterarm mit einer Kamera am Endeffektor montiert. Auf der Kameralinse wurde eine Lichtquelle (D50) angebracht. Das Licht hat die Form eines Kreises voller LEDs mit einem Loch in der Mitte, durch das die Kameralinse passt. Wegen der Geometrie zwischen das Licht und die Kameralinse ( $0^\circ/0^\circ$ ) sind direkte Reflexionen unvermeidbar, aus diesem Grund sind Cross-Polarization Filter unerlässlich in solcher Situation. Die Cross-Polarisation setzt sich aus zwei Polarisationsfiltern zusammen, die so ausgerichtet werden, dass sie einen rechten Winkel zueinander bilden, also einen Winkel von 90 Grad (ähnlich einem Kreuz). Spiegelungen/Reflexionen lassen sich mit solcher Technik eliminieren.

In dieser Arbeit studieren und analysieren wir den Einfluss der Polarisationsfiltern auf Farbmessungsgenauigkeit, Farbkalibrierung und Farbdarstellung. Wir stellen 3+1 Forschungsfragen bezüglich der Verwendung von Polarisationsfiltern und inwieweit sie einen Einfluss auf fotografierte Farben, so wie auf die Lichtquelle selbst haben können. Es wird, zunächst, die Auswirkung von Polarisationsfiltern auf Grauskalas von verschiedenen Materialien (glossy und matt) analysiert. Außerdem werden die Auswirkungen auf die Farbkomponenten CIELAB (*Chroma* und *Lightness*) näher gezogen. Im nächsten Schritt wird die Auswirkung der Polarisationsfiltern auf die Lichtquelle selbst untersucht. Bei direkter Beeinflussung des Lichts wirken sich zwangsläufig Veränderungen auf die Farben aus, auf die das polarisierte Licht einwirkt. Schließlich taucht das Problem mit einem der Color Targets (bzw. Farbziele) auf, da das Material des Color Targets weiterhin Reflexionen aufweist, selbst wenn Cross-Polarization angewendet wird. Daraus sind 2 Fragen entstanden: 1) Wie können Reflexionen solcher Materialien eliminiert und bessere Bildqualität aufgenommen werden? 2) Wie ist es damit umzugehen, wenn die Kamera FOV (bzw. Field-Of-View / Sichtfeld) zu klein ist, um einen kompletten Color Target darin zu passen? – z.B. In dem Fall, in dem eine Makro-Kameralinse verwendet wird und der Wunsch besteht, einen umfangreichen Color Target zu scannen oder zu fotografieren, ergeben sich besondere Herausforderungen. Die für Makro-

---

Linsen geeigneten Color Targets sind in der Regel zu klein und weisen im Vergleich zu größeren Color Targets weniger Farbflecken auf. Darüber hinaus kann der Einsatz von einem großen Color Target bessere Farbkalibrierung garantieren. Die in dieser Forschung vorgeschlagene Lösung adressiert nicht nur das zuvor erwähnte Problem, sondern weist zudem das Potenzial auf, eine Lösung für die Herausforderung der 3D-Farbkalibrierung bereitzustellen.

Folgendes ist die Zusammenfassung der vorliegenden Studie/Forschung:

- Polarizationfilters haben einen unvermeidbaren Einfluss auf fotografierte Farben. Die Farbkomponenten, Chroma und Lightness, sind beide beeinträchtigt, sodass das Lightness der Farben zunimmt und daher zeigen die Farben mehr Brightness auf. Das heißt, die Farben wirken verwaschen/washed-out.
- Polarisationsfilter führen zu einer Unterbrechung der Grauwertlinearität, sodass beim Fotografieren von Graustufen mit Werten im Bereich von  $CIELAB(L^*) \approx 5 \rightarrow 95$  unter Verwendung solcher Filter die lineare Abstufung von  $5 \rightarrow 95$  aufgehoben wird. Dies resultiert in einem Verlust bestimmter Farbstufen, insbesondere in den tieferen Farben.
- Polarisationsfilter führen dazu, dass der Weiße Punkt (WP) eines Lichts und dessen Color-Correlated Temperature (CCT) vom originalen Wert abweichen. Das bedeutet, dass eine D50 Lichtquelle (CCT von  $5000\text{ K}$ ) mit bestimmten  $xy$ -Chromaticitycoordinates, nach dem Einsatz von Cross-Polarization Filtern nicht mehr den gleichen CCT wert und  $xy$ -Chromaticity Coordinates aufweist. Die Abweichung kann im schlimmsten Fall bis zu einem Wert von  $360\text{ K}$  betragen.
- Polarisationsfilter führen ebenfalls dazu, die Neutralität der Lichtquelle in Bezug auf die Werte der Chroma Koordinaten,  $CIELAB(ab)$ , zu beeinträchtigen. Dies bedeutet, dass die Messung der Farbdifferenz zwischen den Chroma Komponenten derselben Lichtquelle vor und nach dem Einsatz von Cross Polarisationsfiltern im ungünstigsten Fall bis zu  $\Delta E \approx 7.3$  und im besten Fall etwa  $\approx 3.6$  betragen kann. Derartige Abweichungen in den Chroma Komponenten einer Lichtquelle haben einen unvermeidbaren Einfluss auf die Darstellung der Farben, auf die das Licht fällt, wenn das Spektrum des Lichts (SPD) mit dem Spektrum des Objekts (Reflexion) interagiert.
- Wir haben eine neuartige Technik vorgeschlagen und untersucht, die es ermöglicht, Farbkalibrierung und Farbkorrektur durchzuführen, insbesondere wenn entweder das Sichtfeld (Field of View, FOV) der Kamera zu klein ist, um das gesamte Color Target zu erfassen (z. B. bei Verwendung einer Makro-Linse), und/oder wenn das gescannte Material sehr reflektierend ist, selbst unter Verwendung einer perfekten Cross-Polarisation. Die vorgeschlagene Lösung dieses Problems trägt auch dazu bei, eine potenzielle Lösung für das Problem der 3D-Farbkalibrierung anzubieten, da die angewandte Technik der Erzeugung einer *uv-map Texture* in 3D ähnlich ist.
- Zum Abschluss dieser Forschung haben wir die ersten Schritte unternommen, um den gesamten Prozess von der Erfassung (Scanning) bis zum 3D-Druck als *proof-of-concept* zu verifizieren. Hierbei wurde ein 2.5D-Gemälde automatisch fotografiert, farbkalibriert, ein 3D-Modell mittels Photogrammetrie generiert und schließlich dreidimensional gedruckt. Eine vorläufige Analyse dieser Ergebnisse wurde am Ende dieser Arbeit präsentiert. Offene Fragestellungen wurden bewusst für zukünftige Arbeiten und Forschungen zurückgestellt, da eine eingehende Untersuchung erfordert wird, um sie angemessen zu adressieren.

Diese Arbeit legt die Grundlagen für ein vertieftes Verständnis des Polarisationsphänomens im Kontext angewandter Forschung und Projekte, die Polarisationsfilter erfordern. Die Studie beleuchtet die Auswirkungen auf die Farbwahrnehmung, wenn sie durch (Cross-) Polarisationsfilter betrachtet werden. In diesem Zusammenhang wird ein weitverbreitetes Missverständnis widerlegt, das besagt, dass Polarisationsfilter keinen Einfluss auf die Farbwiedergabe haben und ihre Auswirkung lediglich auf die Intensität des Lichts beschränkt ist, d.h., die Intensität halbiert wird. Das umfassende Verständnis der Auswirkungen von Polarisationsfiltern auf die Farbgebung stellt einen wichtigen Beitrag dieser Arbeit dar.

# Acknowledgment

First and foremost I would like to thank my supervisor Prof. Dr. Arjan Kuijper for having the patience to guide me throughout this work and all his valuable feedback and input. His positive leadership and imperative advice have made this journey an exceptional learning experience. I would like to express my gratitude, as well, to Prof. Dr. Dr. eh. Dieter W. Fellner for co-refereeing this work and for building a thriving atmosphere for scientific excellence at Fraunhofer IGD.

Much of the gratitude goes to the team with whom I have worked in the past 3 years during my PhD journey in the *Competence Center for Cultural Heritage Digitization (CHD)* at Fraunhofer IGD, especially the head of the department who made the journey possible through his support, vision and management, M.Sc. Pedro Santos. I would like also to express my deep gratitude to M.Sc. Reimar Tausch my mentor and project supervisor with whom I spent countless hours discussing and brainstorming ideas and methods that helped in shaping the presented body of research as it is now. Deep thanks goes to M.Sc. Martin Ritz who made running and managing the project, *EVOCATION Marie Skłodowska-Curie ITN Horizon 2020*, easier through his management. Also, not to forget to thank the rest of the team in the department for their positive comments and feedbacks.

A special thanks goes to Prof. Dr. rer. nat. Philipp Urban, the head of the *3D printing technology* department at Fraunhofer IGD, who never hesitated to offer his advice and insightful feedback whenever I approached him to discuss my doubts and questions in the research area of color science.

I would like to give a special thanks to the family of EVOCATION programme (EU Horizon 2020), mentors, supervisors and research fellows for the atmosphere and the healthy environment they have created through their event organizations, workshops, and all the fruitful and insightful discussions we had together virtually and/or physically on-site despite all the hardships we went through because of Corona epidemic.

I would not be fair if I forget to mention the support I got from my dear friends who were there for me through the time of my research journey, assuring me that I am doing well and believed in me that I will accomplish the scientific goals I set for myself.

My family, parents, brothers and sisters, thanks a lot for being there for me unconditionally, thanks for all the support you have showed throughout my whole life. I would not be here in this position if it were not for you, I am very grateful for having you.





# Contents

<b>1. Introduction</b>	<b>1</b>
1.1. Related Work - State of the Art	2
1.2. Research Questions (RQ)	4
1.3. The Structure of This Thesis	5
1.4. Main Contributions	5
1.4.1. Color Management and Profiling System (CMPS)	6
1.4.2. The effect of cross-polarization on RGB Imaging	6
1.4.3. The effect of cross-polarization on the illuminant's white-point and the color-correlated temperature (CCT)	6
1.4.4. A new mosaic approach for color calibration for non-standard scanning geometry, very shiny surfaces, and small camera field-of-view (FOV)	7
1.4.5. Outlook	7
<b>2. Color</b>	<b>9</b>
2.1. Light and Color	9
2.2. Light	10
2.3. Light Polarization	11
2.3.1. Linear Polarization	11
2.3.2. Circular Polarization	13
2.4. Human Visual System	13
2.5. Color Vision	15
2.5.1. Opponent-Color Theory	16
2.5.2. Human Vision Sensitivity	17
2.6. Colorimetry	17
2.6.1. Color-Matching Function	18
<b>3. Color Spaces</b>	<b>21</b>
3.1. What Is A Color Space?	21
3.2. CIEXYZ Color Space	21
3.3. xy-Chromaticity Diagram	23
3.3.1. Planckian Locus	25
3.3.2. Daylight/Sunlight	25
3.4. A Uniform Chromaticity Scale (UCS)	25
3.5. CIELAB Color Space	27
3.5.1. CIELCh Color Space	27
3.5.2. CIELAB Problem	28
3.6. RGB	28
3.6.1. sRGB, Adobe RGB and ProPhoto RGB	31
3.6.2. Linear RGB - Gamma	31

3.6.3. White-Balance . . . . .	35
3.6.4. Chromatic Adaptation . . . . .	37
<b>4. Designing a Color Management Pipeline</b>	<b>39</b>
4.1. Color Management System (CMS) . . . . .	39
4.1.1. ICC Profile . . . . .	41
4.2. The Problem . . . . .	43
4.2.1. Software . . . . .	43
4.2.2. Hardware . . . . .	45
4.3. Camera Exposure . . . . .	47
4.4. Conclusion . . . . .	49
<b>5. Effect of Cross-Polarization on RGB Imaging and Color Accuracy and Fidelity</b>	<b>53</b>
5.1. Introduction . . . . .	53
5.2. The Experiment . . . . .	53
5.2.1. Hardware . . . . .	54
5.3. Methodology . . . . .	55
5.3.1. Image Conversion . . . . .	57
5.3.2. Demosaicking - Image Decoding . . . . .	57
5.3.3. Color Correction - Calibration . . . . .	58
5.3.4. RGB Linearization - ProPhoto . . . . .	58
5.3.5. ICC Profile Creation . . . . .	60
5.3.6. Color Correction and Validation . . . . .	62
5.3.7. ProPhoto/ROMM RGB → CIEXYZ → CIELAB . . . . .	63
5.3.8. Color Difference $\Delta E$ / CIEDE2000 . . . . .	64
5.3.9. ISO Color Metrics . . . . .	65
5.3.10. Benchmarking Against A Commercial Software . . . . .	67
5.4. Results and Discussion . . . . .	68
5.4.1. Lightness, Chrome, and Polarization . . . . .	70
5.5. Conclusion . . . . .	74
<b>6. A Cross-Polarization as a Possible Cause for Color Shift in Illumination</b>	<b>89</b>
6.1. Introduction . . . . .	89
6.2. The Experiment Setup . . . . .	91
6.3. Objectives . . . . .	91
6.4. Methodology . . . . .	93
6.4.1. Measurement - Data Acquisition . . . . .	93
6.5. Results and Discussion . . . . .	94
6.6. Conclusion . . . . .	98
<b>7. Color Calibration Based on Mosaic Stitching of a Color Target as an Alternative to a Single-Shot Approach</b>	<b>101</b>
7.1. Introduction . . . . .	101
7.1.1. The Problem . . . . .	101
7.2. Stitching Approach . . . . .	102
7.2.1. 2D Planar Image Rectification . . . . .	103
7.2.2. Depth of Field Masking and Vignetting . . . . .	105

7.3. Methodology . . . . .	105
7.3.1. Technical Design . . . . .	105
7.3.2. Experiment . . . . .	106
7.3.3. Data Acquisition . . . . .	108
7.4. Result . . . . .	110
7.5. Discussion . . . . .	111
7.6. Conclusion . . . . .	113
<b>8. Conclusions and Future Work</b>	<b>115</b>
<b>A. Appendix</b>	<b>121</b>
A.1. CIEDE00 - Color Difference . . . . .	121
A.2. COPE - Command Line Executable . . . . .	123
A.3. Argyll - ICC Profiler . . . . .	124
A.4. ProPhoto RGB to CIELAB Formulae . . . . .	125
<b>Bibliography</b>	<b>127</b>
<b>A. Publications and Talks</b>	<b>131</b>
A.1. Publications . . . . .	131
<b>B. Curriculum Vitae</b>	<b>133</b>



# 1. Introduction

Research on color calibration has increased substantially in recent decades and especially in recent years, where the strive towards more accurate color representations, rendition, and color experience for the user has become one of the main goals of many big industries such as virtual museums, objects/artifacts digitization and rendition and AR/VR worlds among others.

Color calibration for imaging and displaying in 2D is, to a good extent, standardized for how to prepare the setup and do data acquisition and how to assess and evaluate the color calibration process based on the ISO standards, namely *ISO 19263-1* & *19264-1* [ISO20, ISO17]. However, such standards are, first of all, strictly tailored for 2D imaging. Second of all, they are strict regarding the lighting geometry setup, and the acquisition equipment for two light sources, at least, should be used to illuminate the imaged 2D sample from both sides at an angle of nearly  $45^\circ$  to guarantee enough and even light distribution. In addition to the fact that the imaging system (e.g. a camera) should avoid any extra components that may impact the image quality and the acquisition in any sense (e.g. filters). These requirements and conditions, however, are not always feasible and easily met or practical, especially when we start talking about various materials and/or 3D imaging.

The technology that was developed at Fraunhofer IGD under the code name *CultArm3D* [Cul23] is designed to be a fully autonomous robotic system for 2D and 3D digitization. The system targets, very well, the cultural heritage sector which requires, undoubtedly, high-quality scan and faithful color representation of the scanned items. For that, the system is designed to have its own light source integrated and attached directly to the camera, which is mounted at the end effector of the robotic arm. In addition to having two circular cross-polarization filters in place to eliminate any chance of undesirable reflections that are very likely to form due to the light/camera alignment as they lie on the same plane in space with  $0^\circ$  relative to one another. The light source must be integrated as part of the camera (i.e. attached to the camera lens) in order to make 3D objects' digitization more feasible as the light will be always moving with the camera and illuminating strongly enough the intended parts of the scanned object that is meant to be captured. On the other hand, the design of the system (*CultArm3D*) diverges in a very drastic way from the ISO standards regarding the light setup and the use of the polarization filters, which would put, consequently, the scan quality in terms of color faithfulness and accuracy in question.

The following research has been conducted mainly for the purpose of understanding the effect of cross-polarization filters on color accuracy and reproduction. Polarization is a well-documented phenomenon and well-understood in physics optics [Hec02a, Shu62]. However, less is known and (publicly) researched on how polarization filters manufacturing process could affect and impact colors, in real-world applications, regarding color reproduction and color accuracy. The published research from our side, which forms the backbone of this doctorate thesis, to the best of our knowledge, is the first research content that is -publicly available- trying to study, analyze, understand, and disseminate the knowledge regarding the effect of cross-polarization on color reproduction and color accuracy.

## 1.1. Related Work - State of the Art

Light polarization is a hot topic in the domain of physics, photography, and computer science (image processing). There are immense efforts that are still trying to capture the state of polarization of light, which is invisible to the human eye, in an attempt to help retrieve more information from the captured image. *Gruev et al.* [GPY10] demonstrate how it is possible to capture the optical properties of partially polarized light by integrating nanowire filters with a CCD imaging array, which enables having more information about the angle, degree of linear polarization, and the intensity information.

On-chip polarization is a new technology that entered the market in recent years such as the camera technology (Polarsens<sup>®</sup>) introduced by Sony<sup>™</sup> [Son18]. It enables sensing and registering the state of light polarization in the captured images which opens the door for various applications. One research group has shown how using Sony technology enables creating HDR images with the help of polarization information, for these on-chip polarizers provide information about the environment in an analogous way to capturing images using multiple exposures [WZH\*20].

Another very important use of light's polarization is underwater imaging where water is a highly scattering medium that makes visibility very limited to impossible in some cases, so with the help of cross-polarization it is possible to retrieve the image signal more clearly [TS09]. Having light polarization information helps, as well, in contrast, enhancement for images under hazy or foggy conditions [SNS06]. In forensics for instance, while making use of light's polarization it is possible to lift latent fingerprints at a low cost and without damaging the scanned surfaces as it was proved by *Lin et al.* [LYENPE06].

Another field in which cross-polarization is very appreciated and valuable is medicine, namely skin and tissue inspections. Cross-polarization proved to be very helpful in various medical procedures such as laparoscopy, endoscopy, cancer examination, bruises detection, diabetic ulcer recognition, and so on. Cross-polarization plays, as well, a very important role in dental prosthetics and restoration to determine teeth color accurately and to eliminate the effect of highlights and reflections teeth depict when they interact with light due to their nature. *Gurrea et al.* [GGB\*16] shows how important it is to use cross-polarization in digital photography for determining the shade and color of dental prosthetic and ceramic replacement. *Robertson and Toumba* [AJR99] showed back in 1999 a strong evidence of how cross-polarization in digital photography helps immensely in making better decisions in assessing enamel defects. Later in 2011 *Edwards* [Edw11] also conducted a study confirming and proving to the people in the field that the use of cross-polarization is of great help for intra-oral photography and helping greatly in medical assessment and decision making. A curious reader may find the review of *Hanlon* [Han18] useful as she has listed the branches of medicine and forensics that make use of cross-polarization.

In computer vision and image processing, reflections and highlights/specularity that are present in an image are a cause of loss in information that would disturb and confuse many algorithms such as stereo reconstruction, object recognition segmentation, and/or object tracking. Such highlights when they become part of the object in an image, they become artifacts rather than being intrinsic characteristics of the object itself, which will cause a loss of the object's geometric and surface details.

*Apopei et al.* [ABB\*21] in their research and attempt to digitize minerals and rocks and make them accessible for pedagogical and scientific purposes, they demonstrate how important it is to use cross-polarization for 3D scanning and 3D reconstruction of minerals with metallic and submetallic luster. Cross-polarization has proved to facilitate and enable the process of 3D reconstruction of highly reflective geological samples. But just like others, they have overlooked and jumped over the fact - despite their use of a color chart for the color calibration process- of how accurate and faithful the captured colors of the samples are compared to the naturally perceived color (i.e. without polarization filters) when captured with cross-polarization.

In a comparative study in 3D digitization of cultural heritage artifacts done by Angheluță and Rădvan [AR20a] they show how the use of cross-polarization is giving superior results to laser scanning when digitizing 3D translucent materials. The study shows how laser 3D scanning suffers from reflections and consequently defects upon creating the texture. While photogrammetry with the help of cross-polarization filters shows higher quality and precision of the 3D reconstructions both in terms of geometry and texture, hence surface color.

Cultural heritage photography and digitization can make very good use of polarization filters and cross-polarization technique in specific as many of the items and the artifacts depict shiny and reflective surfaces (e.g. coins, metallic utensils, bronze weapons and tools, marble, reflective paints, enamel, gold or golden items...etc.). Polarization filters come in very handy in cutting off all undesirable reflections and highlights such types of items would show depending on the lighting setup and its geometry –where positioning and fixing the lighting setup would be challenging.

Toque *et al.* [TMMIE11] showed how the cross-polarization technique could be deployed to enable clean and clear scans of a reflective painting for archiving purposes, and they did their simple demonstration on one Japanese painting. Angheluță and Rădvan [AR20b] made a comparison between two 3D scanning approaches of an artifact in the cultural heritage using a laser scanner against camera photography with cross-polarization to demonstrate that photogrammetry with the help of cross-polarization can achieve very accurate and cleaner 3D models and textures than the laser scanning technique. However, they addressed only issues related to geometry, overlooking by that the effect of cross-polarization on color accuracy and texture color rendition.

All the research and the technologies that are making use of polarization filters, so far, overlook one vital aspect of imaging and that is, namely, *color*. Color accuracy reproduction is rarely addressed in the currently available body of research related to optics polarization filters and color science. Even though, polarization filters solve important problems in imaging, digitization, and in computer vision by removing reflections and highlights from the captured images. Nevertheless, there is, unfortunately, less attention being paid towards the questions of

- **How are polarization filters affecting and influencing the imaged colors?**
- **How accurate are these colors, or how different from the same photograph before and after using polarization filters?**
- **Could any possible problem arise when speaking about colors because of the use of polarization filters?**

These kind of unanswered questions are creating a big gap in understanding the polarization filters' behavior and their influence on color reproduction that need be clearly addressed and explained, and the knowledge needs be assimilated in a way that helps in making the interested audience more aware of the compromise and the actions they need make when they use polarization filters in their systems and applications, especially to those people whose aim is to have a very highly accurate color representation and rendition for their photographs/scans and images such in cultural heritage digitization and archiving sector, virtual museums, or even in medicine for skin and tissues diagnosis.

## 1.2. Research Questions (RQ)

Driven by the design of the new technology (*CultArm3D*) that is developed at Fraunhofer IGD, for scanning and digitization, targeting primarily but not strictly cultural heritage artifacts and 2D and 3D museum collections. The system strives to deliver top-notch quality in terms of capturing fine geometric details as well as faithful and accurate surface color textures. The technology makes use of an integrated light source (ring-light) attached directly to a camera lens that is mounted at the end effector of a robotic arm. Because of the geometry between the ring-light and the optical axis of the imaging system ( $0^\circ$ ), direct light reflections are an inevitable consequence and very likely to occur compromising by that the quality of the captured images eventually. Hence, a set of circular cross-polarization filters was necessary to mount, one in front of the light source directly, and one in front of the camera lens, so as to cut off and eliminate any chance of undesirable surface reflections. However, that has caused multiple unanswered questions to arise summarized in the following research questions:

- *RQ1: Does cross-polarization affect the reality and the accuracy of the captured colors? if so, then which color attributes are the most likely to be affected than others and in which way?*
- *RQ2: Does cross-polarization affect the used light source in the first place, which would consequently affect how colors appear? Is there any observable change in the light source color-correlated temperature (CCT) and hence its white-point (WP)?*
- *RQ3: Perfect cross-polarization may be able to eliminate reflections on certain types of materials' surfaces but not all materials. For example, the highly glossy laminated finish of the NGT<sup>1</sup> color target) can show very disturbing reflections even with perfect cross-polarization in place. This has led to the development and testing of a new technique of Mosaic Color Calibration instead of the standard one-shot color calibration. Hence opening the door for surface color texture capture, which makes color-accurate 3D surface scanning and modeling possible. So, how accurate and viable such an approach for the color calibration process? Does it still pass the ISO standards in term of color accuracy and reproduction?*

Another issue *RQ3* helps in solving is, having a narrow and small camera field-of-view (FOV) so that the whole scanning surface cannot fit all at once such as in using a Macro lens. This application was also strongly in mind while trying to solve the problem of scanning a large color target using a Macro lens.

The system has required us, as well, to devise and develop a fully functional color management module in order to integrate with the software that controls the system, which raised the following research question that is more on the software side and required us to delve deep into understanding color management from the programming perspective.

- *RQ4: How does a color management module (CMM) pipeline work and what are the main components of a CMM? How to implement and integrate a color profiling algorithm so as to create tailored color profiles within the system and apply them?*

Given the scarcity and the ambiguity of the information that surround the topic of how to implement a color management system and integrate color profiling algorithms, beyond just understanding how they work, *RQ4* has demanded from the author a lot of time and efforts until the system was successfully implemented, integrated and deployed as part of the software that runs the technology *CultArm3D* with high efficiency and accuracy competing with other color profiling software on the market (e.g. BasIColor input 6). It is worth mentioning that tackling *RQ 1-3* was dependent on the successful implementation of a fully functional color management and

---

<sup>1</sup><https://heritage-digitaltransitions.com/product/dt-next-generation-target-v2/>  
<https://www.avianrochester.com/>



profiling system *RQ4*. Hence *RQ4* would be the first to be addressed in this work and then it would be followed by *RQ 1-3* sequentially.

### 1.3. The Structure of This Thesis

The structure of the thesis goes in the following order:

- Chapter 1 discusses the importance of (cross) polarization in imaging applications and the latest research and use-cases in the field such as creating HDR images, having more intensity information, capturing light polarization states, enhancing hazy and foggy images, object segmentation, scanning shiny cultural heritage artifacts objects among other topics. We, furthermore, give an overview of related work done in the field of polarization and possibly color science, introduce the research questions and present the main contributions.
- Chapter 2 gives an introduction that describes the color/light phenomenon and human vision. In this chapter, we talk about the physics of light, polarization, and color, and how the human visual system (HVS) works.
- Chapter 3 explains the basics of color and gives a comprehensive overview of color spaces (e.g. CIEXYZ, CIELAB, xyY, RGB...etc.). This chapter lets one understand the relation between the human visual system (HVS) and the devised color spaces, and understand what uniform and non-uniform color spaces are. We talk, as well in this chapter, about how we measure and assess color differences mathematically in correspondence with human perception. Then, a quick tour over common color spaces such as *sRGB*, *Adobe RGB*, *ProPhoto RGB*, the gamma function, white-balance, and finally chromatic adaptation.
- Chapter 4 describes the developed technology at Fraunhofer IGD, its design, and the problem in hand, which was mainly the incentive behind this body of research. We address *RQ4* firstly as it is the backbone of any further analysis down the road in terms of color. We touch on topics like color management systems, color profiles, and camera exposure.
- Chapter 5 addresses *RQ1* in which we explain and demonstrate how grayscale color reproduction is affected by cross-polarization, and how the linearity, as well as the chroma, of a grayscale, are compromised and cannot be guaranteed depending on the imaged material and the used color target used for color calibration.
- Chapter 6 addresses *RQ2* in which we explore how cross-polarization causes a shift in the light source's white-point (WP) and color-correlated temperature (CCT), which eventually would affect the surface color appearance under such light source and affect the assumption of the used mathematical model that helps in predicting the color value.
- Chapter 7 addresses *RQ3* in which we demonstrate and propose a new color calibration mosaic approach to overcome problems such as very reflective surfaces despite the use of cross-polarization, non-standard scanning geometry and/or small camera field-of-view (FOV) (e.g. in case of using a Macro lens).
- Chapter 8 concludes the thesis and gives some directions for future work.

### 1.4. Main Contributions

This body of research was conducted in the biggest part of it solely by the author of this dissertation (*M.Sc. Tarek Abu Haila*). The contributions include the following:

### 1.4.1. Color Management and Profiling System (CMPS)

Planning, devising, and implementing a fully functional color management pipeline from the moment of capturing an image using a camera and processing the raw data, all the way to showing the final color-corrected image on a color-corrected display. Different libraries and tools were used to build a CMPS such as *OpenCV*, *FreeImage*, *LittleCMS*, *Argyll*, *IrfanView* while coding all of that in *C++*. The implemented pipeline was designed such that it fulfills *ISO 19264-1* standards. Measurements and display color calibration were done using *Barbieri*<sup>TM</sup> spectrophotometer and *Spyder*<sup>TM</sup> colorimeter.

The implementation of the CMPS integrates well with the developed software that runs the technology *Cul-tArm3D* and enables accurate color readings, profiling, creating ICC profiles, applying color correction, and viewing and saving images. The CMPS guarantees the consistency and accuracy of the color information throughout the whole life-cycle of the image inside the system.

In addition to that, a smart "exposure algorithm" assistant was also devised, implemented, and integrated into the system that assists the user in choosing optimal camera exposure settings (aperture, shutter speed, and ISO number) so that the captured data adheres to the ISO standards and conforms with the image quality principles, so to achieve the best results in color calibration and correction process.

### 1.4.2. The effect of cross-polarization on RGB Imaging

The first research topic includes devising an experiment and a method in which I was able to quantify in numbers and show in graphs –so as to disseminate the knowledge publicly given that such knowledge is not -till the time of publishing this dissertation- to be found anywhere in the literature to the best of our knowledge- ***how cross-polarization filters affect drastically the process of color correction.***

In this research topic, I have addressed how cross-polarization filters are killing certain color information below certain color thresholds, which is observable by looking at the dark shades of a grayscale as demonstrated by *Munsell Linear Grayscale*. This information is rendered to be lost and it is hard to correct for or rectify again as multiple dark shades of the grayscale will just be flattened out to bear the same value and disintegrate, falling into one perceived shade of color. I showed, as well, how cross-polarization filters would impact different materials differently. For a matt material, for example, like when using the *Spyder ColorCheckr 24* for color correction, the linearity of a grayscale would shift upwards in the sense of increasing the lightness component, *CIELAB(L\*)*, of the grayscale's patches, causing the perception of washed-out drab material upon color correction. Whereas, the problem is solved when a semi-glossy color target is rather used for the process of color correction (e.g. *X-Rite SG*).

### 1.4.3. The effect of cross-polarization on the illuminant's white-point and the color-correlated temperature (CCT)

In the second research topic, I have addressed further the question of ***what happens to the light source's white-point, in the first place, when it passes through a circular cross-polarization filter.*** The findings were in line with the hypothesis I proposed based on the first research topic #1, that the white-point of a light source would not be stable if a set of polarization filters were to be introduced in its path and that is why we see some shift in the color components (lightness and chroma). I have demonstrated using a D50 light source how different brands of polarization filters can shift the light source's white-point in different directions causing a shift, in worst case scenario, of  $\approx 360K$  (Kelvin) in terms of the color-correlated temperature (CCT).

I have, as well, demonstrated how the neutrality of the light source (D50) in terms of chroma components,  $CIELAB(a^*b^*)$ , is not guaranteed anymore after introducing cross-polarization filters in the path of the light source. This is affecting, consequently, how the light's chroma would interact with the surface color of a material placed under this light source. The change in the light source's chroma amounts to a color difference of  $\Delta E \approx 3.5 \rightarrow 7.3$  in best and worst case scenarios respectively (The color difference is expected to be  $\Delta E \leq 1.0$  in normal and ideal case. i.e. less perceptible).

Upon talking with different optics companies, without mentioning any names, their representatives confirmed to us that their (circular) polarization filters should not contribute to any shift in the light source's chroma or CCT nor in the scanned colors through them. However, our experiments and published data say otherwise, unfortunately.

#### **1.4.4. A new mosaic approach for color calibration for non-standard scanning geometry, very shiny surfaces, and small camera field-of-view (FOV)**

Under this research topic, I have addressed an issue of twofold. Firstly, how to overcome the problem of scanning certain types of material that is very prone to direct reflections, despite having cross-polarization filters, when the geometry of the light source is not perfectly adjusted at a sharp angle (e.g.  $30^\circ$  in order to eliminate reflections) relative to the imaging system. With some help in the implementation, from the second author (*Felix Schneider*) of the corresponding research paper, that is in Ch.7, we devised and implemented **a mosaic-stitching scanning technique** in which I was able to prove the validity of such approach for the process of color correction and color calibration in accordance with the ISO standards (*ISO 19264-1*). This new approach opens new doors for scanning large color targets using camera lenses with small field-of-view (FOV) like Macro lenses while preserving the highest quality of the color correction model. Secondly, using this proposed mosaic stitching technique, we have also opened the door for **3D color correction**, which is still a hard case in the industry and has no standards on how to do it up until this moment. Using our approach a 3D texture would be possible to be color-corrected in a very homogeneous and evenly lit way as our proposed technique, of how to scan an arbitrary 3D object and how to extract only the clean, clear, and evenly lit parts of each captured image and then color-correct for them, guarantee that.

#### **1.4.5. Outlook**

Using the knowledge of this work, we are looking forward to standardizing 3D color correction, as well as hoping to push towards better polarization filters that minimize the color capturing error by making the industry more aware of the wishes and desires of the market and the challenges today's applications are facing using the current polarization filter technology in terms of reproducing color faithfulness and accuracy. We, as well, are striving to 3D print color-accurate replicas of any arbitrary scanned object using the system under research *CultArm3D*. During the time of writing this dissertation, we have run already a few successful tests of 3D printing color-accurate replicas of a few scans of 2 and 2.5D objects/paintings. Future work would include more complex 3D objects and more color analysis on the side of 3D printing and measuring the color difference between the original 3D object and the 3D printed replica.



## 2. Color

Color is a phenomenon and not an objective physical reality. In other words, it is a secondary quality to an object and not primary like height, width, or weight.

Newton, in his 1704 *Opticks* [New04], described light as following:

"For the rays, to speak properly, are not coloured. In them there is nothing else than a certain power and disposition to stir up a sensation of this or that Colour"

While Koenderink, in his 2010 *Colour for the Science* book [Koe10], said:

"The pessimistic notion that colors are 'mere mental paint' and have no relation to the physical and chemical constitution of things at all is popular in science and (especially) in philosophy, but it has no basis in fact"

### 2.1. Light and Color

It is well-established, in physics, that light has dual natures, quantum packets of photons, and electromagnetic wave oscillations. We will focus on describing and talking about the latter form of light in this work rather than the former.

Color is, from the physics point of view, no more than the result of the interaction of light with an object, and with the cells of our visual system in the eye. It can be expressed mathematically in a very simple way as follows:

$$C = IOE \tag{2.1}$$

where  $C$  is our perception of color,  $I$  is an illuminant that is shone on an object,  $O$  is an object, and finally,  $E$  is our eye sensitivity function (more detailed description to follow in 2.5). Obviously, the end-perceived color is dependent on all these three factors, and any change to any of these would result in a change in the realized and perceived color.

For a starter, color is highly influenced by the illuminant under which the color/object's surface is being looked at. So, changing the light source that shines on a banana would not, necessarily, result in the same color perception one would see of a banana under the usual daylight on our planet Earth. i.e. Yellow color would appear almost black (very dark) under a blue light source. Secondly, color is influenced by the object's composition itself, of which material it is made up, and what wavelengths (aka. colors) this material absorbs and/or reflects. i.e. A green tree leaf appears green only because it absorbs every other wavelength and reflects strongly green wavelengths. Another example is the finish of a material. A color surface, say red, with a matte finish would look different from a shiny/glossy finish of the same color; glossy surface color tends to look darker than their matte counterparts [TVG17]. Finally, the sensitivity of our visual system and its working range would determine at the end how this color ( $IO$  components) would be perceived to result in  $C$ . i.e. Even when a certain color results out of the interaction between the light and a material together, a limited color sensitivity (aka. color deficiency/blindness) wouldn't be able -necessarily- to capture all the necessary light information in order to perceive the intended color – different animals perceive the same object under the same conditions differently.

The topic of color blindness and its variations and impact on color perception is out of the scope of this work, therefore a curious reader is advised to consult [NN11].

## 2.2. Light

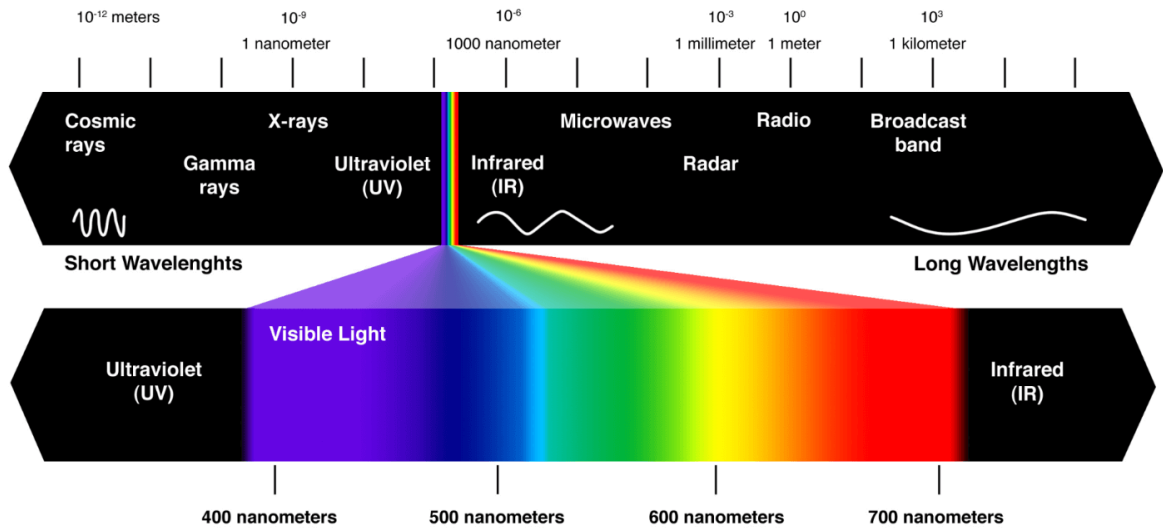


Figure 2.1.: Light spectrum

From the physics' classical point of view, light is considered electromagnetic waves that traverse through space (3D). What we "conventionally" refer to as "white" light is nothing but a composition of a variety of wavelengths all across the visible domain. That was first demonstrated and presented by Newton in 1704 in his prism experiment.

A **wavelength** (denoted by  $\lambda$ ) is a number that signifies the distance between two crests of a light wave and is expressed, usually, in nanometer ( $nm$ );  $10^{-9}$  meters. A short wavelength like  $400\text{ nm}$  lies on the left side of the visible spectrum and has a very high frequency, hence energy. Opposed to a long wavelength (e.g.  $700\text{ nm}$ ) that lies on the opposite side of the visible spectrum (to the right) and of a much slower frequency, hence less energy. The relationship between the wavelength and frequency (energy) is inversely proportional as depicted by the following equations:

$$f = \frac{c}{\lambda} \quad (2.2)$$

where:

$f$ : stands for frequency and is measured in Hertz (Hz) - 1 Hertz corresponds to 1 cycle per second.

$c$ : is, constant, the speed of light and measures to  $\approx 2.998 \times 10^8$  meter/second (m/s).

$\lambda$ : expresses a light wavelength in meter.

and to calculate the energy associated with a given wavelength, it is established that:

$$E = \frac{hc}{\lambda} \quad (2.3)$$

Where:

$E$ : stands for energy and is expressed in *Joule* (J). One *Joule* equals the amount of work/energy expended by the force of one *Newton* over a distance of one meter. Where one *Newton* is the force that produces an acceleration of one meter, per second per second, on a one-kilogram mass in the direction of the force.

$h$ : is *Planck* constant and known to be  $6.626 \times 10^{-34}$  Joules seconds (J.s).

Given that, we can calculate how much energy a given wavelength contains and, hence, check how harmful it could be. Let us take, for example, three wavelengths at both ends of the visible spectrum  $\lambda_1 = 200 \text{ nm}$  (UV-C),  $\lambda_2 = 350 \text{ nm}$  (UV-A), and  $\lambda_3 = 650 \text{ nm}$  (visible red), their corresponding energy, in *Joules*, would be calculated as follows:

$$E_1 = \frac{hc}{\lambda_1} = \frac{(6.626 \times 10^{-34}) \times (2.998 \times 10^8)}{200 \times 10^{-9}} = 9.93 \times 10^{-19} \quad (2.4)$$

$$E_2 = \frac{hc}{\lambda_2} = \frac{(6.626 \times 10^{-34}) \times (2.998 \times 10^8)}{350 \times 10^{-9}} = 5.68 \times 10^{-19} \quad (2.5)$$

$$E_3 = \frac{hc}{\lambda_3} = \frac{(6.626 \times 10^{-34}) \times (2.998 \times 10^8)}{650 \times 10^{-9}} = 3.06 \times 10^{-19} \quad (2.6)$$

To make sense of the numbers consider that the UV radiation energy range is  $5 \times 10^{-19} \leq E \leq 5 \times 2^{-17}$  and the X-Ray energy range is  $2 \times 10^{-17} \leq E \leq 2 \times 10^{-14}$ . So, UV-C of  $\lambda = 200 \text{ nm}$  is of a considerable amount of high energy.

## 2.3. Light Polarization

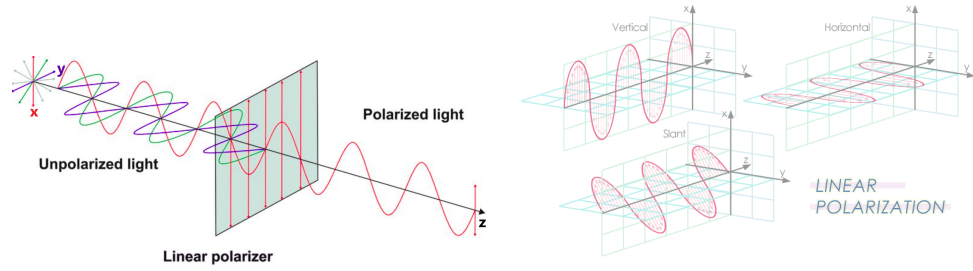
We learned in section 2.2 that light consists of electromagnetic<sup>1</sup> waves (EM) that travel in the 3D space with their direction of propagation being transverse to their vibration (e.g. vibration occurs in  $X, Y$  space while the direction of travel is along the  $Z$  axis), check Fig.2.2(a). These waves oscillate rather randomly in *unpolarized* manner usually. *Polarized light*, on the other hand, is the light whose vibrations depict a preference in oscillation with respect to the transverse direction [Hec02a, Shu62], as shown in Fig.2.2(b) that is described as to be *linearly polarized*.

Light polarization can take two different forms, *linear polarization* or *circular polarization*, defined by the way the light waves oscillate.

### 2.3.1. Linear Polarization

Light is said to be linearly polarized when its electric field takes one specific vibration plane e.g. along  $x$ -axis. It is not necessarily that the vibration plane to be exclusively vertical ( $\theta = 90^\circ$ ) or horizontal ( $\theta = 0^\circ$ ), it can, as well, take any angle in between ( $0^\circ \leq \theta \leq 90^\circ$ ) as long as there is no phase difference between the two of the light wave components on both axes ( $E_x, E_y$ ). While the magnitude and the sign of the electric field vary in time.

<sup>1</sup>Light consists of two forms of vibrations -electric and magnetic- that are orthogonal to one another and have always proportional magnitudes.



(a) An illustration that shows light propagation in the 3D space unpolarized that becomes polarized after entering a polarization filter with vertical slits to become linearly polarized. Source <https://www.codixx.de/en/knowledge-corner/polarization> (b) Illustration on how light EM waves could be linearly polarized. Consider the direction of motion is inwards towards the page. Source <https://jemengineering.com/blog-intro-to-antenna-polarization>

Figure 2.2.: Illustrations of light linear polarization

Consider, now, two perpendicular light waves of the same frequency that are linearly polarized moving in the same direction together that can be expressed as follows:

$$\vec{E}_x(z, t) = \hat{i} \cdot E_{0x} \cdot \cos(kz - \omega t) \quad (2.7)$$

$$\vec{E}_y(z, t) = \hat{j} \cdot E_{0y} \cdot \cos(kz - \omega t + \epsilon) \quad (2.8)$$

where:

$\vec{E}$ : is the electric field moving in the corresponding plane subscript  $x$  or  $y$ .

$z$ : is the moving direction.

$t$ : time.

$\hat{i}, \hat{j}$ : are unit vectors.

$k$ : is the propagation wave vector in the direction of motion where  $k = \frac{2\pi}{\lambda}$ .

$\omega$ : angular frequency/speed;  $\omega = 2\pi f$  where  $f$  is wave frequency.

$\epsilon$ : is the relative phase difference between the waves.

Now, the resultant wave is simply the vector sum of the two waves as follows:

$$\vec{E}(z, t) = \vec{E}_x(z, t) + \vec{E}_y(z, t) \quad (2.9)$$

These two waves are in phase if  $\epsilon = 0$  or multiple of  $\pm 2\pi$ , hence:

$$\vec{E} = (\hat{i}E_{0x} + \hat{j}E_{0y}) \cdot \cos(kz - \omega t) \quad (2.10)$$

In which case, the resultant wave has a fixed amplitude  $(\hat{i}E_{0x} + \hat{j}E_{0y})$  and is linearly polarized at an arbitrary angle. However, if  $\epsilon$  is an odd integer multiple of  $\pm\pi$ , then the two waves are  $180^\circ$  out-of-phase and still linearly polarized, hence:

$$\vec{E} = (\hat{i}E_{0x} - \hat{j}E_{0y}) \cdot \cos(kz - \omega t) \quad (2.11)$$



### 2.3.2. Circular Polarization

Circular polarization, Fig.2.3, is a special case of the more general case which is elliptical polarization. It occurs when two waves have exactly the same amplitude ( $E_{0x} = E_{0y} = E_0$ ) where their relative phase difference is given as follows:

$$\epsilon = -\frac{\pi}{2} + 2m\pi \quad \forall m \in \mathbb{Z} \quad (2.12)$$

Then:

$$\vec{E}_x(z,t) = \hat{i}E_0.\cos(kz - \omega t) \quad (2.13)$$

$$\vec{E}_y(z,t) = \hat{j}E_0.\sin(kz - \omega t) \quad (2.14)$$

Hence, the resultant wave is given as:

$$\vec{E} = E_0[\hat{i}.\cos(kz - \omega t) + \hat{j}.\sin(kz - \omega t)] \quad (2.15)$$

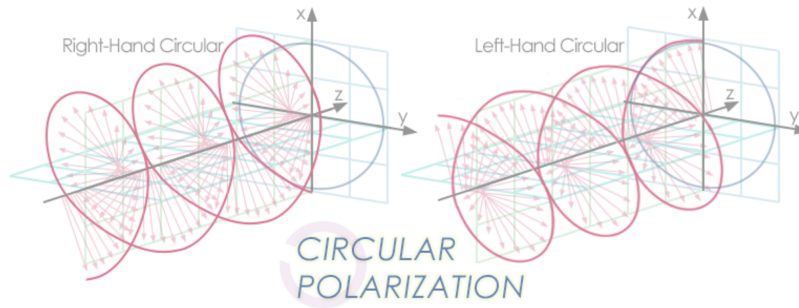


Figure 2.3.: An illustration shows circular polarization. Consider the direction of motion is inwards towards the page. Source as in 2.2(b)

For further details and more in-depth explanation please consult [Hec02a, Shu62].

## 2.4. Human Visual System

**The human visual system (HVS)** is argued to be one of the most complex systems in the human body and more than 50% of the cortex surface, the brain, is devoted to processing visual information according to professor David Williams [Sus12]. To understand the HVS, we need to take a closer look at the anatomy of the human eye and its components. The human eye is considered to be a sphere lodged in the eye socket in the human skull. Fig.2.4 is an illustrative drawing of the eye's cross-section.

Explaining in brevity, the cornea is the most outer glistening convex surface of the eye, it has a refractive index of  $n = 1.376$  and is covered by a tear film. Behind the cornea, there are the iris and the pupil. The iris is the colorful part of the eye where the concentration of the melanin pigment in addition to the iris' structure (stroma) both play a role in the given color the iris shows. The iris can measure up to 12 mm in diameter and 37 mm in circumference. The pupil is, technically, an opening -an orifice- in the middle of the iris through which the light is allowed to enter the eye chamber. The iris stroma is connected to two sets of muscles that contribute to controlling the pupil size and are responsible for its dilation and constriction, namely the sphincter and dilator

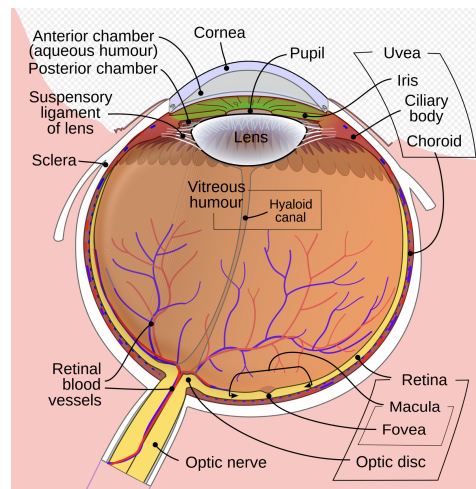


Figure 2.4.: A cross-section of the human eye anatomy

muscles, allowing more or less light to enter the eye eventually. The pupil size can range between  $2\text{ mm}$  up to  $8\text{ mm}$  in diameter. Directly behind the pupil, there is a lens that is responsible for focusing the light rays, that enter, to one exact point so that the looked-at object is in sharp focus whether it is near or far. To do this focusing the refractive power of the lens itself needs to change and that is possible to happen thanks to the lens elasticity and the connecting ciliary muscles where both are essential for what is known as the *accommodation process*. The ability to accommodate worsens while aging, as the lens loses its elasticity, hence reading glasses become indispensable for most people who grow old. It is worth mentioning that, the lens is not only responsible for focusing light but also blocking certain wavelengths in the range  $295 - 400\text{ nm}$  that are considered to be harmful UV radiations in order to protect the retina. The retina is responsible for transducing light into signals in order to transmit them eventually to the brain. The retina main regions, from the anatomical point of view as shown in Fig.2.4, are:

1. The **fovea** - an area of  $1.5\text{ mm}$  in diameter,  $3\text{ mm}$  away from the optic disk. Also referred to by the macula.
2. The **foveola** - an area, inside the fovea, of  $0.35\text{ mm}$  in diameter. It is, technically, a depression in the retinal surface at which the visual acuity (the resolving power) is at its highest.
3. The **optic disk** - it is also known as the blind spot as it contains no retinal layers or photoreceptors, it is technically the exit point for the optic nerves.

The retina as a whole has  $1250\text{ mm}^2$  surface area, and interestingly the photoreceptors that enable us to have the magic of sight lie at the very back of this layer where light needs to travel its way through 4 different groups of cells (Ganglion, Amacrine, Bipolar and Horizontal cells) arranged in 3 cellular layers until it reaches the photoreceptors and being transduced to signals that are transmitted to the brain so that the action of "seeing" happens.

Photoreceptors are categorized in two groups known as **rods** and **cones**. In low light conditions, the rods are dominantly active and they are best at conveying information such as contrast, brightness, and motion. The distribution of the rods is almost everywhere on the retina except for the fovea, they count up to  $100 - 120$  million rods in total with a density of nearly  $30000\text{ rods/mm}^2$ . The light condition under which the rods are active is

### Distribution of rods and cones

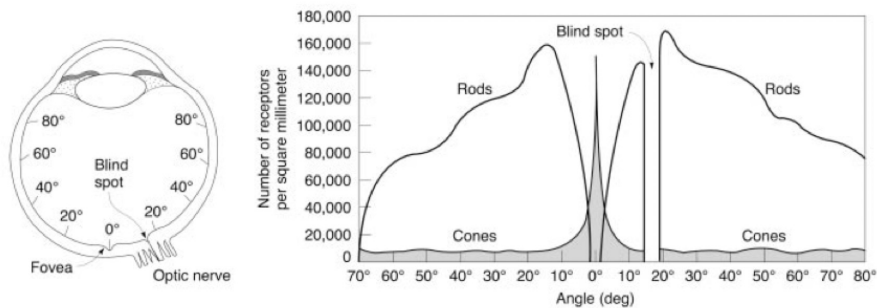


Figure 2.5.: Rods and cones distribution across the retina

referred to as *scotopic*, check Fig.2.6. On the other hand, under bright conditions, aka. *photopic*, the cones are dominantly active and they enable colorful vision. The distribution of the cones is at its highest in the fovea and they count up to 5 – 8 million with a density of nearly  $150000 \text{ cones/mm}^2$ . Fig.2.5 is an illustration of the distribution of both the rods and the cones across the retina. Both rods and cones can be active at certain light conditions where both the photopic and the scotopic light conditions overlap and that is referred to as the *mesopic* vision.

The cones come, as opposed to the rods, in three different types. Each type is sensitive to a different range of wavelengths along the visible spectrum despite their overlap. They are classified, loosely speaking, as Red or long (**L**) cones, Green or medium (**M**) cones and Blue or short (**S**) cones with peak sensitivity at  $\lambda_{Smax} \approx 437$ ,  $\lambda_{Mmax} \approx 533$  and  $\lambda_{Lmax} \approx 564$  as illustrated in Fig.2.7 –if we were to stimulate our cones with the aforementioned wavelengths using monochromatic lights individually, we wouldn't see blue, green, red but rather something like violet, green and yellowish-red respectively. The ratio of L:M:S cones to each others corresponds to 10:5:1 where S-cones are considered to be regularly spaced as opposed to L-M-cones that are more clustered together. Finally, the sensitivity peak of the rods lies around  $\lambda_{max} \approx 498$ , the black curve in Fig.2.7.

Having three types of cones means the color signal is, in principle, a mixture of all three types of cones. In other words, one single cone is not able to measure and report back color by itself. Hence, our visual system is described to be *trichromatic* meaning that the whole light spectrum and the resultant reflectance (remember Eq.2.1) all integrated together to yield just three proportional signals corresponding to *R, G and B* aka. *L, M, S*.

## 2.5. Color Vision

Color vision, in humans, is possible thanks to the three different types of cones and their overlap as shown in Fig.2.7. The theory of three color components in the eye (*trichromacy*), was first proposed by *Palmer* in 1777 and developed by *Thomas Young* later in 1802, then elaborated more by *Hermann von Helmholtz* in 1867, and that became to be known as later as *Young-Helmholtz trichromatic theory*. The trichromatic theory was confirmed by scientists at Harvard and Johns Hopkins who examined the retinal cells under the microscope and reached conclusive evidence about the existence of three types of cones that are sensitive to color in our eyes in 1959.

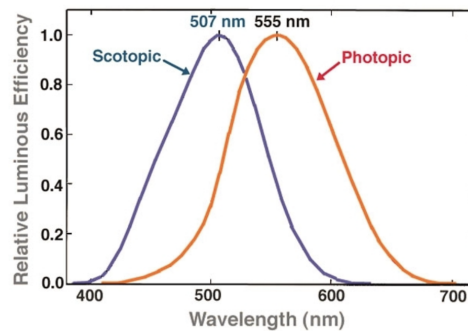


Figure 2.6.: The scotopic and the photopic curves of relative spectral luminous efficiency as specified by the CIE (normalized values)

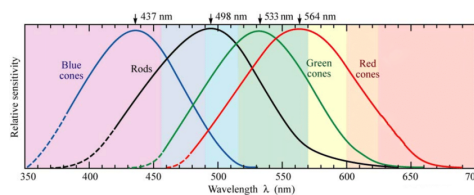


Figure 2.7.: Rods and cones sensitivity range and peaks. Normalized figure. Adopted from Dowling 1987.

*Helmholtz* was, allegedly, the first to conclude through experimenting with different light sources that any color can result as a mixture of only three 'primary' colors. Contrary to the common convention, primary colors do not necessarily mean *Red, Green, and Blue (RGB)* but any set of three colors that are spread enough across the visible spectrum can do the job actually. Also keep in mind that, the choice of *RGB* colors has nothing to do with our types of cones that are assumed, falsely, to be red, green, and blue but more to do with the physiology and psychology of the brain and the eye.

### 2.5.1. Opponent-Color Theory

*Ewald Hering* (1834-1918) has proposed a rivalry theory on how we perceive color known as the *opponent-process theory* that is taking place inside either the brain or the eye. The opponent-process suggests that the perception of color, in humans, happens in a mutually exclusive manner and the primaries responsible for that are *Red, Green, Blue, and Yellow* that are paired as opponents as *Red-Green* and *Blue-Yellow*. Meaning that there is no experience as such that a color would appear *Red-Greenish* or *Blue-Yellowish*, simply there are no such colors and they are referred to as the *impossible colors* or *Chimeric Colors*. *Hering's* theory explains a lot about how we perceive a mixture of colors and also it explains why partially color-blind individuals experience the loss of two colors at a time that are, usually, red and green or blue and yellow together and not just a single color.

*Hering's* theory suggests a third pair responsible for the processing and the perception of *Black and White*. Black and white in *Hering's* theory are spatially dependent, unlike the other two pairs of colors that are rather point-based (i.e. the color distribution in the visual field), and the perception of lightness and/or darkness is relative to the surround with the absence of the hue.

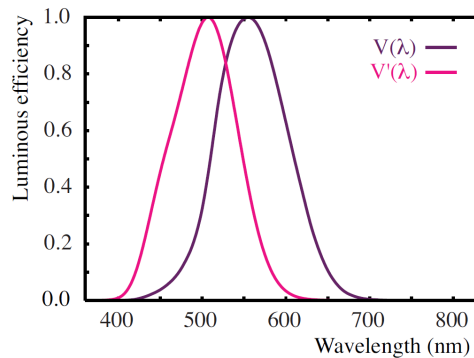


Figure 2.8.: The standardized photopic  $V(\lambda)$  and scotopic  $V'(\lambda)$  luminosity curve sensitivity of the human eye by CIE.

### 2.5.2. Human Vision Sensitivity

As mentioned before, due to the activation of two different sets of cells (rods vs. cones) at different lighting conditions (bright vs. dim), the eye sensitivity differs according to the conditions under which it is being examined. For instance, in the *photopic* domain (bright light) our eye sensitivity peaks at  $\lambda \approx 555 \text{ nm}$  with a gradual decrease towards the two ends of the visible domain (bell curve). The sensitivity curve for the *photopic* domain was measured and quantified in an experiment in the early 1900s where the field of view was set to  $2^\circ$  (e.g. the angular view of our thumb's nail when our arm is extended in front of us) and the measurement was accepted by the *International Commission on Illumination / Commission Internationale de l'Éclairage CIE* in 1924 and referred to as the *photopic luminous efficiency curve  $V(\lambda)$*  - weighted radiometric function check Fig.2.8. Another experiment was set up to measure the sensitivity curve of our *scotopic* vision, in which the rods are most activated, and the measurements were standardized in 1951 by *CIE*, as well, and was referred to as the *scotopic luminous efficiency curve  $V'(\lambda)$*  with a peak sensitivity at around  $\lambda \approx 507 \text{ nm}$ . The visible domain is proposed to be between  $380 - 780 \text{ nm}$  with variability among individuals.

## 2.6. Colorimetry

Colorimetry is the science of measuring and quantifying color in the visible domain. It does not provide a description of how colors look for an observer though. however, it only tries to quantify, conclusively, colors for evaluation and assessment purposes (e.g. whether two colors match or not, color reproducibility accuracy...etc). Colorimetry tries to alleviate all the barriers and difficulties that arise when people try to communicate color to one another, which is, usually, highly subjective. Keeping in mind that *color is an experience more than being a physical reality*.

Mathematics, as always, tries to rule the science of color and how colors behave and appear by formulating everything in a set of mathematical equations. It turned out that colors follow the additive law of Algebra and can be said that if we have four colors  $A, B, C$  and  $D$  where  $A = B$  and  $C = D$  then  $A + C = B + D$ , and that became to be known as *Grassmann's law* as it was first proposed and described by *Hermann Grassmann* in 1853. It is important to keep in mind that this additive property of color is strictly valid when adding up two or more spectral power distributions (spectra) of radiant light sources under the assumption that there is no cross-talk between the

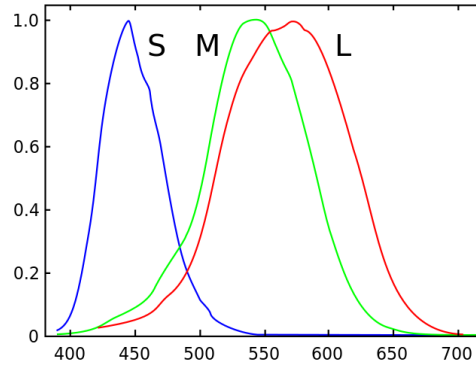


Figure 2.9.: Measured cones response/sensitivity of the human eye L, M, and S in the visible domain.

different wavelengths. Thanks to *Grassmann's additive law*, scientists were able to quantify and measure the cone response of the human eye through a series of experiments in the 1920s.

As a result, for the first time it was possible to model the experience of perceiving color and predicting it by integrating the radiant power of a stimulus  $\phi(\lambda)$  multiplied by the sensitivity of the corresponding cone response (*L, M or S*), Fig.2.9, across all the wavelengths of the visible domain, which is written as following:

$$\begin{aligned}
 l &= \int_{\lambda_{min}}^{\lambda_{max}} \phi(\lambda)L(\lambda)d\lambda, \\
 m &= \int_{\lambda_{min}}^{\lambda_{max}} \phi(\lambda)M(\lambda)d\lambda, \\
 s &= \int_{\lambda_{min}}^{\lambda_{max}} \phi(\lambda)S(\lambda)d\lambda
 \end{aligned} \tag{2.16}$$

and hence the term *tristimulus values* was born. But given that, it means that our perception is shrinking down the whole spectral information into only three values and we are not able, obviously, to distinguish light wavelength by wavelength. Consequently, one would guess, that may lead to an inevitable misperception sometimes as two stimuli can have two distinct spectra, and yet we end up seeing them the same under certain lighting conditions, and that is true! The phenomenon is known as *metamerism* [Ber19].

### 2.6.1. Color-Matching Function

Independently, two scientists, *Wright* in 1928-1929 and *Guild* in 1931, performed experiments in which the observers looked at a projected color, monochrome, through an opening, that measures to  $2^\circ$  (the Fovea size), which is divided into two halves in a complete darkness and asked to match the projected monochromatic color on one half with the additive result of a three-light primaries (red, green and blue) projected on the other half next to it. Because monochromatic colors are usually perceived as rather saturated compared to colors projected from the used broad light primaries (the R, G, and B), it was necessary to de-saturate the monochromatic color by adding the same set of primary lights to it as shown in Fig.2.10 under 'reference field' – it is, technically, making use of the additive properties of color according to *Grassmann's law*. The subject is able to change only the intensity of the light sources without tampering with their spectral power distribution (SPD). Again, thanks to *Grassmann's additive law* for colors that was possible to achieve, check Eq.2.17

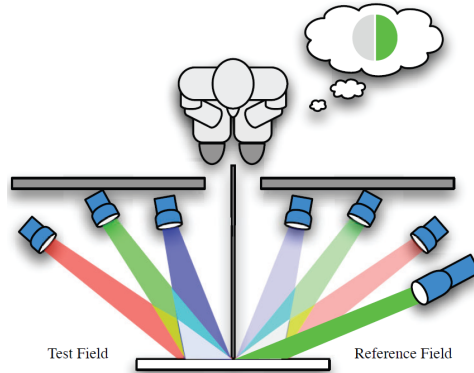
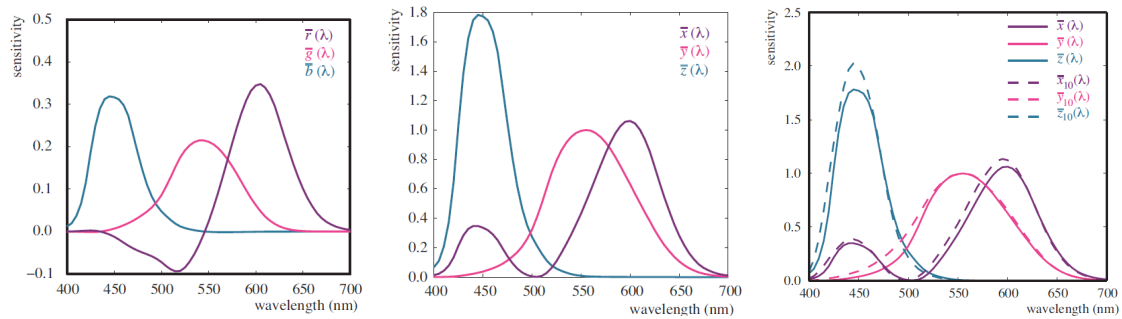


Figure 2.10.: A scheme showing the setup of the experiment that measures the human color-matching function. Source [ROAG08]



(a) The human color-matching function based on the data from *Wright and Guild* after being transformed to *CIE's* primaries, 435.8, 546.1, 700nm. (b) The human color-matching function  $\bar{x}(\lambda)$ ,  $\bar{y}(\lambda)$  and  $\bar{z}(\lambda)$  after making it all positive, for less complex calculations, and aligning one of the primaries with the photopic luminance response  $V(\lambda)$ . (c) The human color-matching function for the standard observer  $2^\circ$  and  $10^\circ$ .

Figure 2.11.: The human color matching function (CMF). Source [ROAG08]

$$R(r) + B(b) + G(g) = \lambda - (R(r_2) + B(b_2) + G(g_2)) \quad (2.17)$$

Where:

$R(r)$ : is the Red light source ( $R$ ) that has a defined amount of intensity ( $r$ ). Likewise the Blue  $B(b)$  and the Green  $G(g)$ .

$\lambda$ : is a monochromatic color produced at a certain wavelength.

As a result, we got what became known as the *color-matching function (CMF)* of the average human observer. The CIE committee transformed and averaged the results of both experiments and made the necessary changes to adjust for the following primaries  $\lambda = 435.8, 546.1$  and  $700.0 \text{ nm}$  to yield what is known as the *standard color matching function* Fig.2.11(b). Fig.2.11 depict the tristimulus values of our visual system CIE  $\bar{r}(\lambda), \bar{g}(\lambda), \bar{b}(\lambda)$  [ROAG08].

The noticeable negative dip in Fig.2.11(a) reflects, technically, the need to add that amount of a primary to the reference color, as the monochromatic reference color at this point seems to be out of the color gamut defined by the chosen set of primaries and impossible to match.

Now, after knowing and anchoring how the "average" human eye responds across the visible spectrum, it is possible to calculate what the expected *tristimulus values* (i.e. R, G and B amount) is (aka. the perceived color) if we have the spectral power distribution (SPD) of a stimulus using the following formulae:

$$\begin{aligned} R &= \int_{\lambda_{min}}^{\lambda_{max}} \phi(\lambda) \bar{r}(\lambda) d\lambda, \\ G &= \int_{\lambda_{min}}^{\lambda_{max}} \phi(\lambda) \bar{g}(\lambda) d\lambda, \\ B &= \int_{\lambda_{min}}^{\lambda_{max}} \phi(\lambda) \bar{b}(\lambda) d\lambda \end{aligned} \quad (2.18)$$

So with the help of these formulae, Eq.2.18, it is possible to judge whether two stimuli would deliver the same response to the human visual system or not, without the need for an actual observer. i.e. it is possible to tell whether two stimuli have the same color or not.

One, usually, encounters rather the color matching function that is shown in Fig.2.11(b) and that is due to the transformation agreed upon to do to the data of the experiments from *Wright* and *Guild* because of the following reasons. First and foremost, for the desire to remove any negative values from the tedious calculation done back then. Secondly, to combine the CIE 1924 photometry CIE  $V(\lambda)$  with the colorimetry system which is reflected in the  $\bar{y}(\lambda)$ .

The new color-matching function bears the  $\bar{x}(\lambda), \bar{y}(\lambda)$  and  $\bar{z}(\lambda)$  notation for the spectral sensitivity curves of the human visual system and the output tristimulus values are referred to as  $X, Y$  and  $Z$  instead of  $R, G$  and  $B$  in order not to confuse it with the actual measurements. This transformation required shifting the primaries to out-of-gamut primaries so to achieve all positive curves. i.e. the new primaries are, physically, impossible to realize and not meant for use if one needs to replicate the results. However, the new system is meant to be used rather for computational purposes.

The new color-matching function became known as *CIE1931 standard observer; 2° observer* and later in 1964 the CIE committee announced the *10° standard observer*, check Fig.2.11(c), based on the two datasets coming from *Stiles* and *Burch*, and *Speranskaya* separately. Notice that, the  $\bar{y}_{10^\circ}(\lambda)$  does not correspond to or match the  $V(\lambda)$  photopic curve sensitivity, and hence it does not correspond to luminance measurements in this case.



## 3. Color Spaces

*Color* is a very elusive realm that has no actual existence in reality beyond the illusion our brain, or any creature's brain for this matter, tries to convince us with. Color is sometimes defined as the interaction between the world and our brain as it is not a solid property of an existing object in a way similar to the object's dimensions for example, but rather it is a secondary property that accepts multiple interpretations based on various factors such as the perception physiology, the mood, the context, and the environment among others.

### 3.1. What Is A Color Space?

A *color space* is a constellation of colors that conglomerate together to form and define a subset of the visible colors, it is also known as *color gamut*.

Any color space is, normally, defined by 3 primaries like *red*, *green* and *blue* (not necessarily with these names exactly). Depending on the choice of these primaries the color space would be described as big or small. For example, have a look at Fig.3.1 which is a 2D illustration that shows the difference between the most popular output color spaces *sRGB*, *Adobe RGB* and *ProPhoto RGB*. However, having 3 primaries is not enough to define, what is commonly referred to as "a color space" and can be misleading when represented on a 2D graph. Nonetheless, The 2D representation helps in showing all the possible colors that could be mixed and reproduced out of those primaries according to *Grassmann's additive law*.

A color space, however, is not just a 2D space but rather 3D, check Fig.3.2. That, in addition to having defined primaries, it has another dimension that represents black and white (aka. lightness). Think of it like this, when the lightness level is 100%, no matter what are the RGB values, the color is just pure white. On the other hand, when the lightness level is 0%, no matter what the RGB values are, the color is just black. Saturated colors have a lightness level of 50%.

### 3.2. CIEXYZ Color Space

After we saw how the CIE committee decided to transform the experiment's results of *Wright* and *Guide*, so that the sensitivity response curves do not show any negative values, for easier calculation. The new sensitivity curves became known as the *CIE 1931 2° standard observer* and much later they agreed on a new dataset that became known as the *CIE 1964 10° standard observer*, check 2.6.1.

The common way of calculating the tristimulus values then became, after just slight replacement in Eq.2.18, as follows:

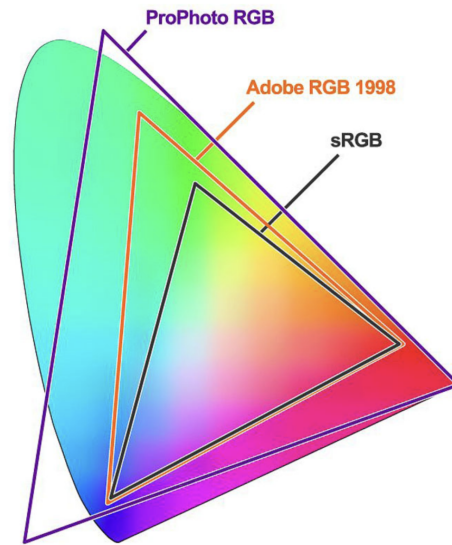


Figure 3.1.: A 2D comparison between the most common color space (sRGB, Adobe RGB, and ProPhoto RGB)

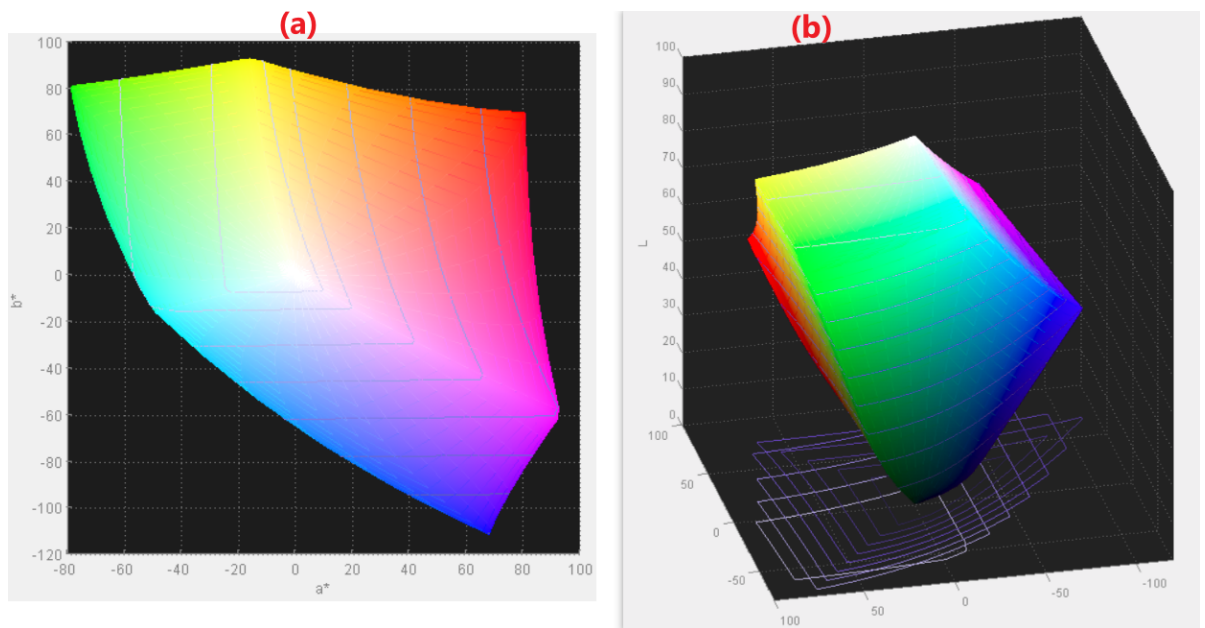


Figure 3.2.: A 3D view of sRGB color space represented in CIELAB. a) is a top view, b) is a view from an angle

$$\begin{aligned}
X &= \int_{\lambda_{min}}^{\lambda_{max}} \phi(\lambda) \bar{x}(\lambda) d\lambda, \\
Y &= \int_{\lambda_{min}}^{\lambda_{max}} \phi(\lambda) \bar{y}(\lambda) d\lambda, \\
Z &= \int_{\lambda_{min}}^{\lambda_{max}} \phi(\lambda) \bar{z}(\lambda) d\lambda
\end{aligned} \tag{3.1}$$

and hence we have what is referred to as *CIEXYZ color space*. Remember that the *CIEXYZ(Y)* component does not reflect the luminance perception when calculated through the data of the 10° observer, but only when 2° observer data are used.

In a real-world scenario, the radiant spectral power distribution (SPD) -what we refer to by  $\phi(\lambda)$ - is two things, one is the light source SPD denoted by  $S(\lambda)$ . Second, the object reflectance, onto which the light source is shining, denoted by  $R(\lambda)$ , and because the measurements in the real world are rather discrete and not continuous we replace the integration by a summation  $\int \rightarrow \sum$ . Measurements are usually arranged in a 5 or 10 nm step ( $d\lambda$ ). Based on that, we re-write Eq.3.1 as:

$$\begin{aligned}
X &= k \sum_{\lambda_{min}}^{\lambda_{max}} S(\lambda) R(\lambda) \bar{x}(\lambda) d\lambda, \\
Y &= k \sum_{\lambda_{min}}^{\lambda_{max}} S(\lambda) R(\lambda) \bar{y}(\lambda) d\lambda, \\
Z &= k \sum_{\lambda_{min}}^{\lambda_{max}} S(\lambda) R(\lambda) \bar{z}(\lambda) d\lambda
\end{aligned} \tag{3.2}$$

where:

$$k = \frac{100}{\sum_{\lambda} \bar{y}(\lambda) S(\lambda) d\lambda} \tag{3.3}$$

$k$  is a scaling factor so that *CIEXYZ* values are relative to the light source luminance itself, which measures to *CIEXYZ(Y)=100* for a perfect diffuser.

*CIEXYZ* color space does not give too much information about the color itself, apart from the *CIEXYZ(Y)* that reflects luminance only for the 2° observer (CIE 1931), as much as it tells about the relative necessarily needed amount of each of the X, Y and Z tristimulus to produce a certain sensation of a color – if it were to be linked directly to the human visual system. Therefore, a variety of color spaces depending on *CIEXYZ* can be calculated that make color evaluation and analysis much easier and more comprehensive as we will see in the next sections.

### 3.3. *xy-Chromaticity Diagram*

*xy-Chromaticity* diagram is a step towards visualizing *CIEXYZ* tristimulus values as it normalizes the *CIEXYZ* coordinates and removes the *CIEXYZ(Y)* contribution (luminance information). At the end, *xy-coordinates* ( $x$ ,  $y$  *small letters*) are nothing but a ratio of the tristimulus values with no magnitude information. That can be calculated as follows:

$$\begin{aligned}
 x &= \frac{X}{X+Y+Z}, \\
 y &= \frac{Y}{X+Y+Z}, \\
 z &= \frac{Z}{X+Y+Z},
 \end{aligned}
 \tag{3.4}$$

given :  $x + y + z = 1$

*xy-Chromaticity* coordinates alone are not real color descriptors and they miss the third dimension that represents the luminance information (lightness). Usually *xy-chromaticity* coordinates come accompanied with one of the *CIEXYZ* coordinates, commonly *CIEXYZ(Y)* value and would be expressed as *Yxy*.

*xy-Chromaticity* diagram in Fig.3.3, by no means, is a representative color space in terms of how an actual color would appear given certain *xy-coordinates* or in terms of calculating the actual distance between two colors, this color space is highly non-uniform. However, for illustrative purposes only it is common to see the *xy-chromaticity* diagram painted in color – which is not considered as a good practice at all.

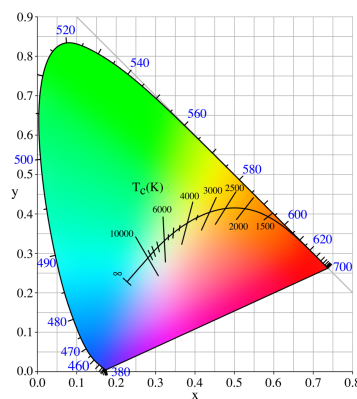


Figure 3.3.: *xy-Chromaticity* diagram with the black-body radiation curve aka. Planckian locus

The boundaries of the *xy-Chromaticity* diagram represents the monochromatic colors at the specified wavelength ( $\lambda$ ) except for the lower "purple" line which is not an actual monochromatic color but rather a result of two stimuli, namely the red and the blue. Everything beyond the boundaries of this diagram is regarded to be *imaginary color* that could result out of some math calculation but has no physical representation in reality. The diagram is, assumed, to encompass all the visible colors to the human eye.

Despite the incompleteness in how the *xy-Chromaticity* diagram represents colors. Though, it is still widely used alongside others, in the display industry, as it helps in visualizing the possible colors a display with three primaries could reproduce by simply connecting them to form a triangle that is referred to, usually, as the display color space or the display gamut encompassing all the possible colors thanks, again, to *Grassmann's additive law* for colors.

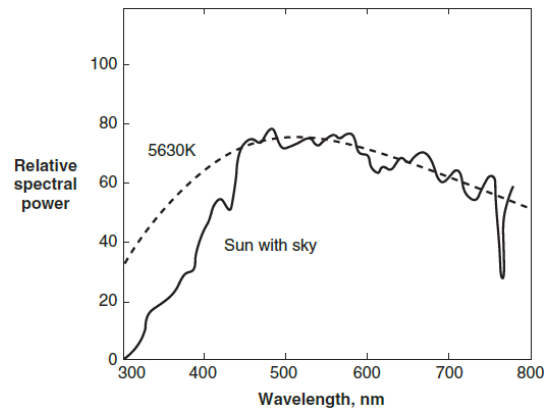


Figure 3.4.: Sun light combined with the sky (solid curve) relative to the black-body radiation curve (dashed) at temperature 5630K. Source [HP11].

### 3.3.1. Planckian Locus

The *Planckian* locus or the *black-body radiation curve* is a curve illustrated on the *xy-Chromaticity* diagram on which lie all the colors an assumed incandescent black-body goes through while being heated up to different temperatures ranging from red at low temperatures, going through orange, yellowish, green... all the way to the blue that reflects a very high temperature. The temperature is, commonly, measured in *Kelvin* ( $K$ ) based on the SI units<sup>1</sup> and called the *Color-Correlated Temperature* abbreviated *CCT* when describing the color of a light source.

### 3.3.2. Daylight/Sunlight

The light originating from the sun is believed to be around 5800  $K$  and because of its interaction with the sun's and the Earth's atmospheres, it measures actually to around 5500  $K$  up in the sky and a bit lower near the horizon.

Fig.3.4 shows the spectrum of the sun light combined with the sky that is not a perfect smooth curve as the one assumed by the black-body radiation curve for the temperature around 5630  $K$ . Sun light suffers, considerably, in the blue region where the Earth's atmosphere is responsible for many of the blue light scattering and reflecting it back to the space (check *Rayleigh's* scattering [ROAG08,Hec02b]). In addition to some dips in the red/near infrared regions (a bit before 800  $nm$ ) of the sunlight caused by the air water vapor that is responsible for absorbing those wavelengths. A common *CCT* of a clear sunny day combined with the sky is 5500  $K$  for solar altitude no less than 30°.

## 3.4. A Uniform Chromaticity Scale (UCS)

*xy-Chromaticity* diagram suffers from the problem of non-uniformity, in the sense that two lines of equal length, say  $\overline{ab} = \overline{cd}$ , if placed on the *xy-Chromaticity* diagram they would not yield the same perceptual color difference (i.e. how much color  $a$  differs from color  $b$  does not amount to the same difference as between color  $c$  and  $d$ ).

<sup>1</sup>The International System of Units - *Système International d'unités* (French)

### 3. Color Spaces

---

Therefore, a need for a more perceptually uniform color space arose and announced the birth of *CIE1976  $u'v'$  color space*, also referred to as *Uniform Chromaticity Scale (UCS) diagram*, Fig.3.5.

The representation of the *CIE1976  $u'v'$  diagram* also lacks, similar to *xy-Chromaticity diagram*, the luminance information. So, it is important when comparing and calculating  $u'v'$  coordinates to ensure that they are coming from light sources of the same luminance level, otherwise interpreting  $u'v'$  data would be completely off.

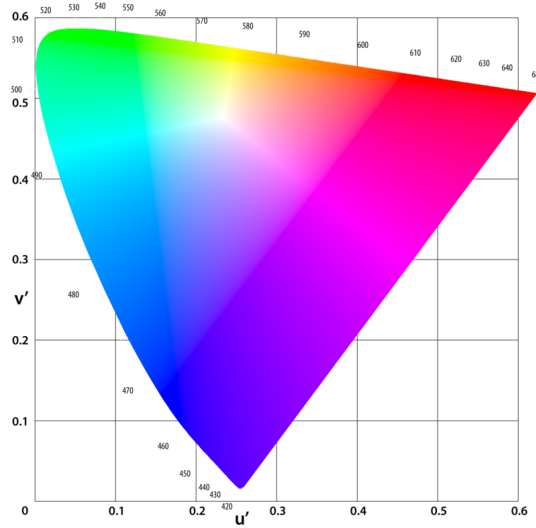


Figure 3.5.: CIE1976 Uniform Chromaticity Scale;  $u'v'$  Chromaticity diagram

The following formulae show the transformations how to reach *CIE1976  $u'v'$  coordinates* from either *CIEXYZ coordinates*:

$$\begin{aligned} u' &= \frac{4X}{X + 15Y + 3Z}, \\ v' &= \frac{9Y}{X + 15Y + 3Z} \end{aligned} \quad (3.5)$$

or from *xy-Chromaticity coordinates*:

$$\begin{aligned} u' &= \frac{4x}{-2x + 12y + 3}, \\ v' &= \frac{9y}{-2x + 12y + 3} \end{aligned} \quad (3.6)$$

The inverse transformation from *CIE1976  $u'v'$  coordinates* into *xy-Chromaticity coordinates* is given by:

$$\begin{aligned} x &= \frac{9u'}{6u' - 16v' + 12}, \\ y &= \frac{4v'}{6u' - 16v' + 12} \end{aligned} \quad (3.7)$$

### 3.5. CIELAB Color Space

An attempt in the 1940's by *Elliot Quincy Adams* to have a perceptually uniform color space directly from *CIEXYZ* coordinates was the seed that resulted in the birth of *CIELAB* color space during 1973 CIE Colorimetry Committee meeting. Which, later on, was standardized in 1976 to become known as *CIELAB color space* and its coordinates  $L^*$ ,  $a^*$ ,  $b^*$ . It was, undoubtedly, cumulative efforts throughout the years originating from *Adams* (1942), *Nickerson and Stultz* (1944) and *Glasser and Troy* (1952).

The formulae to derive *CIELAB* coordinates out of *CIEXYZ* are given as follows:

$$\begin{aligned} L^* &= 116f\left(\frac{Y}{Y_n}\right), \\ a^* &= 500\left[f\left(\frac{X}{X_n}\right) - f\left(\frac{Y}{Y_n}\right)\right], \\ b^* &= 200\left[f\left(\frac{Y}{Y_n}\right) - f\left(\frac{Z}{Z_n}\right)\right] \end{aligned} \quad (3.8)$$

where:

$$f(x) = \begin{cases} x^{\frac{1}{3}} & \text{if } x > \left(\frac{24}{116}\right)^3 \\ \left(\frac{841}{108}\right)x + \frac{16}{116} & \text{if } x \leq \left(\frac{24}{116}\right)^3 \end{cases} \quad (3.9)$$

The subscript  $n$  in  $X_n, Y_n, Z_n$  refers to the *CIEXYZ* coordinates of a known illuminant that is used as a light source (e.g. *CIEXYZ* of D50 [0.96422, 1.00000, 0.82521]).

It is common to see *CIELAB* color space represented as in Fig.3.6, giving the impression that  $+a^*$ ,  $-a^*$  &  $+b^*$ ,  $-b^*$  correspond to red, green, yellow, blue respectively. However, CIE documentation refrains actually from any sort of naming explicit colors when defining *CIELAB*. It is worth mentioning that *CIELAB* color space is heavily used in the printing and materials industries.

The  $L^*$  stands for *lightness* while the combination of both  $a^*b^*$  coordinates are referred to as the *chroma* ( $C$ ). It is common to move the rectangular coordinates of *CIELAB* into polar coordinates representation, *CIELAB*  $\rightarrow$  *CIELCh*, to illustrate that more easily and comprehensively on the hue circle Fig.3.6.

#### 3.5.1. CIELCh Color Space

*CIELCh* color space is a direct derivation from *CIELAB* color space, it represents only the color components, in a different manner, in polar coordinates rather than in rectangular coordinates. Hence, it separates the color in each of the  $a^*, b^*$  components into hue  $h_{ab}$  and chroma  $C_{ab}$  while preserving the  $L^*$  as it is. The following formulae show how to perform the transformation from *CIELAB* coordinates:

$$\begin{aligned} C_{ab}^* &= \sqrt{(a^*)^2 + (b^*)^2}, \\ h_{ab} &= \begin{cases} \frac{180}{\pi} \arctan2(b^*, a^*) & \text{if } \arctan2(b^*, a^*) \geq 0 \\ \frac{180}{\pi} \arctan2(b^*, a^*) + 360 & \text{otherwise} \end{cases} \end{aligned} \quad (3.10)$$

where the  $\frac{180}{\pi}$  is to convert *radians* ( $\arctan2$ 's output) into *degrees*. Going back from polar coordinates into rectangular coordinates is given by the inverse formulae as follows:

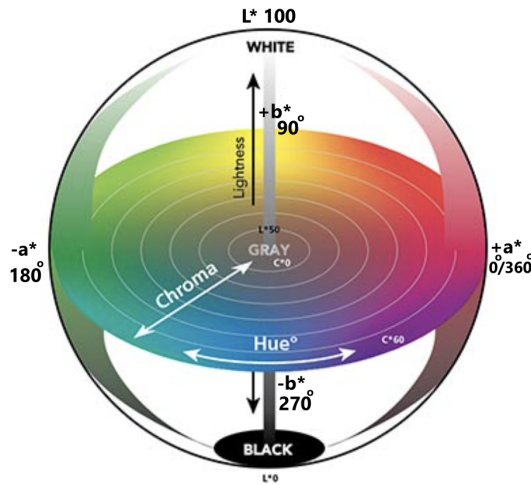


Figure 3.6.: CIELAB color space 1976, the hue circle represents the chroma and the hue angle based on  $a^*b^*$  coordinates, while  $L^*$  is represented by the vertical axis. Source (X-Rite).

$$\begin{aligned} a^* &= C_{ab}^* \cos\left(\frac{\pi}{180} h_{ab}\right), \\ b^* &= C_{ab}^* \sin\left(\frac{\pi}{180} h_{ab}\right) \end{aligned} \quad (3.11)$$

It is important to be aware of what the terminology means and how it should be interpreted. *Hue* refers to the color itself, what we usually, in our spoken language, refer to as (red, green, yellow...etc.). While *chroma*, on the other hand, expresses the strength or the saturation of that chosen hue (i.e. if we fix the lightness component to  $L^* = 50$ , set hue at an arbitrary angle and *Chroma*=0 it means the color, no matter what, is perceived rather as a tone of dark gray (close to the center), while if the *chroma* is set to the maximum then the color is perceived fully saturated (close to the circumference of the circle)).

### 3.5.2. CIELAB Problem

Despite the great success *CIELAB* model shows in uniformity and color representation and prediction, *CIELAB* suffers quite much from correctly predicting blue and purple colors that seemed to be problematic and quite challenging based on the collected data that were quite off (i.e. one notices shift for what should be predicted as blue towards the purple), check [Ber19]. We will see, later, how it was tried to account for when calculating the color difference.

## 3.6. RGB

*RGB* is an additive color space in which *R:Red*, *G:Green* and *B:Blue* are the chosen primaries. Based on color theory, a mixture of these additive primaries (think of them as light sources) in different ratios can, virtually, yield any desired color. It is, technically, the underlying principle of all the technologies available in our hands e.g. smartphones, cameras, displays, cinema projectors...etc.



White color is simply the mixture of all these three primaries when all set to the maximum (*i.e.*  $R = 1.0$ ,  $G = 1.0$ ,  $B = 1.0$ ) given that  $R, G, B \in [0.0 - 1.0]$ . Keep in mind, however, that there is nothing called an *RGB color space* in the abstract sense, as there is no standard or fixed *RGB* primaries that are agreed-upon that yield a pre-defined "RGB color space". When it is being called an *RGB color space* it is, usually, meant the color space in which a device (e.g. camera, monitor, projector...etc.) operates and encodes the photometric data, a space of colors defined by the set of primaries (e.g.  $R, G$  and  $B$ ) chosen by the manufacturer. Such primaries could be  $R, G$  and  $B$  of any wavelengths that yield these colors (broadly speaking) or they could be even a set of any other disparate primaries. Regardless of which, the set of primaries when fixed on *xy-Chromaticity* diagram, in a similar fashion to Fig.3.1, they would define an enclosed space that is commonly known as "*RGB color space*" or "*RGB color gamut*" of the device in hand. Because such *RGB "color space"* varies between products and manufacturers, usually it is referred to as *device-dependent color space*.

*Device-dependent color space* means that, for example, if we capture a photo using a camera and the camera encodes the photometric data in its own internal "*RGB color space*" that is defined by a set of primaries chosen by the manufacturer, then each color/pixel in the photo will have certain *RGB* values that corresponds to that color only in that pre-defined "*RGB color space*" of the camera. Now, if we take these, *device-dependent RGB* values and try to pass them to a computer display that, obviously, has its own set of primaries chosen by the manufacturer as well in which the display is able to show a certain set of colors, the *RGB* values from the camera do not, necessarily, correspond to the same expected colors when interpreted by the display and there may be a huge discrepancy in how the output colors would look like. In other words, there is no universal language yet between these two devices and a set of *RGB values of e.g. 100, 244, 88 in the range [0-255]* do not necessarily represent the same color when set on different *RGB* devices.

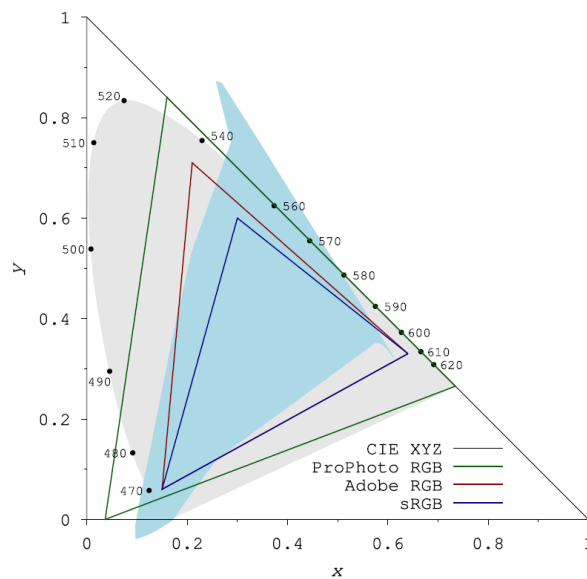


Figure 3.7.: Nikon D700 raw RGB color space (shaded cyan), optimized for D65 illuminant, plotted on *xy-Chromaticity* diagram against sRGB (blue), Adobe RGB (red) and ProPhoto (green). Source [Row20]

Check Fig.3.7, it shows the internal "*RGB color space*" of a Nikon D700 plotted (shaded cyan) on *xy-Chromaticity* diagram against the most common color spaces (*sRGB, Adobe RGB and ProPhoto*). Nikon D700 camera raw

space is estimated using a characterization matrix that was optimized for CIE illuminant D65 [Row20]. The camera's internal *RGB* color space looks to extend well beyond the defined boundaries of the *xy-Chromaticity* diagram, which defines all the visible colors to the human eye, mainly because the camera sensor violates *Luther-Ives* condition, in addition to the influence of the optimization matrix that links between the camera *RGB* response and the tested set of monochromatic colors, more details in [Row20]. Another example illustrates how different devices have their own internal "*RGB* color space" can be seen in Fig.3.8.

*Luther-Ives* condition, briefly, is satisfied when an imaging system response (spectral sensitivity curves) is a direct linear transformation of the human color matching function (*CIEXYZ* tristimulus values). In which case, the imaging system is, then, qualified to be described as a *colorimetric* device [ROAG08, Bal03]. Unfortunately, in reality, most imaging systems do not satisfy *Luther-Ives* conditions.

Having *device-dependent color spaces* means that there should be an opposite to that, and indeed there is. That is known as *device-independent color spaces*, more details on that later in section 4.1. Which act as a universal language for colors that alleviate ambiguity among different devices. Examples of such *device-independent color spaces* are the ones mentioned in the previous sections such as *CIEXYZ* and *CIELAB* color spaces. It is a common practice to convert the *device-dependent RGB* values of a device into one of the *device-independent color spaces* (e.g. *CIELAB*). Then from that point on, it is possible to share color information with another device so that the *device-independent color values* will be converted to what suits this device's internal "*RGB* color space". In color management, as we will see later, *CIEXYZ* and *CIELAB* color spaces are referred to as *Profile Connection Space (PCS)* as they act as a mediator between color spaces and devices.

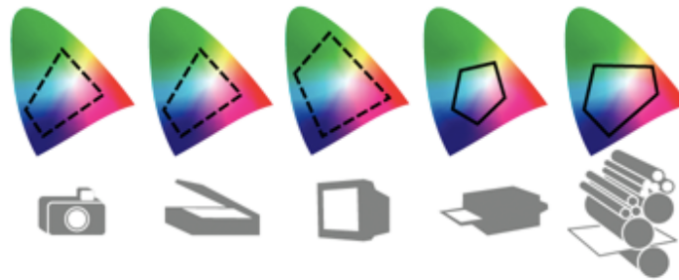


Figure 3.8.: Illustration on how different devices have their own *RGB*-dependent color space. Source: Adobe

It is important to notice that *RGB* color spaces come in two different varieties:

1. Unrendered color spaces; scene-referred.
2. Rendered color spaces; output-referred.

**Unrendered color spaces (scene-referred)** are those used, rather, for image manipulation and mathematical calculations purposes. They are wide enough to cover almost the whole visible colors defined by the *xy-Chromaticity* diagram and to preserve high-dynamic range data. Such color spaces do not need to be real or feasible. *RIMMRGB (Reference Input Medium Metric)* is one of the scene-referred color spaces, that has imaginary primaries that allow mathematical color manipulation over a very wide range of colors [RIM02]. Such color spaces operate, usually, in a high bit-depth as well such as 12-16 bits.

**Rendered color space (output-referred)** are the commonly used color spaces in the various types of devices and software to render out images/colors (also known as *output color spaces*). The most commonly used output color space is the *sRGB* color space [AMCS96], which is the default nowadays if not otherwise mentioned. These

color spaces are, usually, smaller, device-dependent, and have lower bit-depth (e.g. 8 bits)<sup>2</sup> and hence it would have less dynamic range as a consequence.

It is worth mentioning that, most cameras provide data only in a rendered color space even in their raw formats, and do not allow any access to the earlier data before this transformation has taken place (i.e. the transformation from an unrendered color space → a rendered color space) [SBS99].

### 3.6.1. sRGB, Adobe RGB and ProPhoto RGB

*sRGB*, *Adobe RGB* and *ProPhoto RGB*, remember Fig.3.1, are the most common standardized rendered / output color spaces. Because they have a pre-defined and agreed-on set of primaries and white points, for that they serve as universal color spaces. Check Table 3.1 in which the standardized *Yxy* coordinates of each of the aforementioned color spaces are listed.

Standardizing such types of color spaces makes it easier for a manufacturer to do the necessary transformations and calculations to move their *device-dependent* color values into one of these commonly used color spaces directly. Because these color spaces got wide acceptance, it became common that most of the digital imaging/displaying devices are programmed to handle them well. This means, that exchanging color information between different devices becomes now easier than before and less dependent on the device itself so that color values, if encoded correctly in one of these color spaces and flagged accordingly, would be interpreted as expected by any other device that supports the corresponding color space by reading the flag indicator. In simpler words, if a camera has the option to export its photos in *sRGB* color space and one's monitor supports also *sRGB* color space, then exporting the photo from one's camera and importing it onto one's PC/laptop should result in the same colors as the camera intended to render them, and there should be no misinterpretation of the color information.

In 1996 it was proposed, after the joint efforts from both *Microsoft* and *Hewlett-Packard*, to have a more standardized color space. In which, *Microsoft OS*, *HP products* and the Internet can operate, so as to have consistency in the color information and to make color management easier across platforms and applications [AMCS96]. The proposed *RGB* color space to be standardized is called *sRGB* and was, in 1999, officially accepted and announced by the *International Electrotechnical Commission (IEC)* under the code *IEC 61966-2-1:1999*.

*sRGB*, *Adobe RGB* and *ProPhoto RGB* are known as output-referred color spaces. Of course, there are plenty of other output color spaces designed for different purposes such as for the TV's, cinema projectors, motion picture, printing industries, and others. However, that is beyond the scope of this research to cover them all.

### 3.6.2. Linear RGB - Gamma

Of the aforementioned output-referred color spaces, *sRGB* was specially optimized to the behavior of the output devices (e.g. TV, monitors...etc.) at the time through the choice of its primaries, white-point, and its gamma correction function, so that the output voltage of a device results in a meaningful and reasonable brightness, color tone and hue.

It is well-known that the human visual system sensitivity is far from linear, i.e. doubling the amount of the intensity of a light source does not result in doubling the perceived brightness, check Fig.3.9(a). It, rather, follows -broadly speaking- a logarithmic / power function for we are more sensitive under low light conditions to the nuances and the shade's details more than under the bright light conditions – remember that we have more

<sup>2</sup>Keep in mind that we are talking here about the capability of an output device to support certain bit depth. Meaning, that even if your image is encoded in 16-bit depth in an output color space, if the output device (e.g. monitor) does not support sending/rendering signals in 16-bit depth then the image data will be converted to whatever bit-depth the monitor supports (8-bit commonly)

sRGB (D65)			
	Red	Green	Blue
x	0.6400	0.3000	0.1500
y	0.3300	0.6000	0.0600
Y	0.212656	0.715158	0.072186
Adobe RGB (D65)			
	Red	Green	Blue
x	0.6400	0.2100	0.1500
y	0.3300	0.7100	0.0600
Y	0.297361	0.627355	0.075285
ProPhoto RGB (D50)			
	Red	Green	Blue
x	0.7347	0.1596	0.0366
y	0.2653	0.8404	0.0001
Y	0.288040	0.711874	0.000086

Table 3.1.: Xyy coordinates of the most common output-referred color spaces for each of their primaries (R, G, and B).

rods in our eyes than cones. In other words, doubling the values at high-intensity levels does not necessarily trigger any drastic change in the response of our visual system compared to doubling the intensity at low light levels. Checking Fig. 3.9(a), the x-axis represents the luminance levels  $CIEXYZ(Y)$  (brightness)<sup>3</sup> of a light source, while the y-axis represents the lightness ( $V$ ) aka. perceived brightness. The different curves in the figure are elicited from different experiments under different conditions such that: different backgrounds (e.g. neutral gray, white background...etc.) and at different luminance levels (e.g. curves #1, #3 and #4 at luminance level of 20% while curve #6 at 50%). The idea is that, regardless of the background and the luminance level, the trend in which the human visual system perceives luminance (brightness) is quite the same; very noticeable change in the magnitude of perception at low luminance levels while slower change in magnitude of perception at higher luminance levels [WR05].

From *digital-encoding* perspective, we may be wasting too much space while encoding too many values of bright intensities that wouldn't elicit too much change in our visual system at the expense of not encoding the low-intensity values more properly instead. i.e. if we take a camera that encodes images in 8-bit depth, it means it encodes the impinging light, photometric data, on the sensor in  $2^8 = 256$  levels as integers, so we have the following:

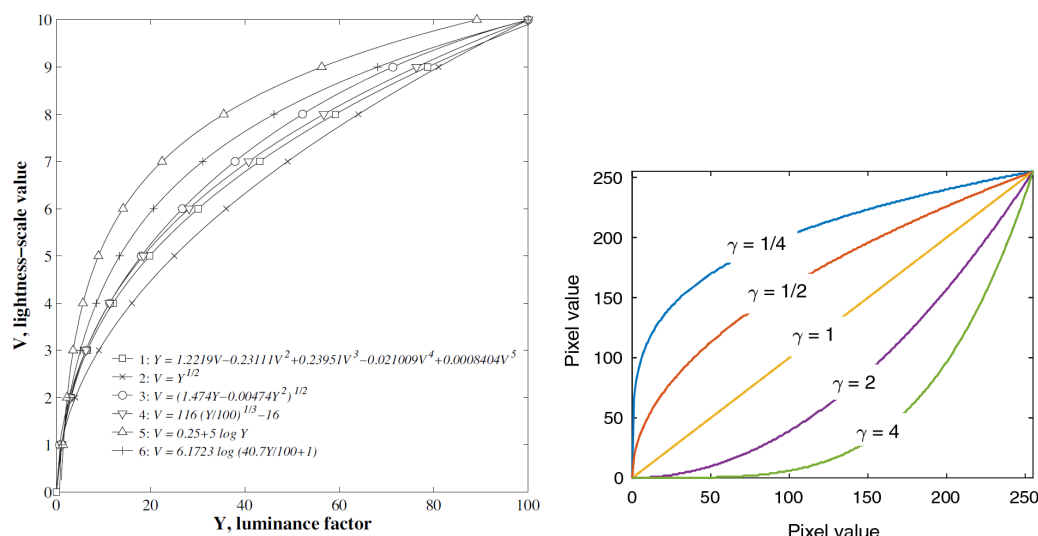
256 is doubling 128, which means the encoded light intensity has doubled in value/intensity, also referred to as increment of  $1 f-stop$  in photography terminology. The same for  $64 \rightarrow 128$ ,  $32 \rightarrow 64$ ,  $16 \rightarrow 32$ ,  $8 \rightarrow 16$ ,  $4 \rightarrow 8$ ,  $2 \rightarrow 4$ ,  $1 \rightarrow 2$ . That is in total  $8 f-stops$ . Cameras usually choose to encode in a higher bit-depth (e.g. 10-, 12- or 14-bit) to have more representative  $f-stops$  that try to keep up with the human eye that is capable of nearly 20  $f-stops$  which correspond to a contrast ratio of 1,000,000 : 1 [CMD13]. The number of  $f-stops$  translates directly

<sup>3</sup>Quick definitions based on [Ber19]

Brightness: describes how much an area looks to emit/reflect more or less light.

Luminance: defines the amount of light generated by a source.

Lightness: is the perceived brightness of an area judged relative to the brightness of a similar area that looks white.



(a) A set of various functions relate the x-axis which is the input luminance ( $CIEXYZ(Y)$ ) of a light source (aka. brightness) to the y-axis which represents the lightness levels. Source [WR05]

(b) Gamma family curves.

Figure 3.9.: Gamma function concept.

to the *dynamic range* of a scene/photo, which is -briefly- the difference between the lowest darkest value and the highest brightest value a camera sensor is capable of registering at the same time and before being saturated.

Looking at this linear encoding method shows clearly that low light levels get barely any chance to be encoded properly when compared to high light levels (i.e. bright light encoding is taking already half the range between 128  $\rightarrow$  256) even though we are not as sensitive to the differences for the bright light levels as we are for the low light's levels.

Understanding all of that about the human visual system dictates on us the use of what is known as the **Gamma correction** function that is denoted, commonly, by the Greek letter  $\gamma$ . Gamma correction is a successful attempt to transform the camera's linear response to light into a more human-like logarithmic curve, check Fig.3.9(b) where the x-axis is the input pixel value or input signal, and the y-axis is the output pixel value or output signal in the range 0-255. The mapping of the curves where  $\gamma < 1.0$  ensures that the lower values in the range enjoy a wider range for representation than the higher values at the other end of the range. In other words, shadows and dark values will have the opportunity to expand over a wider range in the output domain in contrast to the bright values that would rather be compressed, and hence the encoded data would have a better contrast in general. Signal data encoding is achieved through a simple formula as follows:

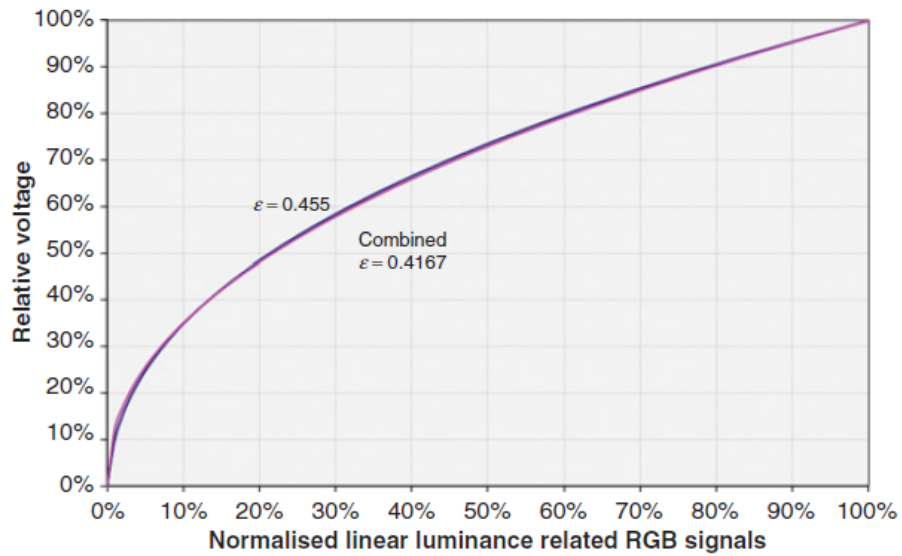
$$V_{out} = AV_{in}^{\gamma} \quad (3.12)$$

where:

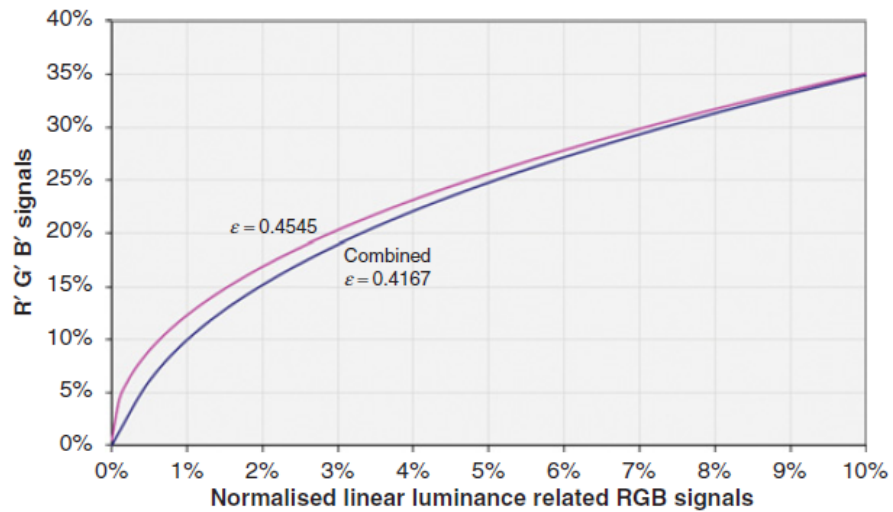
$V_{out}$ : is the output signal.

$V_{in}$ : is the input signal (the camera linear response).

A: a scaling factor (commonly  $A = 1.0$ ).



(a)



(b)

Figure 3.10.: Two sRGB gamma transfer functions, in red a simple law function as in Eq.3.12, and in blue a combined function (power law + linear function). a) x-axis luminance RGB signals vs. y-axis the relative output voltage over the whole range. b) a close-up view of the range between 0% - 10% in order to see the difference between both formulae. Figures are taken from [Too16].

$\gamma$ : is an exponential power for encoding/decoding depending on the range;  $\gamma < 1.0 \rightarrow$  encoding (aka. compressing),  $\gamma > 1.0 \rightarrow$  decoding (decompressing/expansion).

Commonly, *sRGB* color space has a decoding  $\gamma = 2.4$  ( $\gamma = 1/2.4$  for encoding), but not all over its range. *sRGB* was designed to behave as such that any corresponding signal input of  $V_{in} \leq 0.00304$ , then the value will be treated as it is, linearly ( $\gamma = 1.0$ ) [AMCS96, Too16]. Check Fig.3.10, which illustrates how *sRGB* gamma correction behaves. Two curves are compared here, one with the simple power law as in Eq.3.12 (red line) where  $\gamma = 1/2.2 = 0.4545$  is set everywhere. On the other hand, the blue curve is the power law applied with  $\gamma = 1/2.4 = 0.4167$  only when  $V_{in} > 0.00304$  otherwise a linear  $\gamma = 1.0$  is applied with a linear gain of 12.92. Both calculations yield almost very similar curves showing that a power function with a  $\gamma = 1/2.2$  is a very good approximation to the standard calculations of *sRGB*. Although, slight differences especially in the range below 4% are noticeable when we zoom in, Fig.3.10(b). For more information consult [Too16].

### 3.6.3. White-Balance

White-balance is the process of adjusting and adapting an imaging system's reference white-point (WP) to match the scene's actual white-point, it is expressed in *Kelvin*( $K$ ) and commonly referred to as adjusting the *color-correlated temperature* (*CCT*). A system's reference white-point is the sort of "white" a system (e.g. camera, monitor...etc.) shows when all its three primaries (e.g. *RGB* system) are set to the maximum values (*i.e.*  $R = 1.0$ ,  $G = 1.0$ ,  $B = 1.0$ ). Different systems may have different reference white-points depending on their choice of those primaries e.g. a printing system WP: D50  $\approx 5000 K$  vs. a monitor/display system WP: D65  $\approx 6500 K$ .

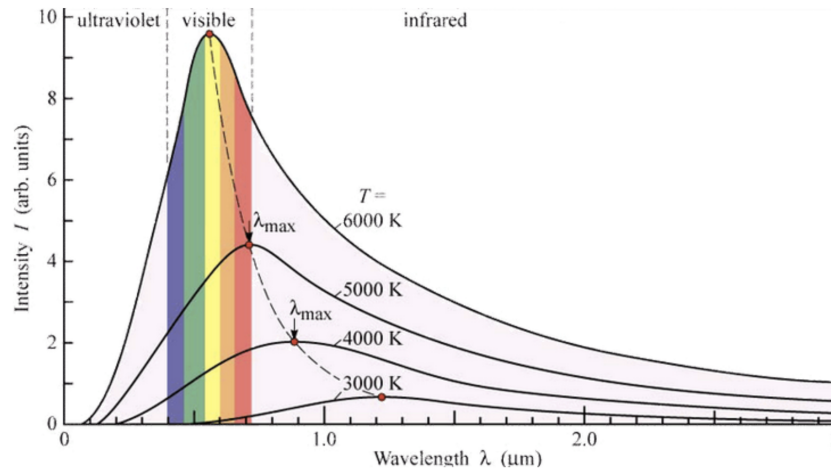
A series of spectral measurements (around 600) of the sun/sky irradiation, from different places on the globe at different times, helped in defining the common-known illuminants and their nomers thanks to the efforts of Judd's, MacAdam's and Wyszecki's, who found a correlation between the measured SPD's and the black-body radiator's color temperature [JMW\*64]. The colors a black-body goes through when heated up, check Fig.3.11(a), are drawn on *xy-Chromaticity* diagram and known as the *Planckian Locus* as it was mentioned before in sec.3.3.1 and shown in Fig.3.3. The correlation between the measurements and the colors that can be expressed on the *xy-Chromaticity* diagram are given in Table 3.2.

At different times throughout the day, the white-point of the daylight changes constantly, and consequently, the colors of the objects outside under the sun are influenced. Though, the human visual system is capable, through a mechanism known as *Chromatic adaptation* [CIE07], to adapt to the light source white-point and perceive the white and adjust all other colors accordingly without feeling much of a shift in the perception of how we are used to seeing certain colors (e.g. a house painted white and a yellow banana will almost always appear white and yellow to us respectively whether we look at them during the sunrise, sunset or virtually at any other point in the day despite the fact that the white-point of the sun illumination is changing in the range between 6500  $K$  to 3000  $K$ ) throughout the day. Chromatic adaptation is addressed in the coming section.

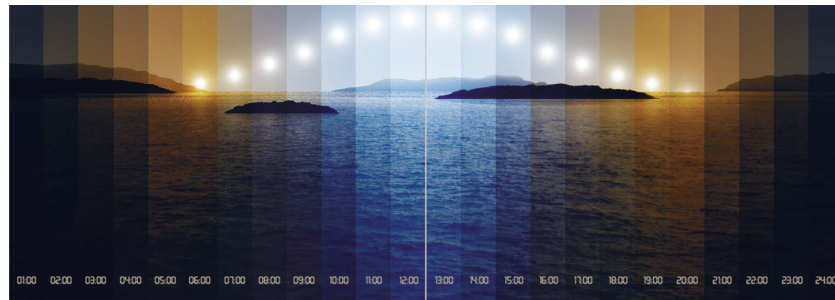
CCT in Kelvin	x	y
4000	0.3802	0.3767
5000 (D50)	0.3444	0.3513
5500 (D55)	0.3314	0.3405
6500 (D65)	0.3118	0.3224

Table 3.2.: A few color-correlated temperatures (CCT's) of a black-body radiator and the corresponding *xy-Chromaticity* coordinates in CIE1931. Source [ROAG08]





(a) Black-body radiation at different temperatures ( $T$ ) in Kelvin



(b) A simulation of the daylight throughout the day every hour starting from 01:00 until 24:00 (right). Source <https://www.greatermainlandelectric.com>

Figure 3.11.: The black-body radiation and daylight color simulation.



The same applies to the artificial lights indoors, whether one is using a fluorescent lighting system that is nearly 4500 – 5500  $K$  (e.g. office environment) which is seemingly blue(ish) or cool color, or whether one has a cozy feeling atmosphere under tungsten bulbs/candle lights that are around 2000 – 3500  $K$  that are considered warm colors and red(ish)/orange. Objects under either of the situations would appear to us to bear always the same color (e.g. a banana would look always yellow more or less).

So if one can see the problem now, a camera with fixed sensitivity curves defining its peaks for the used primaries ( $R, G$  and  $B$ ) must adjust these primaries by weighting them differently so that when the camera is pointed towards a white surface it reads a correct white, not yellow, not red, or any other color. Obviously, if camera channels are weighted as such that, a mid-day light (D55) reflected off a white wall looks indeed white. Then moving, say, indoors to an artificially lit environment with Tungsten bulbs (CCT of  $\approx 3500 K$ ) or waiting until sunset time outdoors and then pointing the camera again at a white surface, the white surface would not look actually white if no adjustment happens to the camera weighted channels again under the new conditions (aka. white-balance).

### 3.6.4. Chromatic Adaptation

Chromatic adaptation is an automatic process runs by the *Human Visual System (HSV)* so that a certain surface color looks the same regardless of the change in the source illumination falling on it (e.g. a banana will look yellow regardless of whether it is viewed under daylight (5500  $K$ ), Tungsten light (3500  $K$ ) or any CCT in between). The phenomenon is known as *color constancy* in which the *HSV* is capable of discounting the differences in illumination settings so that objects bear always the same color appearance to the human eye. Color constancy is an important field in computer graphics especially when moving materials from one medium to another (e.g. moving an image from a display to a printer) or even when rendering certain materials that need to be viewed under different simulated light conditions (e.g. simulation of a cloth fabric under indoor and outdoor light conditions).

There are various methods and algorithms on how to run chromatic adaptation digitally. Cameras, try to mimic the *HSV* automatic chromatic adaptation through the *white-balance* functionality. The general steps each chromatic adaptation model takes are summarized as follows:

1. moving from tristimulus values  $CIEXYZ$  into cone response space  $LMS$  (L:Long, M:Medium, and S: Short).
2. moving the cone response values from the source to the destination illuminant (e.g. D65  $\rightarrow$  D50).
3. moving back from cone response space into the tristimulus values  $LMS \rightarrow CIEXYZ$ .

#### 3.6.4.1. Von-Kries Model

*Von-Kries model* is one of the most famous transformation models for chromatic adaptation. The model suggests that the source and the destination tristimulus values ( $CIEXYZ$ ) are linked together by a  $3 \times 3$  conversion matrix such as:

$$\begin{bmatrix} X_d \\ Y_d \\ Z_d \end{bmatrix} = c \begin{bmatrix} X_s \\ Y_s \\ Z_s \end{bmatrix} \quad (3.13)$$

where  $d, s$  subscripts are, respectively, the destination and the source values.  $c$  is a sequence of transformations given as such:

$$c = M^{-1}DM \quad (3.14)$$

where superscript  $(-1)$  is the inverse of a matrix.  $M$  is a  $3 \times 3$  matrix that transfers the *CIEXYZ* tristimulus values into cone response space  $(L, M, S)$ , whereas the  $D$  matrix transfers the cone response values from the source to the destination  $(L_s, M_s, S_s) \rightarrow (L_d, M_d, S_d)$ . The  $D$  matrix is a diagonal matrix and is given as follows:

$$D = \begin{bmatrix} L_{wd}/L_{ws} & 0 & 0 \\ 0 & M_{wd}/M_{ws} & 0 \\ 0 & 0 & S_{wd}/S_{ws} \end{bmatrix} \quad (3.15)$$

where  $ws, wd$  are the white-point cone response coordinates of the source and the destination illuminant respectively. Regarding the  $M$  matrix, There is virtually an infinite amount of transformation that satisfies the  $M$  matrix.

The cone response coordinates of an illuminant are given by a transformation moving the illuminants *CIEXYZ* coordinates as follows:

$$\begin{bmatrix} L_{ws} \\ M_{ws} \\ S_{ws} \end{bmatrix} = M \begin{bmatrix} X_{ws} \\ Y_{ws} \\ Z_{ws} \end{bmatrix} \quad (3.16)$$

For more information and for checking different Chromatic adaptation methods and models refer to Ch.4 in [Kan06a].

## 4. Designing a Color Management Pipeline

The current technology that is emerging at Fraunhofer Institute for Computer and Graphics Processing (*Fraunhofer-Institut für Graphische Datenverarbeitung - IGD*) and is developed by the *Competence Center Cultural Heritage Digitization - CHD* under the name *CultArm3D*<sup>1</sup> has grown into a spin-off company by the time of writing this dissertation under the name *Verus Digital*<sup>2</sup>, was the project under which the current body of research has been conducted.

The technology comprises a robotic arm (Universal Robots<sup>TM</sup>)<sup>3</sup> equipped with a high-end camera at its end effector (PhaseOne<sup>TM</sup> iXG 100MP<sup>4</sup>) and a light source designed by the department that has a ring shape to fit on top of the camera lens referred to as the ring-light. The whole surface area of the ring-light is covered by little LEDs all over except for the opening where it attaches itself to a camera lens, Fig.4.1(b). The LEDs have a light color-correlated temperature of D50 measured and confirmed by us, to be discussed in detail in Chapter 6 (*Research Paper II*), using a spectrometer and a perfect diffuser. Finally, there is a rotatory table on which an object would be placed to scan, also known as the turn-table. Check Fig.4.1(a).

The system has been developed to operate in a fully autonomous way. The aim is to scan 2D and 3D objects and then run photogrammetry on the captured images afterward so as to have a digital 3D model at the end with very accurate geometric and texture color resolutions. Because the system is fully autonomous, the robot/camera must move all around an object to capture all its surface details, hence the need for a light source that is, rather, attached directly to the camera following its movement so that all the captured images are well-lit and crystal clear. Whereas fixing a couple of light stands nearby to light up the 3D scanned object would not be very practical and would inevitably cast shadows, also the light will not reach some parts of a scanned 3D object, as the robot/camera is moving all around the object and the object could have virtually any arbitrary geometry making fixing lighting setup very tricky.

The focus of this project was, besides the resultant research papers that were accepted and published at different conferences, a full implementation of a functional color management module and a color profiler that ensures the quality of the captured images in terms of color accuracy and fidelity throughout the whole life of the image inside the software.

### 4.1. Color Management System (CMS)

A color management system (CMS) is a process, on both software and hardware levels, that ensures that a pixel color in a digital image is always interpreted correctly regardless of the medium in which the pixel resides (e.g. camera, display, projector, smartphone...etc.). Remember from section 3.6, every digital device and every manufacturer has their own technology and hardware/software that operate differently from other devices and other brands when it comes to storing and showing colors. Therefore, moving an image was captured by a

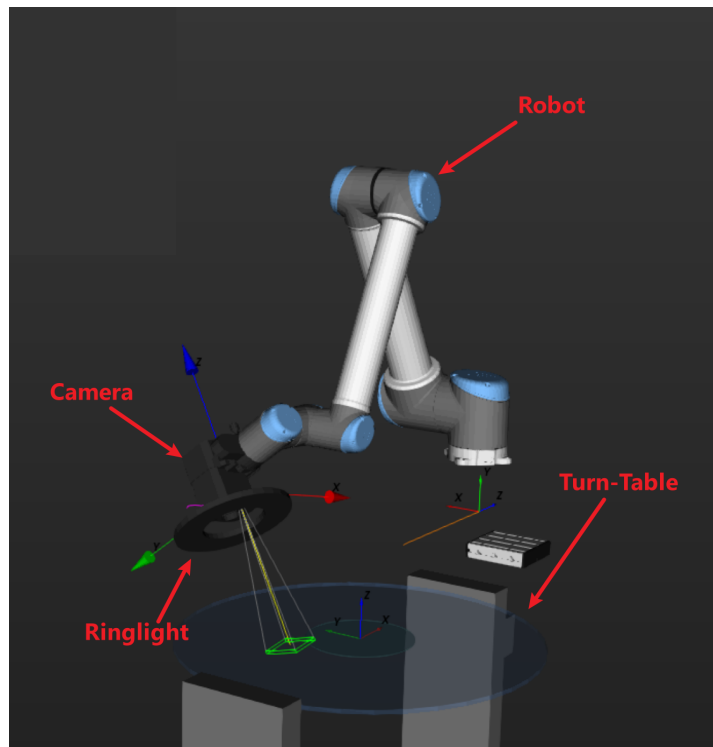
---

<sup>1</sup><https://cultarm3d.de>

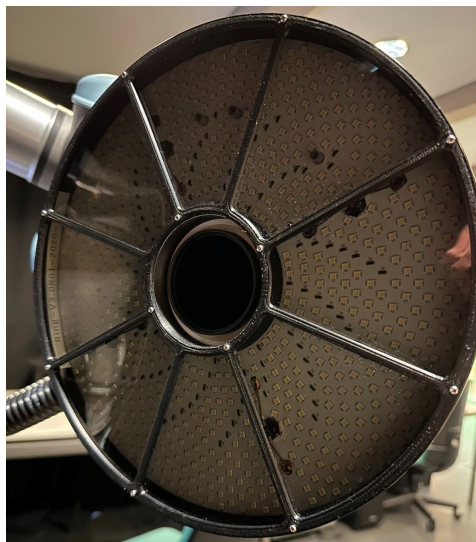
<sup>2</sup><https://verus.digital>

<sup>3</sup><https://www.universal-robots.com>

<sup>4</sup><https://www.phaseone.com>



(a) An illustration of the scanning station annotated with its different components.



(b) The designed ringlight attached to the camera.

Figure 4.1.: *CutlArm3D Scanning Station.*



Figure 4.2.: A comparison between two different software (a) not color-managed, (b) color-managed viewing the same image but showing different tone color and different RGB values.

camera  $X$  to a display  $Y$  or to a printer  $Z$ , without taking care of an existing and enabled CMS, would, very likely, result in different colors for the same pixel values on each medium. So, to account for the differences in each digital device and to ensure correct color representation/interpretation a CMS, through what is known as *Profile Connecting Space (PCS)* would take care of translating the source input information so that to match the way in which the destination output device represent colors. A simple example is, we have an image  $x$  that is viewed using two different software  $a$  and  $b$  as shown in Fig.4.2. Clearly, the same image of a green patch does not show the same values, nor the same color tone on both software. The reason behind the discrepancy in the green color is due to the lack of a functional CMS in software  $a$ , whereas software  $b$  is, indeed, color-managed and that is how the color green is supposed to be read, rendered, and perceived in actuality. For this exact reason, both software should, first, support CMS so that the color information from the input data (image) is translated and interpreted correctly by how the software reads and shows color information. Secondly and most importantly, the image itself must contain certain data indicating the encoding method it used to save the color values it contains and that is achieved through an *ICC profile - International Color Consortium*<sup>5</sup>.

#### 4.1.1. ICC Profile

An ICC profile is the type of file responsible for identifying the color information of image data and it acts as a universal identifier so that wherever the image data end up (e.g. on the web, photo editing software, a printer...etc.) the color information/values can be identified in which way they were encoded (i.e. in which color space) so they could be transformed accordingly to match the new medium's color space (e.g. An image from a camera  $\rightarrow$  imported by Adobe Photoshop needs to have clear identifiers that tell the software how to handle the color information inside the image). A PCS acts as an intermediate universal color channel that is described as *device-independent color space* and it is usually expressed in either *CIEXYZ* or *CIELAB* color space, check Fig.4.3.

For example, a color of a *CIELAB* value of ( $L^* = 51.9$ ,  $a^* = -35.27$ ,  $b^* = 37.14$ ) would correspond, always, to the same green color that is found on the X-Rite<sup>TM</sup> SG Color Checker (F4), check Fig.4.4, regardless of the software, the display or the camera that would display and capture it. The idea is that an image, say created by a camera, is encoded at first in the camera's internal RGB color space, which is dependent on the camera sensor's

<sup>5</sup><https://color.org>

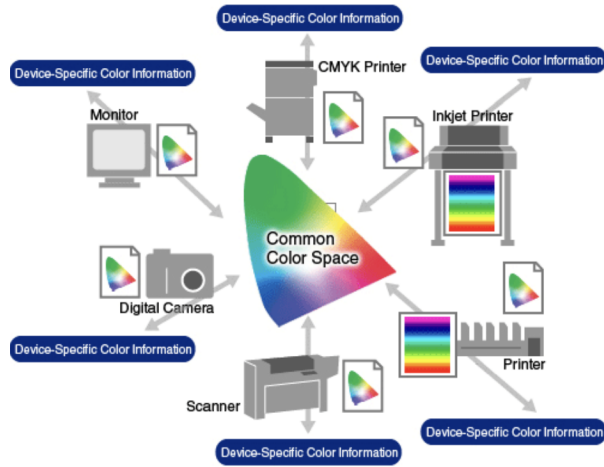


Figure 4.3.: An illustration shows how a profile connection space (PCS) serves as a universal communication channel for exchanging color information between various devices that carry, usually, device-specific color information.



Figure 4.4.: X-Rite SG ColorChecker

$$CIELAB - L^* = 51.9, a^* = -35.27, b^* = 37.14$$

RGB Space	WP	R	G	B
sRGB	D65	78.55	137.82	56.16
Adobe	D65	100.00	136.64	64.48

Table 4.1.: An example of moving color values from a device-independent color space (CIELAB) into a device-dependent color space such as sRGB or Adobe RGB that are widely used by different software/hardware.

sensitivity curves. Then, the color information would be converted into an unrendered color space where all the necessary image mathematical calculations would take place, then moving into a more generic widely accepted, and standardized rendering color space such as *ProPhoto RGB*, *Adobe RGB* or even *sRGB* through the use of an ICC profile that is linking the internal camera RGB space to one of these output color spaces through either CIEXYZ or CIELAB ( $camera\ RGB \longleftrightarrow CIEXYZ/CIELAB \longleftrightarrow ProPhoto/Adobe/sRGB$ ).

An ICC profile has always to be embedded in the image to act as an identifier everywhere the image travels. Without an embedded ICC profile, it is hard to predict the source of the color values and in which space they were encoded, which leads to an erroneous interpretation consequently as shown in Fig.4.2. *sRGB* color space is the default assumption for any image that lacks an embedded ICC profile (e.g. all the images on the web). So, our previous *CIELAB* values of a green color should correspond to the following RGB values when a device operates either in *sRGB* or *Adobe RGB* color space as shown in Table .4.1

More in-depth details about ICC profiles and how to use them can be found in [Sha18, KG10].

## 4.2. The Problem

Given the nature of the developed system *CultArm3D*, a problem of twofold that needs to be solved arose here:

- The system does not support or enable the use of a color management system (CMS) yet, hence captured colors cannot be guaranteed to be accurate or faithful at all as intended for the objective of the system which is namely "cultural heritage digitization".
- The system does not comply with the recommended standard geometry for archiving systems and the best practice in cultural heritage [ISO17] given its technical design and objective of extending beyond just scanning 2D but also 3D.

### 4.2.1. Software

From the software perspective, the development of *CultArm3D* dictated the need for an independent and fully functional CMS module to be integrated into the software that operates and runs the technology. The module was developed, answering *RQ4* as part of this research, independently with the following elements:

- A color-managed environment for reading and viewing images with embedded ICC profiles.
- The capability of decoding raw images in a correct way that is adequate for the color correction procedure.
- The capability of creating an ICC profile / color correction.
- The capability of applying an ICC profile / color correction transformations.

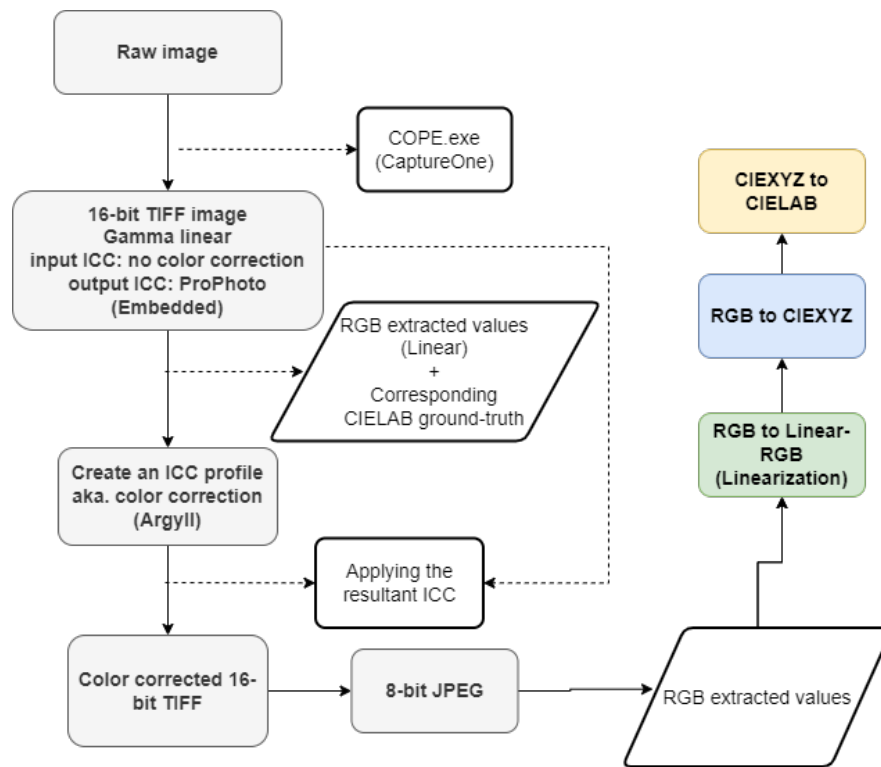


Figure 4.5.: Color profiling and correction pipeline.

- The capability of embedding an ICC profile into the color-corrected and saved image (e.g. 16-bit or 8-bit TIFF/PNG/JPEG).

Different tools made this possible after a deep understanding of how a color management workflow works algorithmically given the scarcity of the materials that explain how to implement and build a color management system. Tools like *OpenCV*, *Argyll*, *LittleCMS* and *FreeImage* libraries were used for the development of a fully functional CMS.

Our developed CMS has been benchmarked against other commercial software for the sake of comparison and proof-checking as it will come up later in the coming chapters.

The developed pipeline can be explained with the following general steps that are outlined and illustrated in Fig.4.5 for the case of creating a color profile using a color target as follows:

1. Images are captured in their raw formats, proprietary to the camera manufacturer.
2. Raw images are converted into *16-bit TIFF* format -best- using the camera manufacturer's converting engine e.g. COPE/CaptureOne for PhaseOne cameras.
3. Ensuring that the conversion happens under these conditions:
  - Gamma is linear ( $\gamma = 1.0$ ).
  - input color profile: None
  - output color profile: ProPhoto RGB



- output format: 16-bit TIFF

4. RGB values are then extracted from the image and linearized.
5. *Argyll* will cook an ICC/ICM color profile based on the extracted RGB values + the ground-truth *CIELAB* values.
6. Using *LittleCMS* we apply the resultant ICC/ICM color profile on the intended image data.
7. Now, it is possible to export and save the color-corrected image in *8-bit JPEG* or any other desired format either in *Adobe RGB* or *sRGB* color space as desired.
8. In the case of a color target, we extract the RGB values once again and linearize them.
9. Converting the linearized and color-corrected RGB values into *CIELAB* color space to calculate the color difference between the actual *CIELAB* spectral measurements of the color target and the color-corrected ones. Hence, evaluating the color correction model accuracy.

Using this pipeline, we enable our software to color-calibrate and color-correct every single captured image with the system so as to ensure high-quality color and fidelity. More details about the performance of our implemented pipeline will be discussed later in CH.5.

### 4.2.2. Hardware

On the hardware level, the problem is exhibited by the technical design of the system which comprises, as mentioned earlier, a robotic arm with a camera mounted at its end effector. The camera bears a ring-light (D50) attached to its lens and both the lens and the ring-light are covered by circular polarization filters (CPL) that are aligned so as to form perfect cross-polarization.

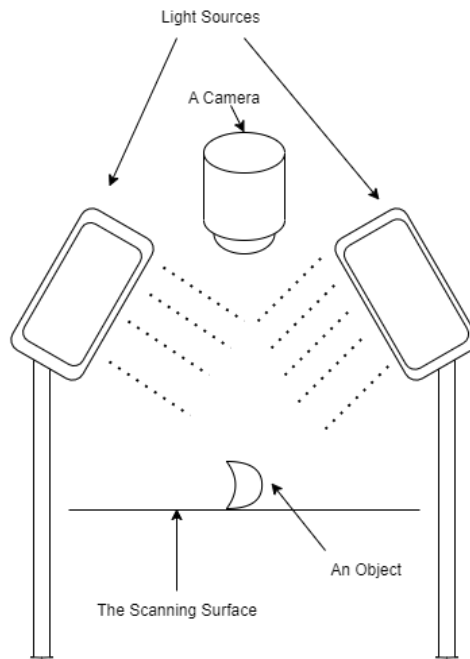
Given the design of the system, the light setup, clearly, does not conform with the ISO standards recommendations for photographing cultural heritage materials that dictate a lighting setup of  $35^\circ - 45^\circ$  angle relative to the normal of the target to-be-imaged whereas the optical axis of the camera should be positioned normal (in front of) to the target [ISO17], check Fig.4.6(a) for illustration. In our case, the light source is completely parallel to the camera plane, which is not optimal and can result in a lot of undesirable reflections as the optical axis and the light source are aligned to the same angle as illustrated in Fig.4.6(b).

The idea of mounting the light source directly to the camera body (attached to the lens) is that the system is designed to scan 3D objects (e.g. museum artifacts) for photogrammetry purposes so as to build a 3D digital model at the end. To make a successful photogrammetry, the 3D object must be captured from all directions to ensure enough coverage of all its surface details, which would require the camera (the robot) to move all around the object. So, having the light source fixed at one position and letting the robot move around the object would introduce more issues related to light fall-off distribution, exposure, and shadow casting. Hence, the need for a light source that moves in accordance with the camera (robot) movement is a necessity so as to ensure good lighting and exposure at all times for virtually every point of any scanned surface.

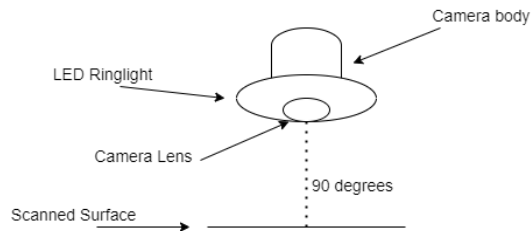
However, fixing the light source on the same plane as the camera's optical axis would introduce undesirable reflections when scanning certain materials (e.g. metal objects, glossy/semi-glossy/polished surfaces, coins, utensils... etc.) and to eliminate such kind of reflections cross-polarization come very handy to help solving the issue.

The questions that incentivized the research were:

- How much are the color calibration and color correction processes affected by the polarization filters?
- How much is the light source itself affected by the polarization filters?



(a) An illustration shows a lighting setup for data acquisition according to the ISO standards. The light sources are nearly at an angle  $\approx 40^\circ$  and the imaging system lies on the normal of the scanned surface.



(b) Our lighting setup and data acquisition scheme.

Figure 4.6.: Lighting setups.

- How do colors behave (chroma, lightness), if at all, when the light is being polarized? e.g. is neutrality and linearity still preserved when compared to the same photographs without polarization?

and that is where the journey of the following research began!

### 4.3. Camera Exposure

The selection of a correct camera exposure is a vital part of designing a well-behaving color management pipeline as it affects essentially the amount of light reflected by each color. Hence, defining the ratio and range between what is considered to be white and what is considered to be dark (black).

Camera exposure is, technically, defined by how much light a camera sensor is allowed to absorb during a pre-defined period of time. It is defined and controlled by the following three elements:

- Aperture size
- Shutter speed
- ISO number

**Aperture size** defines how big the opening is that would allow light into the camera; Think of it as the pupil of the human eye. The aperture size defines, as well, the *depth of field (DoF)* in which either the whole captured scene would appear sharp and in-focus (deep DoF) or only close objects to the camera lens would appear sharp and in-focus while everything in the background would appear rather blurry/out-of-focus (shallow DoF), check Fig.4.7(a).

Aperture size can range from being very wide  $f/1.4$  to very small down to  $f/32$ . Aperture size is expressed in *f-number (N)* - written  $f/N$  conventionally, and it expresses the ratio between the diameter of the lens' entrance pupil ( $D$ ) in mm to its focal length ( $f$ ) in mm such in:

$$N = \frac{f}{D} \quad (4.1)$$

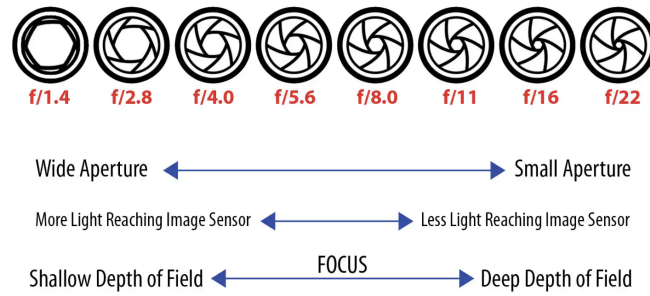
So, the smaller the f-number is, the wider the aperture size/entrance pupil of the lens is, and vice-versa.

**Shutter speed** defines how quickly the opening of the aperture would react to the action of opening and closing that allows light in. A slower shutter speed allows more light in (adequate for dim/dark lighting conditions), whereas a faster shutter speed allows less light in (adequate for bright lighting conditions). One needs to be careful when the shutter speed is slow for the registered images are more prone to *ghosting effect* as a result of an unsteady camera. In other words, when choosing a slower shutter speed one needs to pay attention to fix the camera on a tripod or such to prevent the camera from moving or any possible shaking during the time of capturing. The same applies to the objects in the scene.

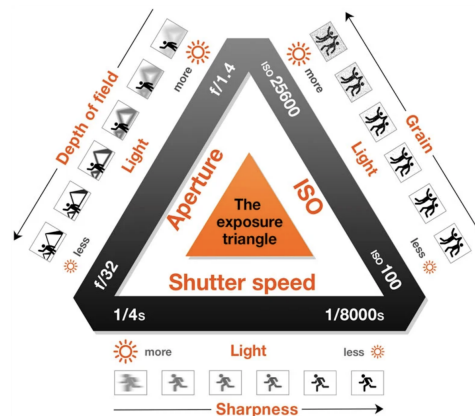
Shutter speed measures in seconds and can range from  $1/8000$  (very fast) all the way up to  $2''$  (slow) seconds. Of course, in astrophotography, it is common to control the shutter speed and allow 15 – 30 seconds of exposure –sometimes even much longer- with the help of an external controller.

**ISO number** was originally proposed and standardized by the *International Organization for Standardization (ISO)* to define the sensitivity of analog films back in the time (e.g. 100, 200...etc.).

In digital cameras, the ISO number is a gain factor that controls artificial brightness enhancement. In the sense that setting a higher ISO number would artificially brighten up the captured photo more, and consequently more noise or grains would be visible in the photo. Hence, it is advised to keep the ISO number always to the minimum as much as possible, so as to keep the signal untouched by any digital digital enhancement process as much as possible.



(a) An illustration shows the relationship between the size of a camera aperture, the amount of incoming light and the focus



(b) Exposure triangle. The three factors that define the exposure of a camera. Source <https://petapixel.com/exposure-triangle>

Figure 4.7.: Camera exposure tirangle.

All three factors mentioned previously are known as the *exposure triangle*, check Fig.4.7(b), and any modification to one of them would affect the other two consequently.

What defines a good exposure is a well-distributed image histogram that stretches from the lower end up to the higher end of an acceptable range without trespassing either of the ends (no clipping). i.e. Highlights and shadows should be preserved by choosing proper exposure settings so that the image pixels are neither all the way saturated (highlight clipping) nor all the way darkened (shadows clipping). Hence, a healthy histogram would never touch either of the ends of the image range e.g. for 8-bit  $[0 - 255]$ . Also, a proper exposure should be set as such that a pre-defined gray patch with a certain lightness level  $CIELAB(L^*)$  is reproduced correctly, even before the color correction process takes place. More details will follow when delving more into the research in the next chapter.

The design of the color management pipeline included devising and implementing an algorithm that automatically assists the user with what would be possibly optimal exposure settings. The algorithm, basically, is initialized by random starting values (aperture size, shutter speed, and ISO number), check Fig.4.8(a). Then, it reads how much light is hitting the sensor by taking an image of a color checker (e.g. X-Rite SG) and converting

it *Raw* → 16-bit *TIFF* linear and with no color profile correction so as to read a pre-determined color patch with a known lightness value of  $CIELAB(L^*) \approx 65$  that was previously measured spectrally. Based on the outcome  $\pm$  tolerance threshold, the algorithm will determine the change in direction for one of the 3 parameters. The 3 exposure parameters are sorted out and given priorities by the user in the sense of which parameter to change first, which last, and which never to touch (if needed), check Fig.4.8(b), it shows the possible values *PhaseOne iXG 100MP* offers for the shutter speed. As well, we define an acceptable operating range for each of the parameters (e.g. ISO number [50 – 400]). Given that, the algorithm will start checking what is the closest value it can get for that specific gray patch by changing the first parameter, if the output cannot converge to be within a pre-defined tolerance but very close, then it will start changing the second allowed parameter one step at a time, depending on how far it is from the goal value. When changing the second parameter starts to show a big divergence, the algorithm will try to set the parameter to the closest value that converges to the goal value, and then it will start changing the third parameter, if available, one step at a time, depending on how far it is.

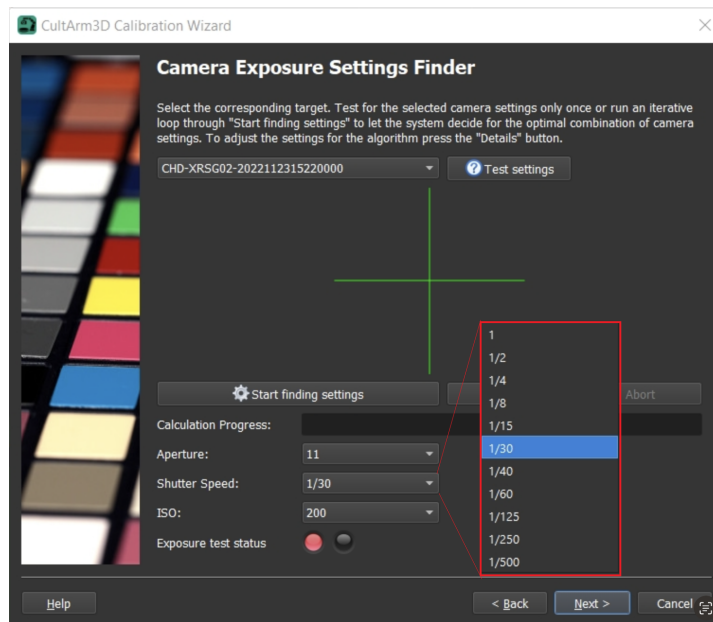
The first possible valid option, that would satisfy the condition, would be then proposed to the user to choose and proceed. There are also cases where convergence is not possible, where the convergence falls in a vicious cycle iterating between two values that are on either ends but beyond the defined tolerance threshold. In such case, the algorithm will abort when it starts to feel that it is falling into an endless loop and it will ask the user to change the starting values of the parameters or change the acceptable range. It needs to be kept in mind that the convergence depends highly on the range every camera offers in terms of what the allowed minimum step between every two successive options (aperture sizes, shutter speeds, or ISO numbers) for some cameras may offer finer steps than others. The tolerance threshold was defined heuristically and primarily depending on the camera model we have for how close it can reproduce an exact value (e.g.  $CIELAB(L^*) \pm 2$ ).

How the algorithm runs will be demonstrated in the demo video that will come along with this work. Check the flowchart that also illustrates how the algorithm works in Fig.4.9

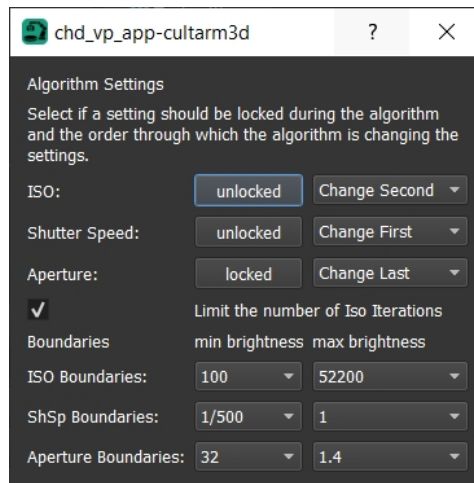
## 4.4. Conclusion

In this chapter, we have presented the system, *CultArm3D* around which this body of research revolves. We have explained what a color management system (CMS) is, why it is important, and how *CultArm3D* needs one to put it right on track in its mission towards "accurate and faithful digitization in the culture heritage sector". We explained our implementation of a CMS pipeline and the tools we have used.

On the hardware side, we have explained how the technical design of the system deviates from the recommended standards [ISO17] and how that introduces a challenging problem in understanding how it may affect accurate color imaging, calibration, and correction. We then talked about camera exposure and what parameters contribute to adjusting it. We addressed what makes a good choice of exposure parameters and how we implemented successfully a smart algorithm assistant to help the user in making decisions in that regard.



(a) The interface that allows the user to run the automatic exposure algorithm assistant. The user has the possibility to choose the values to initialize the parameters. The figure shows the possible options when pressing on the shutter speed dropdown menu.



(b) When pressing on "Details" from the interface, the user is allowed to set the priorities for each of the exposure settings parameters, by pressing "locked/unlocked" we allow the algorithm to change or never change the corresponding parameter. In the lower part of the window, the user has the possibility to define the range over which the algorithm is allowed to iterate.

Figure 4.8.: Exposure algorithm assistant interface.

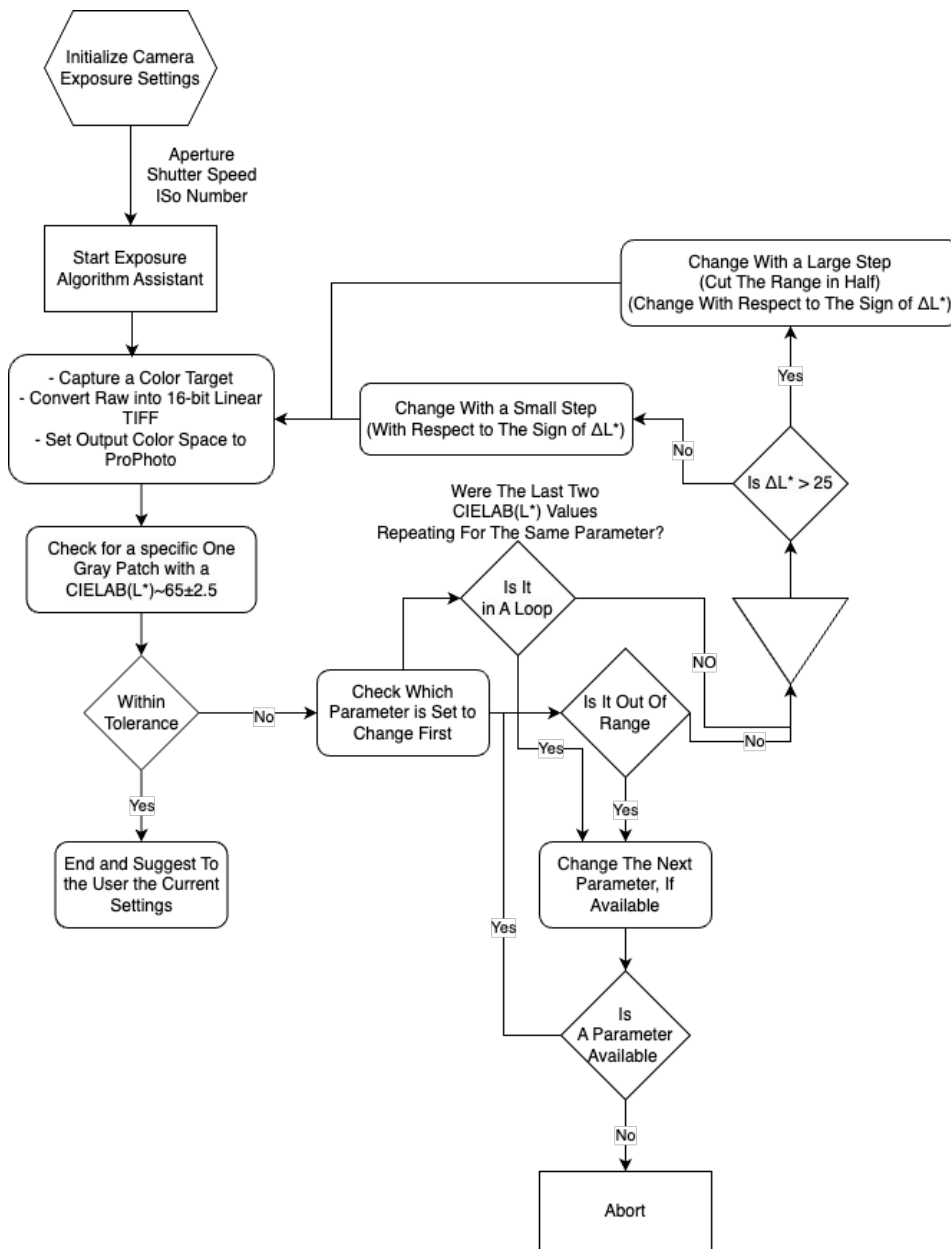


Figure 4.9.: Flowchart explaining how the exposure algorithm assistant takes a decision.





## 5. Effect of Cross-Polarization on RGB Imaging and Color Accuracy and Fidelity

In this chapter, we are addressing *RQ1* and alleviate the misconception around how cross-polarization filters do not affect, supposedly, the imaged color accuracy. We inspect closely the effect and the impact of cross-polarization on two materials *matt* and *(semi-)glossy* while color calibrating and correcting using two color targets, namely the *X-Rite SG* and *DataColor Spyder24*. We show how the use of cross-polarization comes always with a cost and a compromise at the expense of color fidelity.

### 5.1. Introduction

Polarization filters are indispensable parts of the design of the system *CultArm3D*. As well as the strive for color accuracy in digital reproduction. Hence, the need for studying, analyzing, and understanding how much the process of color calibration is impacted by introducing circular polarization filters was vital to the project and it was the main incentive behind the research in hand.

In this topic, we address what happens to the colors and more closely the two main color components (*chroma* and *lightness*) when running color calibration/profiling after being imaged using the cross-polarization technique. We examine different color targets of different materials such as *X-Rite SG*<sup>1</sup>, *DataColor SpyderCheckr 24*<sup>2</sup>, *Munsell Linear Grayscale*<sup>3</sup> and the *SFR grayscale*<sup>4</sup>, check Fig.5.1. It turned out, that each of the aforementioned targets behaves differently depending on its finish and the material.

Given that *CultArm3D* scanning station does not conform completely with the ISO standards regarding the camera and light setups that should follow, normally, the standard  $0^\circ/45^\circ$  [ISO17]. So, we decided to eliminate the factor of "non-standard" geometry from our analysis. Hence, we designed an experiment that conforms to and follows the ISO standards recommended light/camera geometry in which the optical axis of the camera is perpendicular to the scanned surface, and the lighting setup is fixed on the sides of the scanned surface tilted at an angle nearly  $45^\circ$ . With this standard acquisition geometry, we can be sure that no error or undesirable effect would be introduced due to the system design itself.

### 5.2. The Experiment

The aim of this experiment was to understand what happens to color under a cross-polarization setup and if there is any drastic change that is worth taking notice of. We hypothesized that cross-polarization not only reduces the light intensity but also affects different wavelengths along the visible spectrum differently depending on the

<sup>1</sup><https://www.xrite.com/categories/calibration-profiling/colorchecker-digital-sg>

<sup>2</sup><https://spyderx.datacolor.com/shop-products/>

<sup>3</sup><https://www.imagescienceassociates.com/munsell-linear-grayscale.html>

<sup>4</sup>[https://www.image-engineering.de/content/products/charts/qa62/downloads/QA-62\\_data\\_sheet.pdf](https://www.image-engineering.de/content/products/charts/qa62/downloads/QA-62_data_sheet.pdf)

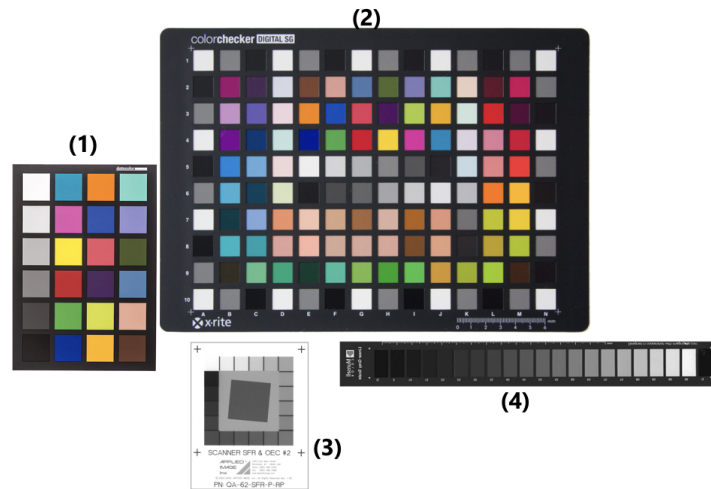


Figure 5.1.: The used color targets for the experiment. (1) Spyder24, (2) X-Rite SG, (3) SFR Grayscale, and (4) Munsell Linear Grayscale (MLG).

material. So, We decided for this experiment to start with the fundamental understanding of what happens to achromatic colors, namely a linear grayscale. We aimed to analyze the behavior of two linear grayscales, one is matt and one is semi-glossy, in terms of their lightness components ( $CIELAB(L^*)$ ) and their chroma components ( $CIELAB(a^*b^*)$ ). For if polarization filters only reduce light intensity we should observe primarily a change in the lightness component only. Whereas, the chroma component that expresses color should remain unaltered in any way.

We chose two color targets with two different finishes, one is matt and the other is semi-glossy, to run the color calibration process as it is important to match the type of the material used in the color calibration process the material that needs to be color-corrected (also known as profiling).

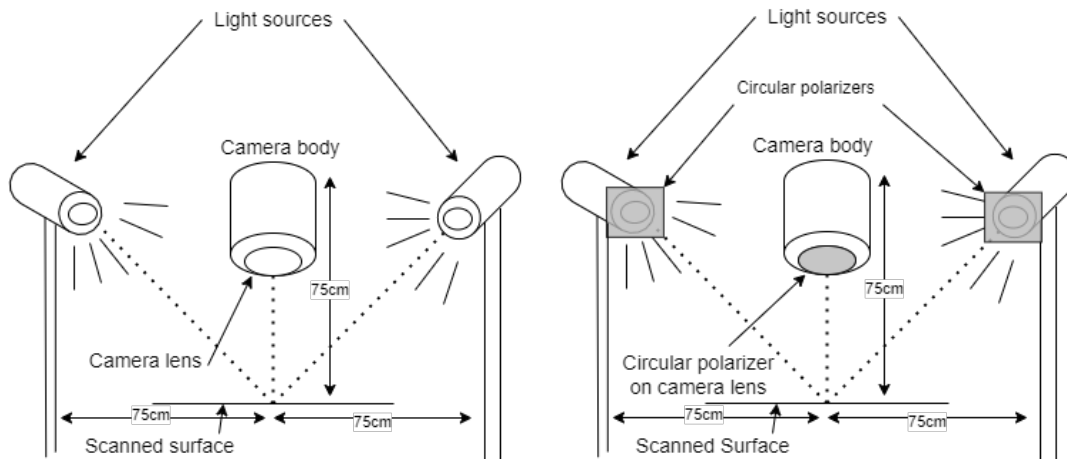
### 5.2.1. Hardware

In order to run the experiment, a completely dark room was necessary. A camera was fixed perpendicular to the scanned surface at a distance of  $\approx 75cm$ . Two headlights were mounted on both sides of the scanned surface at an angle nearly  $\approx 45^\circ$  operating in the visible domain and have a color-correlated temperature (CCT) of D55. Two color targets for calibration were chosen with two different finishes (matt vs. semi-glossy), as well as two linear grayscales for the analysis. All the used components in detail are listed below.

- A camera - PhaseOne iXG100MP<sup>5</sup>.
- Two standard light sources - Dedolight D55.
- A set of color targets including:
  - X-Rite SG (SG).
  - DataColor SpyderCheckr 24 (Spyder24).
  - Munsell Linear Grayscale (MLG).

---

<sup>5</sup><https://heritage-digitaltransitions.com/phase-one-ixg-cultural-heritage-camera>



(a) A sketch of the experiment using external lights with no polarization filters. (b) A sketch of the experiment using external lights with polarization filters on both the light sources and the camera lens

Figure 5.2.: A sketch depicts the setups of the experiment.

- SFR Linear Grayscale (SFR).
- A set of circular polarization filters for the visible domain:
  - Two circular polarization films to be fixed in front of the light sources.
  - A circular polarization filter to be fixed in front of the camera lens.

Fig.5.2 shows in two sub-figures schematic sketches of the experiment setup; 5.2(a) without polarization and 5.2(b) with cross-polarization. A complete darkness in the room was ensured upon starting the data acquisition process.

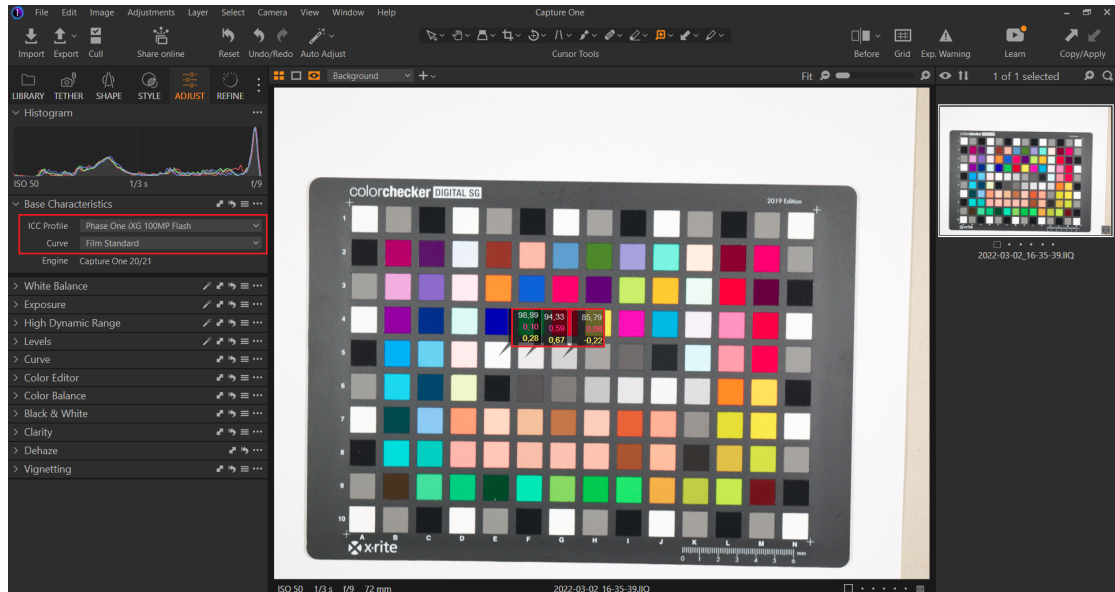
## 5.3. Methodology

First of all, all the color targets were measured spectrally using a spectrophotometer *Barbieri LFP qb* that provides *CIELAB* and *CIEXYZ* values along the spectral data all across the visible range 380-780 nm. The *CIELAB* values are prepared while taking the 2° observer into account so as to anchor down the ground-truth values. The instrument is equipped with a D50 light source.

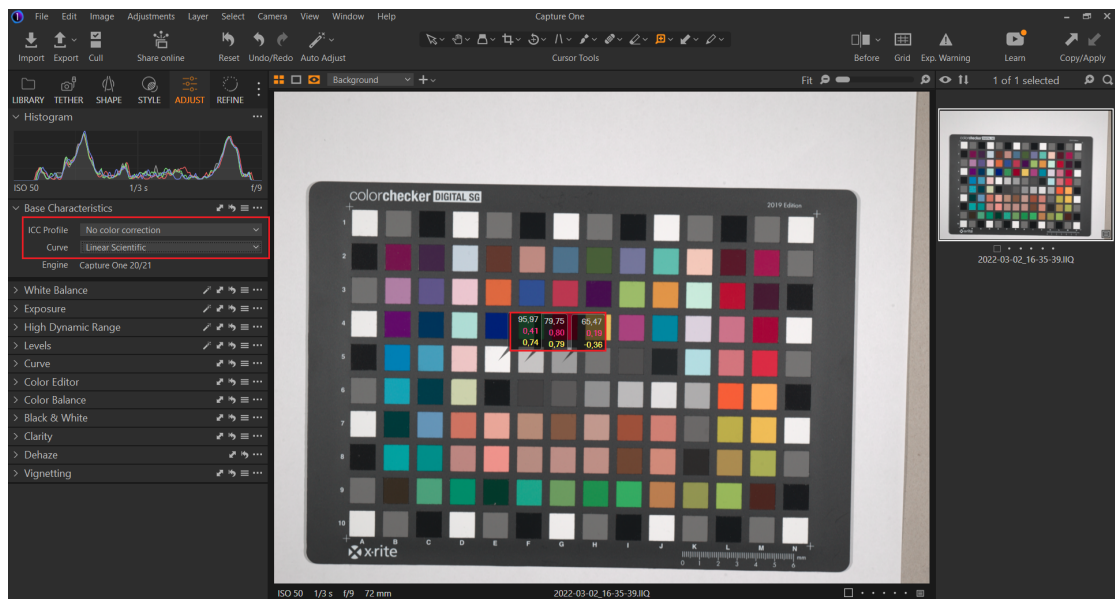
The camera was set to the correct white-balance manually, before any capturing, using a gray patch – that also can be corrected for using the white-balance functionality on the raw image directly, if needed. The exposure settings were chosen based on a gray patch of  $CIELAB(L^*) \approx 65$  as recommended by the ISO standards [ISO17] (e.g. patch G5 on X-Rite SG) so that when inspecting the captured image, in *CIELAB* color space, after setting gamma to linear ( $\gamma = 1.0$ ) and the input ICC profile to "no correction", the patch's  $L^*$  value must be reproduced very closely even before running the color correction process yet. Check Fig.5.3

When the exposure settings are all set correctly, as well as the input ICC profile and the linear gamma, only then the image is ready to be processed for creating an ICC color correction profile.

5. Effect of Cross-Polarization on RGB Imaging and Color Accuracy and Fidelity



(a) X-Rite SG ColorChecker **before** choosing the correct settings so as to read the raw data. Default camera output readings.



(b) X-Rite SG ColorChecker **after** choosing the correct settings that allow inspecting the raw data without any tampering with the camera data. Setting input ICC profile to "no correction" and gamma to linear

Figure 5.3.: Previewing a captured image of the X-Rite SG color target in CaptureOne software before and after choosing the correct input ICC profile and gamma.

### 5.3.1. Image Conversion

The data are captured in their raw format (*IIQ*), usually proprietary. In order to decode/demosaic them in the best way it requires the corresponding raw image converter engine from the same manufacturer so as to guarantee the highest image quality as they know the best their camera and all the nuances that may affect the image quality (software and hardware).

We used *COPE* engine, which is a simplified *API* (*Application Programming Interface*) executable of the manufacturer's software *CaptureOne*<sup>6</sup>. The executable allows, with the help of certain commands, to decode/demosaic the raw images along with the possibility of controlling other parameters e.g. image format, image quality, exposure adjustment, modifying highlights, contrast, gamma curves...etc. Check Fig.A.1 in the Appendix for the whole list of possible parameters.

In our case, the parameters we wanted to control are specifically the following:

- Image format.
- Image bit depth.
- Input ICC profile.
- Output ICC profile.
- Gamma curve.

and the command used for that looks like the following:

```
COPE.exe input_raw_image_IIQ output_decoded_image
-outputformat=tif
-bits=16
-filmcurve="PhaseOneIXG100MP-Linear Scientific.fcrv"
-inputprofile="Phase One Effects - No color correction.icm"
-outputprofile="ProPhoto.icm"
```

where the chosen parameter for *input profile* guarantees that no color modification of any sort is being applied to the raw color information, the *output profile* guarantees that the color space in which the color values are encoded is large enough so that no mapping or any transformation of any sort that could distort the color information would happen when moving from the camera RGB color space to this output color space, and finally the *film curve* guarantees that the color values are not gamma-encoded and still have their linear response as received by the camera sensor.

### 5.3.2. Demosaicking - Image Decoding

Image decoding or demosaicking, in brevity, is the process of building up an image out of the registered information by the sensor to form a complete fully-colored or monochromatic image by the means of interpolation given the underlying architecture of the sensor that is known as *Color Filter Array* (*CFA*), check Fig.5.4.

Sensors are designed as such that each  $4 \times 4$  block contains two green-sensitive photosites, one red-sensitive area, and one blue-sensitive area, after the famous *Bayer's* pattern [Bay76,Pal01]. *Bayer's* pattern, though, is not the only pattern used in sensors out there, other different patterns and color combinations of sensitivity photosites were also proposed and have been tested for various purposes, check [AF15,LP05]. However, *Bayer's* pattern is, still, the most widely used pattern among all the others.

---

<sup>6</sup><https://www.captureone.com>

The reason why *Bayer's* pattern bears double the amount of green photosensitive sites, as compared to the reds or the blues, is due to the human eye's great sensitivity in the green region of the visible spectrum whether it is in color or in luminance. Remember section 2.5.2. In addition to the fact that the green information in the image is usually correlated with the luminance data actually.

### 5.3.3. Color Correction - Calibration

The image must be exported, first, in a *16-bit TIFF* format with an embedded ICC color profile either the camera's own color profile – usually an unrendered internal RGB color space but most of the time cameras do not offer that or in *ProPhoto* color space, of which the camera own RGB color space usually is a subset, so the original data do not undergo any alteration. ProPhoto color space is considered to be an output color space, large enough that allows mathematical manipulation while preserving the color information in their original gamut (considering all devices' gamuts out on the market are subsets of the imaginary ProPhoto color space) [SGW00]. Which is recommended to use according to the ISO standards for best practice [ISO17].

The image now is ready for collecting the color information from each patch of the captured color targets in order to prepare them for the creation of a color correction model / an ICC profile. The color information needs to be read and processed their linear RGB form (without any gamma encoding). Hence, remember section 3.6.2, all rendered color spaces (e.g. ProPhoto RGB, Adobe RGB, sRGB) are designed with various gamma encoding (i.e. non-linear), so to get back to the original camera RGB response these values need to be gamma-decoded (aka. linearized) accordingly depending on the color space in which the image is exported (in our case ProPhoto RGB).

### 5.3.4. RGB Linearization - ProPhoto

First, let us understand a bit the idea behind *ProPhoto RGB* color space. We have mentioned in the section 3.6 that RGB color spaces are device-dependent and hence they vary across products' models depending on the used technology (e.g. optics, sensor sensitivity, light source...etc.), let alone across different manufacturers. On the other hand, device-independent color spaces such *CIELAB*, *CIEXYZ* are not designed for color manipulation or to carry out mathematical operations of any sort efficiently (e.g. tone mapping, white-balancing...etc.). Therefore, the need dictated to develop an RGB color space that is less device-dependent and serves as a more universal standardized color space in which it is still possible to preserve and maintain the original color values coming from different devices/manufacturers and to perform the necessary mathematical operations with as little artifacts and alteration to the original raw data as possible.

Such a color space has to satisfy, among other conditions, that it encompasses all the possible observable colors in real-world scenes and are reproduced eventually by different imaging and displaying technologies. Hence, it must have a wide enough color gamut. Check Fig.5.5. Also, such a color space needs to have a direct connection to PCS (Profile Connection Space). As well as the possibility to move to other more realizable color spaces such as *sRGB* and *Adobe RGB*. It must be mentioned here that, other output (device-dependent) color spaces (e.g. sRGB), inherently, have the problem of limited encoded color gamut and luminance dynamic range, which the new color space (ROMM RGB / ProPhoto RGB) came to solve too.

That is in brevity the background story of ProPhoto RGB color space or more officially referred to as *ROMM RGB (Reference Output Medium Metric)*. More in-depth information can be found in [SGW00].

Image color values that are encoded in ProPhoto RGB color space are recommended to have a depth of *16-bit* to make use of this wide color gamut and its ability to represent a wider range of colors. RGB values must be

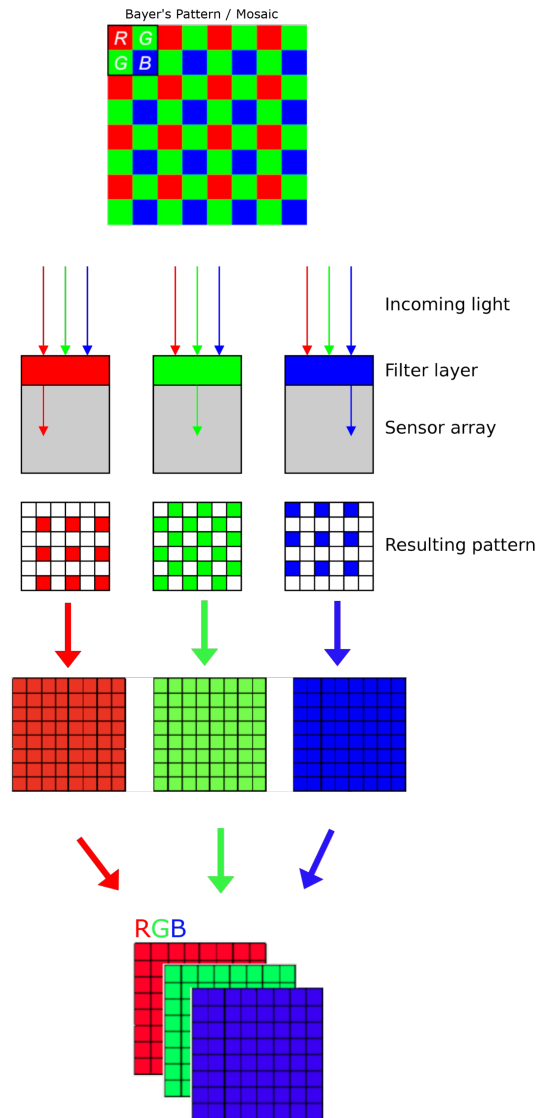


Figure 5.4.: Bayer mosaic pattern; RGB sensor design also known as Color Filter Array (CFA)



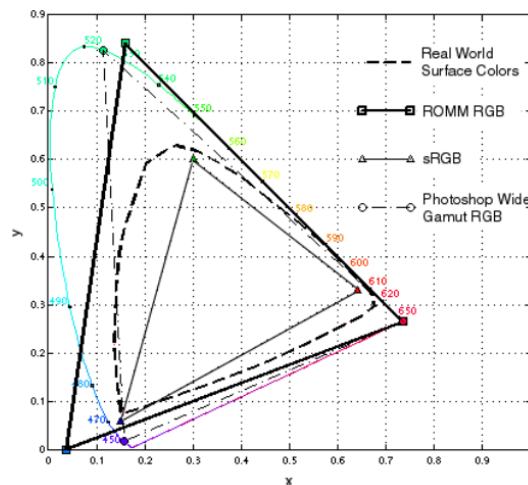


Figure 5.5.: A comparison of the color gamuts of different color spaces (ROMM/ProPhoto RGB, sRGB, Photoshop wide gamut RGB, and real-world surface colors) on xy-Chromaticity diagram. Source [SGW00]

normalized in the range between [0.0 – 1.0] for the process of ICC profile creation or scaling them to the range that is expected by the profiling software as we will see next.

### 5.3.5. ICC Profile Creation

After reading and extracting the values of all the color patches of an imaged color target and getting sure that the gamma is linearized, then normalizing the data between [0.0 – 100.0], the values are now ready to go to the next step for creating an ICC color correction profile using *Argyll*<sup>7</sup> (The software expects the RGB values to be in this range). The data are arranged in the following manner that each color patch has the camera RGB linear response values next to its corresponding ground-truth values in *CIELAB* as shown in Fig.5.6, so that *Argyll* is capable of creating a correction model (e.g. Look-Up Table, correction matrix, ...etc.) that will map the camera linear RGB output (sensor response) of certain colors (the patches of a color target now) to how these color must appear and get rendered based on the collected ground-truth data that were accurately measured using a spectrophotometer instrument (the *CIELAB* values).

*Argyll* allows the user to choose the type of color correction transformation whether it's based on a Look-Up Table (LUT/CLUT), a matrix transformation, a simple power function (gamma curve), or any combination of these. Check Fig.A.2 in the Appendix for the list of commands *Argyll* offers.

The command we have chosen to create the corresponding ICC color profile looks like the following by calling the executable *colprof.exe*:

```
colprof.exe -V -Z a -qh -al -R -ua -bh
```

where:

-V : for verbose.

<sup>7</sup><https://www.argyllcms.com/>



```

1  CTI3
2
3  DESCRIPTOR "Argyll Calibration Target chart information 3"
4  ORIGINATOR "Argyll target"
5  CREATED "Thu Feb 09 16:57:08 2023"
6  DEVICE_CLASS "INPUT"
7  COLOR_REP "LAB_RGB"
8
9  NUMBER_OF_FIELDS 7
10 BEGIN_DATA FORMAT
11 SAMPLE_ID LAB_L LAB_A LAB_B RGB_R RGB_G RGB_B
12 END_DATA_FORMAT
13
14 NUMBER_OF_SETS 130
15 BEGIN_DATA
16 A1 97.165 -1.18533 3.79767 88.4317 91.6274 98.1733
17 A10 96.2577 -1.26233 2.621 88.6999 91.9931 98.4756
18 A2 21.5483 -8.908 -1.97133 6.40794 6.74183 8.17064
19 A3 79.8767 -33.335 0.521333 38.0216 39.537 42.5657
20 A4 81.482 -25.4847 44.7127 92.1365 95.9262 99.2099
21 A5 97.0877 -1.048 3.68867 7.15957 7.53594 9.10996
22 A6 46.9203 -0.685333 0.740333 38.7472 40.3198 43.4778
23 A7 51.6757 44.109 43.6483 92.2137 96.0777 99.2389
24 A8 38.845 -30.4967 -29.5813 6.6772 7.02572 8.50589
25 A9 71.1847 -23.4653 -18.0097 37.3262 38.8573 41.9577
26 B1 24.3397 -27.231 4.124 36.4713 37.9212 40.7607
27 B10 51.7417 -20.8227 -18.9127 36.4959 37.9545 40.9354
28 B2 42.2103 -21.208 -1.19533 32.4702 18.5408 27.3611
29 B3 62.2047 -40.7637 -1.16533 59.1072 51.5979 67.093
30 B4 68.541 -7.64467 -31.1827 28.4458 16.8327 39.6891
31 B5 38.4833 57.6643 2.02167 35.7347 45.3044 76.3931
32 B6 35.4897 5.20667 2.15567 43.6441 50.013 76.5577

```

Figure 5.6.: A snippet of data arrangement for ICC color creation using *Argyll*.

-*Za*: for intent absolute colormetric.

-*qh*: for quality high.

-*al*: for algorithm based on CIELAB CLUT (Color Look-Up Table).

-*R*: for some restrictions on the white, black, and primary values to be more compatible.

-*ua*: for forcing absolute intent for input profiles.

-*bh*: for high quality B2A CLUT (device-dependent to device-independent transformation).

The parameters were chosen heuristically as these are the ones that showed the best results after many tests.

**A (Color) Look-Up Table LUT/CLUT** is a way of mapping certain input values to specific output values in one-to-one relation. CLUTs are used as they offer higher precision when it is not possible to map precisely the values between the input and the output using linear transformations (e.g. matrix transformation, power function...etc.). CLUT does not, necessarily, contain all the possible values. However, it contains a sample of pre-defined input/output values allowing by that the interpolation of the missing values in-between [KG10].

Simply put, the job of a CLUT is to map the camera linear RGB response (input) to the ground-truth/expected values of certain color patches of a captured color target (output), for which we have prior knowledge of their actual values (spectrally measured). Doing that, the camera is said to be calibrated after using this resultant mapping (ICC profile).

It is important to keep in mind that, ICC profiles are valid only for the specific imaging system it was produced for and only under the very same conditions under which the calibration took place (i.e. camera exposure settings, lighting conditions, ambient light, camera orientation... etc.). A new ICC calibration profile is always advised to be created, if any of the aforementioned conditions have changed, for more accurate results.

Another important aspect to keep in mind when creating and using an ICC profile is the *rendering intent*. **Rendering intent** is a gamut compression scheme that comes in four different flavors:

- Perceptual.

- Relative colorimetric.
- Absolute colorimetric.
- Saturation.

The most important thing to know here is that colorimetric intents, whether it is relative or absolute, both try their best to preserve high color accuracy in reproduction. *Absolute colorimetric intent* is more desirable when the exact colors of the original medium need to be reproduced with little to no alteration, as possible [Mor03].

Discussing all the details about ICC profiles<sup>8</sup> is out of the scope of this work and hence the curious reader is advised to consult [KG10, Sha18] two extensive books dedicated solely to ICC profiles and color management.

To summarize, a raw image coming directly from a camera in its proprietary format must be converted into an actual RGB image (demosaicking), the image must preserve the color information with no alteration possible by decoding it in the highest bit-depth (e.g. 16-bit) *TIFF* format, with "*No Color Correction*" as its input ICC profile (i.e. do not change the input data), *ProPhoto RGB* as its output color space (i.e. widest possible rendered output color space), while RGB values must retain their linearity by setting the gamma to linear (i.e. no gamma encoding). At this moment, the image is ready for color values extraction, and RGB linearization (i.e. decoding the gamma of the output color space) so to map these color values to their corresponding ground-truth using ICC profiling software. Fig.5.7 shows a quick summary of these steps.

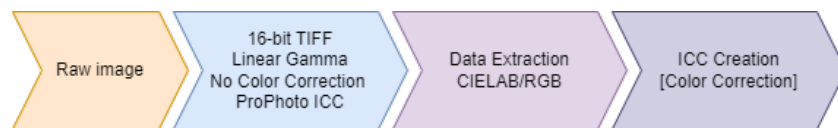


Figure 5.7.: Summary of the steps up until creating a color correction ICC profile.

### 5.3.6. Color Correction and Validation

Up until this stage, we should have the color correction ICC profile that calibrates our camera device. Now, it is possible to capture and reproduce more colorimetrically accurate color images.

To test the viability and the validity of the resultant color correction ICC profile, an image of a color target must be profiled (color corrected) and validated against its ground-truth color values (CIELAB).

With the help of *LittleCMS*<sup>9</sup> library, our software is capable, after successful integration, of continuing right after the previous step -after ICC profile creation using *Argyll*- to apply the resultant ICC color profile onto the input image of the captured color target directly for validation. *LittleCMS* enables us to apply the color correction transform on the image data and then to create the necessary transformations into one of the rendered output color spaces (e.g. ProPhoto RGB, Adobe RGB, or sRGB). The transformation will map the camera linear RGB response  $\rightarrow$  to colorimetrically corrected RGB  $\rightarrow$  to one of the standardized output color spaces (e.g. ProPhoto RGB).

Now after the correction has been carried out and color values are encoded in a standard output color space, we validate the correction by extracting the color values of the color patches once again to compare them against their corresponding ground-truth CIELAB values. The comparison must happen in CIELAB color space, hence we need to move the RGB color values into CIELAB color space in a series of steps ( $RGB \leftrightarrow CIEXYZ \leftrightarrow CIELAB$ ) as it is explained next.

---

<sup>8</sup>An ICC-profile file has the extension *ICC* or *ICM* interchangeably.

<sup>9</sup><https://www.littlecms.com/>

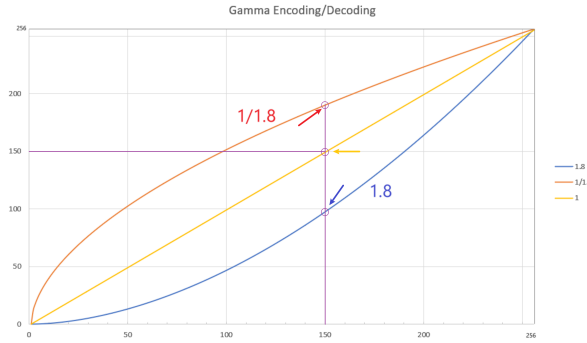


Figure 5.8.: Gamma curves at 1.8 (blue) and 1/1.8 (red) when applied on a linear curve at  $\gamma = 1.0$  (yellow).  
 $n = V^\gamma$ .

### 5.3.7. ProPhoto/ROMM RGB $\rightarrow$ CIEXYZ $\rightarrow$ CIELAB

As mentioned in section 5.3.4, ProPhoto RGB color space was designed to be large enough to contain all the possible surface colors, and to encapsulate all possible gamuts of different devices on the market. It was designed, as well, with the idea in mind, to move easily from and to device-independent color spaces such as CIEXYZ/CIELAB, which is what we are about to do.

To move from ProPhoto RGB into CIEXYZ color space, first, gamma should be inverted or decoded (i.e. RGB linearization) and that could be done easily through the gamma power function as follows:

$$n = V^\gamma \quad \exists \gamma \in \mathbb{R} \quad (5.1)$$

Where:

$V$  : is the encoded value  $V \in \{R, G, B\}$ .

$n$  : is the decoded value  $n \in \{R, G, B\}$ .

Basically, when an image is encoded in ProPhoto RGB color space, it usually has its pixel values compressed/encoded based on a certain gamma value (i.e.  $\gamma = 1/1.8$  for ProPhoto RGB), the red curve in Fig.5.8, and to return the pixel values into their original values (i.e. before being encoded), the gamma should be decoded/decompressed to get to the yellow line in Fig.5.8. Check the example in Eq.5.2 for how gamma encoding/decoding works. An arbitrary value, say,  $v = 150 \in [0 - 255] \rightarrow V = 150/255 \approx 0.59$

$$V^\gamma = \begin{cases} 0.59^{1.8} & \approx 0.39 \rightarrow 0.39 \times 255 \approx 99 \quad \exists \gamma = 1.8 \\ 0.59^{1/1.8} & \approx 0.75 \rightarrow 0.75 \times 255 \approx 191 \quad \exists \gamma = 1/1.8 \end{cases} \quad (5.2)$$

Now the linear corrected RGB values are ready to undergo a transformation to move from *ProPhotoRGB*  $\rightarrow$  *CIEXYZ* based on the following matrix transformation while assuming the values are for illuminant D50, Eq.5.3

$$\begin{bmatrix} X_{PCS} \\ Y_{PCS} \\ Z_{PCS} \end{bmatrix} = \begin{bmatrix} 0.7977 & 0.1352 & 0.0313 \\ 0.2880 & 0.7119 & 0.0001 \\ 0.0000 & 0.0000 & 0.8249 \end{bmatrix} \begin{bmatrix} R_{ROMM} \\ G_{ROMM} \\ B_{ROMM} \end{bmatrix} \quad (5.3)$$

The inverse of this transformation is given by the following matrix transformation to move from  $CIEXYZ \rightarrow ProPhotoRGB$  back as in Eq.5.4

$$\begin{bmatrix} R_{ROMM} \\ G_{ROMM} \\ B_{ROMM} \end{bmatrix} = \begin{bmatrix} 1.3460 & -0.2556 & -0.0511 \\ -0.5446 & 1.5082 & 0.0205 \\ 0.0000 & 0.0000 & 1.2123 \end{bmatrix} \begin{bmatrix} X_{PCS} \\ Y_{PCS} \\ Z_{PCS} \end{bmatrix} \quad (5.4)$$

The transformations in 5.3 and 5.4 are taken from [SGW00]. Whereas, the numbers we have used are from BruceLindbloom<sup>10</sup> website that are technically the same only with more decimal precision.

Given that ProPhoto/ROMM RGB color space's white-point is D50, there is no need to run some Chromatic adaptation on the obtained CIEXYZ values, as our ground-truth CIELAB values are also measured under D50 illuminant. Consult Ch.5 in [Too16], Ch.6 in [HP11] for more on Chromatic adaptation.

Now after having the CIEXYZ values, we are ready to move them into CIELAB color space, in which we can run the color analysis and calculations easily. The transformation can be carried out by following the following set of equations that were mentioned earlier in Eq.3.8 (we copy them here once again for the ease of reading):

$$\begin{aligned} L^* &= 116f\left(\frac{Y}{Y_n}\right), \\ a^* &= 500\left[f\left(\frac{X}{X_n}\right) - f\left(\frac{Y}{Y_n}\right)\right], \\ b^* &= 200\left[f\left(\frac{Y}{Y_n}\right) - f\left(\frac{Z}{Z_n}\right)\right] \end{aligned}$$

where:

$$f(x) = \begin{cases} x^{\frac{1}{3}} & \text{if } x > \left(\frac{24}{116}\right)^3 \\ \left(\frac{841}{108}\right)x + \frac{16}{116} & \text{if } x \leq \left(\frac{24}{116}\right)^3 \end{cases}$$

The subscript  $_n$  in  $X_n, Y_n, Z_n$  refers to the CIEXYZ coordinates of a known illuminant that is used as a light source (e.g. CIEXYZ of D50 [0.96422, 1.00000, 0.82521]).

The color values are, finally, in CIELAB color space. Now, it is possible to measure, analyze, and quantify the color difference between the corrected color target and its corresponding ground-truth CIELAB values that were measured spectrally beforehand.

### 5.3.8. Color Difference $\Delta E$ / CIEDE2000

Measuring a color difference between two given color values mathematically, in CIELAB color space, has started as simple as calculating an Euclidean distance, at first, and evolved throughout the years in an attempt to match more closely the actual human perception with respect to the physical characteristics of the measured color substance and how different hues would be perceived differently (based on their position on the hue circle). All of that contributed to the current formula that is commonly used in the colorant industry and known as the *CIEDE2000*, usually written as  $\Delta E00$ <sup>11</sup>, color difference formula that was standardized by the CIE committee [CIE01]. The color difference formula is described as follows [LCR01, SWD05]:

$$\Delta E00 = \sqrt{t^2 + r^2 + k^2 + R_T r k} \quad (5.5)$$

<sup>10</sup><http://www.bruceindbloom.com>

<sup>11</sup>*E* stands for "Empfindung" the German word for perception/sensation.

Where:

$$t = \frac{\Delta L'}{K_L S_L}, \quad r = \frac{\Delta C'}{K_C S_C}, \quad k = \frac{\Delta H'}{K_H S_H} \quad (5.6)$$

Given two stimuli (color patches) and their corresponding CIELAB values, it is possible now to quantify their color difference mathematically more accurately, in the sense of how they would appear to an average human observer.

The *CIEDE00* formula has its deep roots in the field of color science, and a detailed explanation of the used terms can be found in several places such in [SWD05, LCR01, CIE01] among others, which is outside the scope of this thesis to explain here in detail. But briefly, the numerators in the equation 5.6 indicate that the calculation happens on the difference in the lightness, chroma, and hue respectively. While the denominators have some weighting factors. First, the  $S_L, S_C, S_H$  that compensate for the non-uniformity that exists in *CIELAB* color space, along with the rotational term  $R_T$  in Eq.5.5. Second, the terms  $K_L, K_C, K_H$  compensate for the viewing conditions. All the calculations and the necessary equations can be found in the appendix A.1.

### 5.3.9. ISO Color Metrics

Besides the famous  $\Delta E00$  as a metric for color difference, a set of other metrics are recommended by the *ISO standards* [ISO20] to use, as one single metric may not be enough to paint the whole picture and cover all the aspects in the color difference nuances. The set of metrics that we have used during this work is summarized in Table 5.1 and listed as follows:

- Tone Response Curve / TRC.
- Gain Modulation / GMod.
- Root Mean Square Noise / N-RMS.
- White-Balance chroma / WB-Chroma.
- Color Difference /  $\Delta E00$ .

	Level A	Level B	Level C
TRC	$\Delta L^* \leq \pm 2$	$\Delta L^* \leq \pm 3$	$\Delta L^* \leq \pm 4$
GMod	$0.7 \leq GMod \leq 1.3$	$0.6 \leq GMod \leq 1.4$	$0.3 \leq GMod \leq 1.6$
N-RMS	$RMS \leq 1.6$	$RMS \leq 2$	$RMS \leq 2.2$
WB-chroma	$\Delta E_{ab^*} \leq 3$	$\Delta E_{ab^*} \leq 4$	$\Delta E_{ab^*} \leq 5$
$\Delta E00$	$\text{mean}(\Delta E00) \leq 4.0$ $\text{max}(\Delta E00) \leq 10.0$	$\text{mean}(\Delta E00) \leq 5.0$ $\text{max}(\Delta E00) \leq 15.0$	$\text{mean}(\Delta E00) \leq 5.0$ $\text{max}(\Delta E00) \leq 15.0$

Table 5.1.: A chosen set of metrics that are recommended by the ISO standards to check for the quality of color reproduction of an imaging system. The evaluation happens for 3 defined quality levels each with certain tolerance thresholds. TRC: Tone Response Curve, GMod: Gain Modulation, N-RMS: Root Mean Square Noise, WB-Chroma: White-balance chroma and  $\Delta E00$ : Color difference CIEDE2000.

### 5.3.9.1. Tone Response Curve / TRC

It is expressed in  $CIELAB(L^*)$  and reflects the opto-electronic conversion function (OECF) of the input light. Ideally, the obtained digital values should correspond to the same original luminance  $CIELAB(L^*)$  values of the captured patches. It measures a grayscale that ranges in values from  $L^* \approx 5 \rightarrow 95$ .

### 5.3.9.2. Gain Modulation / GMod

It describes the slope variation of the OECF given the original  $CIELAB(L^*)$  values (spectrally measured) compared against the reproduced values. Ideally, the slope measures to 1.0. It is calculated using the following Equation Eq.5.7.

$$g_i = \frac{L_{img\ i+2}^* - L_{img\ i}^*}{L_{org\ i+2}^* - L_{org\ i}^*} \quad (5.7)$$

If the used grayscale patches have a spacing of  $L^* < 10.0$ , then the slope is calculated for every second patch compared to the current patch i.e.  $i = 1$  and  $i = 3$ ,  $i = 2$  and  $i = 4$ ...etc.

### 5.3.9.3. Root Mean Square Noise / N-RMS

It is, technically, the root mean square error of  $CIELAB(L^*)$  values of a grayscale. It is calculated according to Eq.5.8.

$$\sigma = \sqrt{\frac{1}{n} \sum_{j=1}^n (L_j^* - \hat{L}_j^*)^2} \quad (5.8)$$

where:

$n$ : is the number of grayscale patches.

$L^*$ : is the system output  $CIELAB(L^*)$  of a given patch  $j$ .

$\hat{L}^*$ : is the ground-truth  $CIELAB(L^*)$  value of the patch  $j$ .

### 5.3.9.4. White-Balance chroma / WB-Chroma

It measures the deviation of grayscale patches in their chroma component using, technically,  $\Delta E_{00}$  color difference formula (Eq.5.5) while omitting the  $L^*$  component. It is written as  $\Delta E_{ab}$ .

### 5.3.9.5. Color Difference / $\Delta E_{00}$

The color difference is defined by Eq.5.5. It measures the color reproduction accuracy of an imaging system by calculating the difference between the original color target values in  $CIELAB$ , that are spectrally obtained, and their digital corresponding values after running color correction and converting the color values from  $RGB \rightarrow CIELAB$  color space.

Fig.5.9 summarizes all the steps from the moment of capturing the data (raw images) up to collecting the final statistics after running color correction.

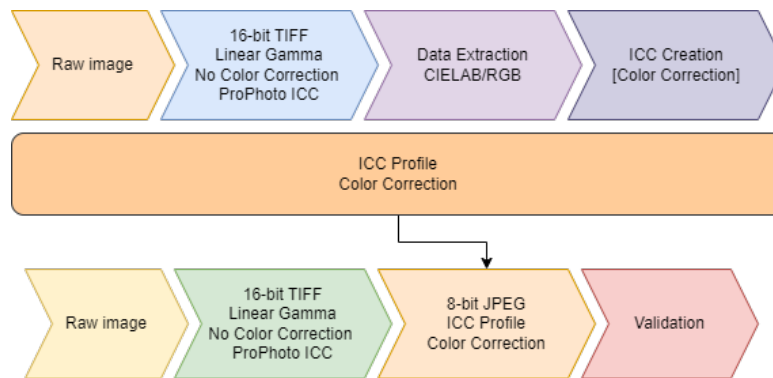


Figure 5.9.: A summary of the implemented workflow from the moment of capturing raw images up to the validation step where all the statistics are collected.

### 5.3.10. Benchmarking Against A Commercial Software

For the sake of double-checking the accuracy of our implemented *CMS* pipeline, we have decided to run the same images through a completely commercial software that are heavily used by professional who seek, as well, color accuracy reproduction in the field.

We have chosen to go with *CaptureOne / C1*<sup>12</sup> software for developing and exporting raw images, as well as for applying color correction ICC/ICM profiles. *CaptureOne* is a well-known photography software developed by *PhaseOne* directly. For creating a color correction ICC/ICM profile we have used *BasIColor Input 6*<sup>13</sup>, a very well-known software in the domain.

The workflow for the commercial pipeline is described as follows:

1. A raw image of a color target is imported by CaptureOne.
2. White-balance is set by a certain gray patch on the color target.
3. Input ICC profile set to "no color correction", and gamma curve to "linear scientific".
4. Image is exported in 16-bit TIFF, and with an embedded camera profile.
5. BasIColor Input 6 is provided first with the corresponding ground-truth CIELAB values of the intended color target (e.g. X-Rite SG, DataColor SpyderCheckr 24).
6. The 16-bit TIFF color target image is imported into BasIColor Input 6.
7. Adjusting the setting for ICC profile creation that is compliant with CaptureOne profiles + choosing ICC profile for Repro/Archiving purposes.
8. Creating an ICC profile.
9. Importing the color correction ICC profile into CaptureOne.
10. Correcting for the color target image using the created ICC profile as an input profile.
11. Reading the corrected CIELAB color values.

<sup>12</sup><https://www.captureone.com>

<sup>13</sup><https://www.basicolor.de/en>

## 5.4. Results and Discussion

Initially, the validation of the color correction is calculated only in terms of the color reproduction accuracy  $\Delta E_{00}$  as most profiling software, such as *BasIColor Input 6*, yields these statistics upon creating a color correction ICC profile for a given target as shown in Table 5.2. The table presents the average and the maximum color difference,  $\Delta E_{00}$  of the color correction on the same color target that was used to create this color correction, which is usually insignificant information, for the training and the testing data are the same. The table lists as well the color difference for the two images with and without cross-polarization filters. **The forward-slash symbol "/" separates between the performance of our pipeline (left) and the commercial pipeline performance that we call "BasIColor+C1" (right).**

	SpyderCheckr24		X-Rite SG	
	Unpolarized	Polarized	Unpolarized	Polarized
Avg	0.51 / 1.26	0.67 / 1.25	1.06 / 1.72	1.22 / 2.33
Max	0.94 / 2.73	1.61 / 3.27	4.43 / 4.31	4.24 / 7.85

Table 5.2.: [Our Pipeline / BasIColor+C1]  $\Delta E_{00}$  Stats showing the performance of the generated ICC profiles when being applied on the same color target used for profiling.

Table 5.3, on the other hand, shows cross-validation statistics when a color correction ICC profile that was created from a color target  $X$  (base-ICC) being applied on a color target  $Y$ . The following statistics show the average  $\Delta E_{00}$  and average 90% which is the average  $\Delta E_{00}$  after discarding the top 10% of the statistics after sorting them in a descending order (max  $\rightarrow$  min) i.e. discarding the maximum outliers. In addition to the minimum, the maximum, and the standard deviation.

For a fair comparison against the *Spyder24 ColorChecker*, we chose to opt for the color difference statistics only of the common 24 patches of the *X-Rite SG*<sup>14</sup>.

We have, in addition to calculating the usual  $\Delta E_{00}$ , also calculated the color difference as recommended by the ISO standards – when the application is more oriented towards the digitization of cultural heritage artifacts- by setting the following parameter to unity  $S_L = 1.0$  in the Eq.5.6 [ISO20]. **Note that everywhere in this research  $S_L$  is weighted normally (i.e.  $S_L \neq 1.0$ ) unless it is explicitly mentioned otherwise.**

A clear observation one can make by looking at Table 5.3 is that the errors are almost doubling under polarization. In general, the average and the max  $\Delta E_{00}$  do not go beyond 5.0 and 10.0 respectively whether it is polarized or unpolarized except for that in our pipeline and using Spyder24 as a base-ICC the max tips a little bit over 10.0. When  $S_L = 1.0$  the numbers also get a little worse in general, regardless of the used pipeline, for the average tips a bit over 5.0 under polarization. Nevertheless, the mentioned statistics in Table 5.3 are, to a good degree, compliant with the ISO recommendations regarding an acceptable color difference limit (i.e. in terms of average  $\Delta E \leq 4.0/5.0$  and  $\max(\Delta E) \leq 10.0/15.0$  for levels  $A$  and  $B$  respectively). However, good  $\Delta E$  statistics do not tell much about the visual appearance and the actual color perception [Bal03].

For this reason, we have decided to start looking at another target that could help fundamentally in understanding the behavior of the created ICC color correction profiles and the effect of polarization on that. We chose two grayscale targets, *Munsell Linear Grayscale (MLG)* that has a glossy/semi-glossy finish, and the *SFR & OECF target (SFR)*<sup>15</sup> with its matt finish. Using the grayscale targets, it is possible to assess and evaluate the ICC profiles' behaviors and capabilities of reproducing grayscale linearity and neutrality better. This would help in

<sup>14</sup>The common 24 color patches on X-Rite SG starts on E2 and ends by J5.

<sup>15</sup>SFR: Spatial Frequency Response. OECF: Opto-Electronic Conversion Function. [https://www.image-engineering.de/content/products/charts/qa62/downloads/QA-62\\_data\\_sheet.pdf](https://www.image-engineering.de/content/products/charts/qa62/downloads/QA-62_data_sheet.pdf)



understanding how the color correction, using a certain ICC profile, would appear visually as it would give a clear idea of any possible lightness/chroma shift. Both targets consist of 20+1 patches (20 are linearly spaced).

	Weighted SL		SL=1.0	
	Unpolarized	Polarized	Unpolarized	Polarized
X-Rite SG (Spyder base-ICC)				
avg	2.80 / 4.10	4.82 / 4.77	2.99 / 4.51	5.32 / 5.25
avg(90%)	2.33 / 3.76	4.19 / 4.50	2.50 / 4.09	4.67 / 4.88
min	0.45 / 1.30	2.15 / 0.89	0.52 / 1.50	2.67 / 0.89
max	8.52 / 6.91	11.93 / 6.98	8.80 / 8.19	11.96 / 8.08
std	1.83 / 1.51	2.17 / 1.51	1.86 / 1.80	2.19 / 1.70
SpyderCheckr (SG base-ICC)				
avg	2.63 / 3.12	4.64 / 4.87	2.78 / 3.31	5.17 / 5.54
avg(90%)	2.33 / 2.67	4.20 / 4.55	2.44 / 2.80	4.64 / 5.12
min	0.47 / 0.89	2.17 / 2.21	0.50 / 0.89	2.35 / 2.80
max	5.21 / 7.08	8.18 / 7.71	6.13 / 7.90	9.65 / 9.02
std	1.25 / 1.67	1.62 / 1.55	1.33 / 1.78	1.92 / 1.82

Table 5.3.: [Our Pipeline / BasICColor+C1]  $\Delta E_{00}$  stats showing the validation performance of the generated ICC profile of one of the color targets when applied on the other. For SG CC the stats reflect only the common 24 patches' behavior.

MUNSELL LINEAR GRAYSCALE $\Delta E_{00}$				
	Weighted SL		SL=1.0	
	Unpolarized	Polarized	Unpolarized	Polarized
MLG (Spyder base-ICC)				
avg	3.26 / 2.68	4.09 / 4.79	3.46 / 3.26	5.45 / 6.26
avg(90%)	2.53 / 2.53	3.24 / 3.95	2.71 / 3.06	3.96 / 4.80
min	0.57 / 1.24	1.08 / 1.67	0.57 / 1.25	1.10 / 2.40
max	8.16 / 3.64	9.88 / 10.66	8.44 / 4.93	15.53 / 16.25
std	2.37 / 0.74	2.49 / 2.48	2.42 / 1.02	4.11 / 4.06
MLG (SG base-ICC)				
avg	2.25 / 1.74	2.94 / 2.15	2.46 / 1.92	3.40 / 2.61
avg(90%)	1.94 / 1.52	2.29 / 1.63	2.10 / 1.64	2.46 / 1.80
min	0.60 / 0.44	0.54 / 0.65	0.60 / 0.44	0.54 / 0.65
max	4.32 / 3.42	7.89 / 6.16	4.94 / 4.04	10.45 / 8.79
std	1.09 / 0.76	2.06 / 1.58	1.24 / 0.93	2.80 / 2.39

Table 5.4.: [Our Pipeline / BasICColor+C1]  $\Delta E_{00}$  stats of Munsell linear grayscale reproduction used to validate the generated ICC profiles' behavior and capability.

Tables 5.4 and 5.5 show the color reproduction statistics when linear grayscales (Munsell with its semi-glossy finish and the SFR/OECF with its matt finish) are color corrected using the created ICC profiles of the corresponding color targets (X-Rite SG and Spyder24).

For MLG when profiled using Spyder24, Table 5.4, the error is noticeably high for some outliers especially when polarized. The max values, for BasICColor+C1, amount to nearly  $\approx 10.0$ , and up to 16.0 if  $S_L = 1.0$ . In

SFR/OECF LINEAR GRAYSCALE $\Delta E_{00}$				
	Weighted SL		SL=1.0	
	Unpolarized	Polarized	Unpolarized	Polarized
SFR (Spyder base-ICC)				
avg	2.52 / 3.60	2.09 / 4.57	2.66 / 4.26	4.98 / 5.18
avg(90%)	2.25 / 3.23	1.71 / 4.19	2.38 / 3.90	4.50 / 4.68
min	1.66 / 2.12	0.18 / 1.59	1.73 / 2.18	2.25 / 1.73
max	5.21 / 6.22	6.97 / 7.38	5.51 / 6.92	8.30 / 9.00
std	0.88 / 1.21	1.32 / 1.48	0.93 / 1.38	1.75 / 1.88
SFR (SG base-ICC)				
avg	2.80 / 2.45	2.34 / 2.04	3.00 / 2.65	2.87 / 2.31
avg(90%)	2.50 / 2.16	1.93 / 1.64	2.68 / 2.36	2.39 / 1.80
min	0.40 / 0.95	0.84 / 0.29	0.46 / 1.04	1.35 / 0.29
max	5.36 / 4.54	7.30 / 5.90	5.78 / 4.57	7.81 / 8.27
std	1.12 / 1.00	1.39 / 1.44	1.16 / 1.04	1.53 / 1.84

Table 5.5.: [Our Pipeline / BasICColor+C1]  $\Delta E_{00}$  stats of SFR linear grayscale reproduction used to validate the generated ICC profiles' behavior and capability.

general, our pipeline and BasICColor+C1 workflow are very closely on the same par when looking at the *avg* and *avg(90%)*, despite that BasICColor+C1's max values are noticeably better under the unpolarized conditions.

The numbers get much milder when the ICC color correction profile is that of the X-Rite SG (SG base-ICC) and both workflows (ours and BasICColor+C1) are performing very much similarly. However, setting  $S_L = 1.0$  under polarization still shows few outliers with their big color difference that maxes up to  $\approx 10.0$  for our pipeline and  $\approx 8.8$  for BasICColor+C1.

To understand better the role of the material's finish in the color correction process, we have repeated the same experiment however this time on a linear grayscale with a matt finish (The SFR/OECF target) whose statistics are presented in Table 5.5. Our pipeline in this case, when Spyder24 is used as a base-ICC, shows obviously a better performance than BasICColor+C1 workflow when looking at the *avg* and the *avg(90%)*. These differences in the workflows' performances are minor, however, when X-Rite SG is used as the base-ICC.

Despite all these statistics and the numbers that may seem to be very compliant, to a good degree, with the defined tolerances for color accuracy according to the ISO standards, we still think that they are not enough to paint the picture clearly to understand the behavior and the reliability of the resultant ICC color correction profiles. For this reason, we have decided to analyze the influence of the ICC profiles on different components of color by separating color values into *lightness* and *chroma* and inspecting their behavior separately and more closely in *CIELCh* color space.

#### 5.4.1. Lightness, Chrome, and Polarization

Color information was converted into *CIELCh* color space, which is a direct derivative of *CIELAB*, that makes visualizing the lightness and the chroma component (the color and its hue angle) easier to grasp and deliver.

Starting with the lightness component  $CIELAB(L^*)$ , regardless of the followed workflow and regardless of the grayscale finish (matt or semi-gloss), it is obvious that when correcting using the Spyder24 color target the lightness increases noticeably. The effect is, yet, more drastic under polarization, which yields in the end a washed-out look for the final corrected image as colors gain more lightness into them. Check the red curves, for

MLG and SFR<sup>16</sup>, in Fig.5.10 how it elevates above the ground-truth, and the unpolarized curves noticeably are causing the patches to appear brighter than they should be, and giving an overall sensation as if the colors are washed-out.

On the other hand, when looking at the MLG correction reproduction, Fig.5.10(a) and Fig.5.11(a), one notices that it is never the case that the lowest part of the curve matches or comes even close to the ground-truth, and this are namely the first few dark black/gray patches of the MLG grayscale. The lowest corrected value is always starting way above its ground-truth counterpart (i.e. 11.8/18.5 vs. 3.15 ; actual black is becoming less black in comparison, it is gaining more lightness.). In addition to the fact that these first few black patches are getting all flat, no distinction would be observable anymore on the final corrected image among them (i.e. lost information/losing shades). The actual ground-truth value of the darkest gray patch on MLG accounts to  $CIELAB(L^*) \approx 3.1$  while it is slightly higher without polarization  $CIELAB(L^*) \approx 6.7$  and  $\approx 6.5$  respectively upon using either SG or Spyder24 color targets for color-correction. However, under cross-polarization conditions, the  $CIELAB(L^*)$  value of that patch increases drastically up to  $\approx 11.8$  and  $\approx 18.5$  respectively. It is, as well, observable that there is barely any difference in  $CIELAB(L^*)$  values among the first 3 patches under cross-polarization as the values range only between  $\approx 11.8 \rightarrow 12.7$  or  $\approx 18.5 \rightarrow 19.0$  when either SG or Spyder24 color targets were used. Whereas, the actual range of these 3 patches goes between  $\approx 3.1 \rightarrow 12.0$  when the ground-truth was collected spectrally. Without polarization, this range is between  $\approx 6.7 \rightarrow 11.1$  and  $\approx 6.5 \rightarrow 9.9$  for SG and Spyder24 respectively. All these differences are clearly perceptible upon examining visually Fig.5.12.

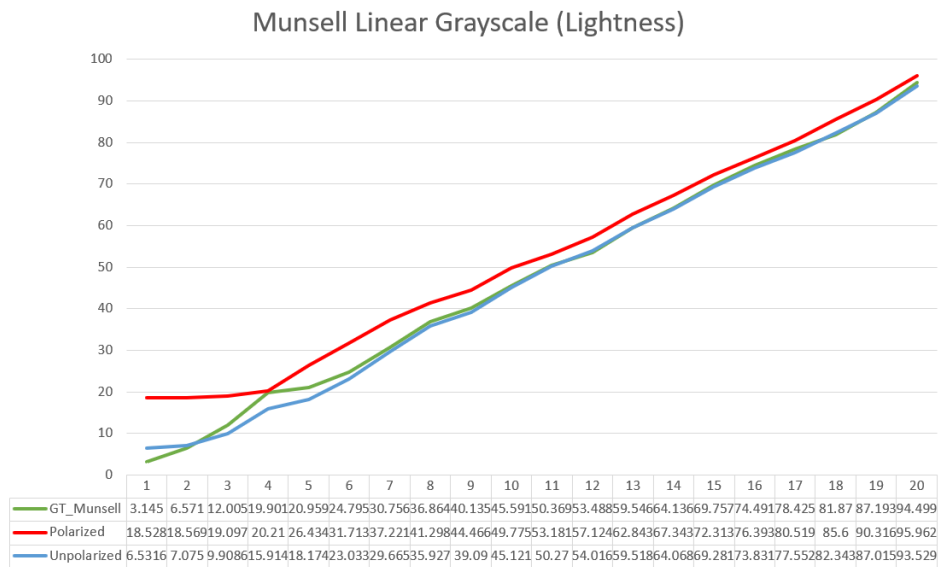
All the figures related to lightness can be compared between our workflow and the commercial workflow in Fig.5.15, Fig.5.16 and Fig.5.17.

Moving to observe the chroma behavior, we notice that despite the aforementioned statistics, we can observe now how each ICC profile influences and affects the grayscale "color" reproduction and breaks its assumed neutrality. Both followed workflows –our pipeline and BasICColor+C1- tend to shift the chroma in different directions across the hue circle, and there seems to be no general trend here. For instance, correcting for a matt grayscale (SFR target), our pipeline shows a chroma shift rather towards the yellow sector on the hue circle, regardless of the used color target, for most of the points whether polarized or unpolarized. Check Fig.5.13. Whereas, the commercial workflow –BasICColor+C1- tends to push the chroma points more in two lines, one in the yellow direction and the other in the green direction. Check Fig.5.20(a) and Fig.5.20(b). All points, under either of the pipelines, spread inside the second inner circle  $Chroma \leq 4.0$  in most of the cases.

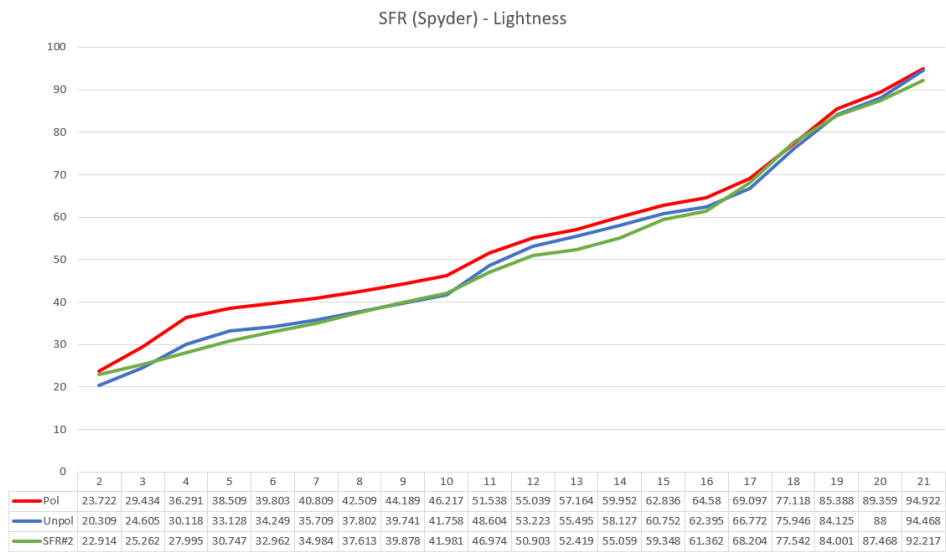
Looking at the hue circle of the MLG BasICColor+C1 workflow shows that the chroma shift is dominating only the left half. In the case of Spyder24, the shift concentrates near the greenish-gray region while in the case of X-Rite SG the chroma shift tends to spread out more with few outliers that go deep in the cyan region and the greenish/yellowish region. Our pipeline correction shows more outliers in the case of X-Rite SG that go deep in the blue/cyan region, as well as in the deep green when polarized. Whereas in the case of Spyder24, the outliers are limited to only one or two points that go deep in the green region. Apart from that, most of the points tend to concentrate near the center, however, in different gray directions. Check Fig.5.19 for clear visualization and comparison.

All in all, regardless of the used method or software, and regardless of the finish of the used target (matt or (semi) glossy), and regardless of the number of color patches it contains whether it is only 24 or 140, a chroma shift seems to be an inevitable consequence of the color correction process, and polarization would accentuate the effect to make it yet more dire. Dark patches get flattened out, linearity shifts upwards making the patches brighter which would make them appear washed-out. Some shift in the chroma, as well, is causing certain tinge to be added to certain gray "neutral" patches.

<sup>16</sup>SFR linear grayscale patches start at patch #2 to #21. The first patch is the central patch of the target and is discarded.

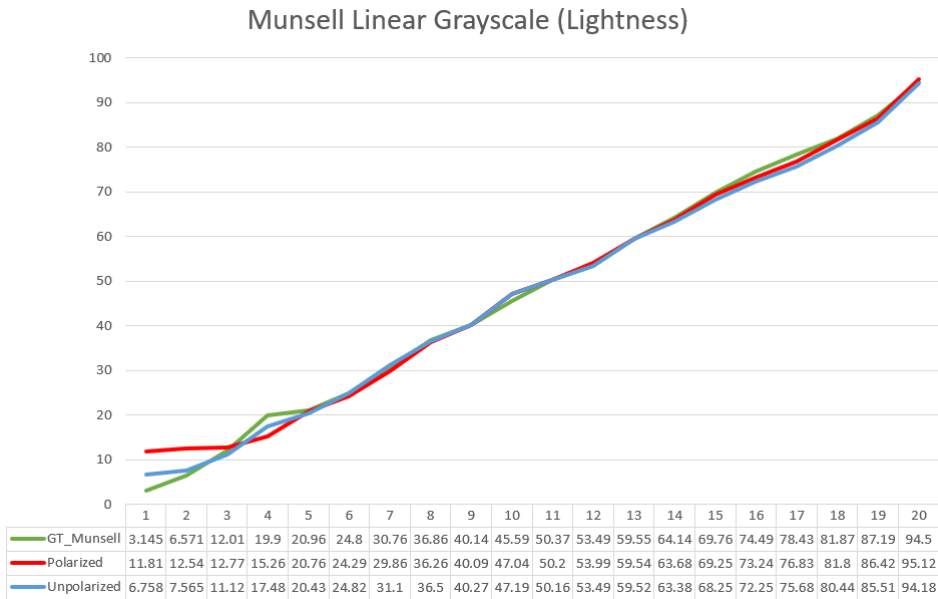


(a) MLG by our workflow with base-ICC (Spyder24).

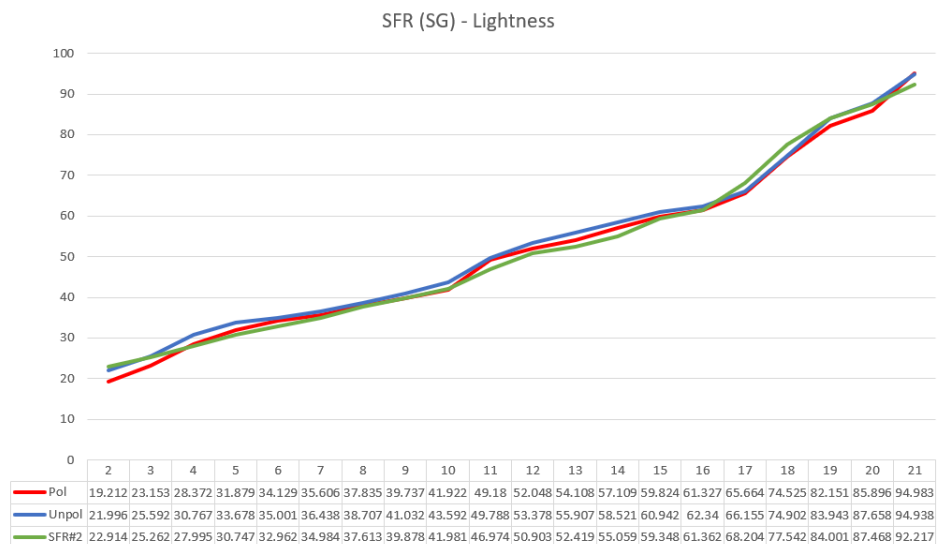


(b) SFR by our workflow with base-ICC (Spyder24).

Figure 5.10.: Munsell linear grayscale (MLG) and the SFR grayscale lightness component CIELAB(L\*) reproduction upon applying the generated ICC profile using Spyder24 color chart using our own pipeline. Ground-truth (green), polarized (red), and unpolarized (blue).



(a) MLG by our workflow with base-ICC (SG).



(b) SFR by our workflow with base-ICC (SG).

Figure 5.11.: Munsell linear grayscale (MLG) and the SFR grayscale lightness component CIELAB(L\*) reproduction upon applying the generated ICC profiles of the corresponding color targets indicated inside the parentheses using our own pipeline. Ground-truth (green), polarized (red), and unpolarized (blue).

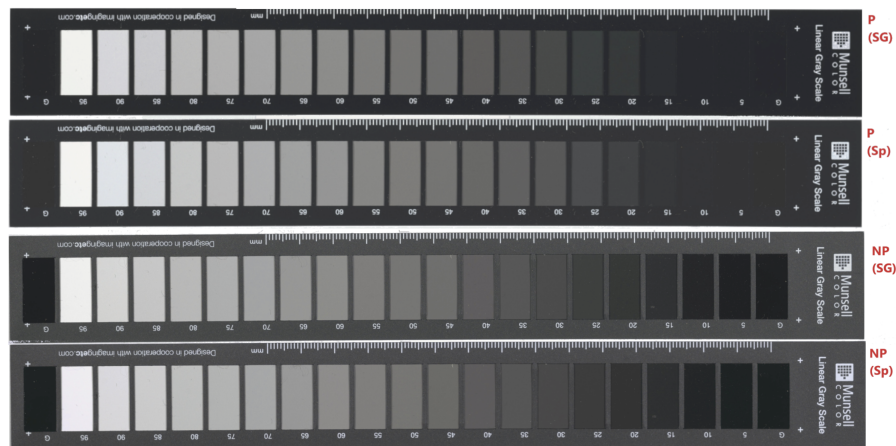


Figure 5.12.: A comparison showing the end result of profiling the Munsell Linear Grayscale (MLG) under two different lighting conditions polarized (P) and unpolarized (NP) based on X-Rite SG (SG) and Spyder24 (Sp) captured in the standard geometry  $0^\circ/45^\circ$ . Notice how under polarization some of the deep black shades are completely lost and getting the same color value.

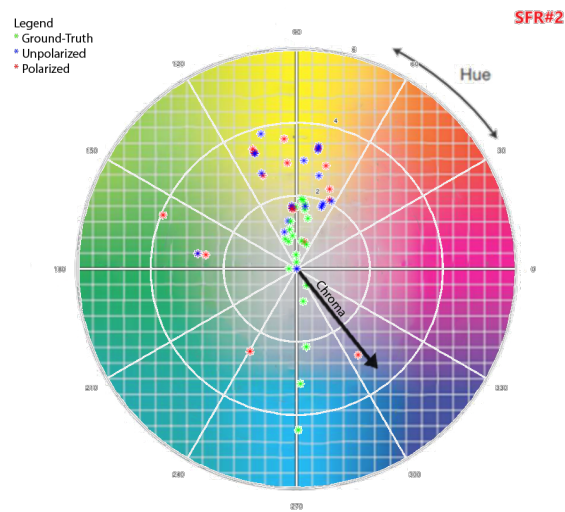
It may not carry any significance to some people in certain domains as the shift, in some cases, is minimal and unobservable while affecting only certain shades. However, it is something that would raise big concerns in the cultural heritage communities for their attempts to preserve historical artifacts in a digital format with little to no alteration in surface color to the possible extent. One needs, at least, to be aware of the color changes that are inflicting the digital replica, especially when such a replica may be an asset of a virtual museum, or if the digital replica were to be used for research and analysis purposes (e.g. think of digitizing Rembrandt's *The Night Watch*).

## 5.5. Conclusion

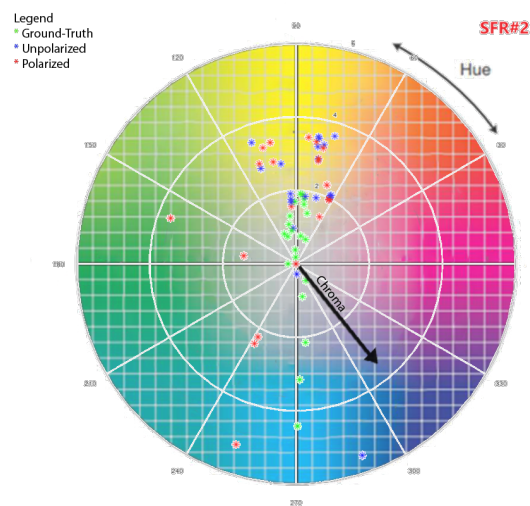
In this first research topic, we have inspected the ICC profiles created using two common and well-known color targets, the *X-Rite SG* and the *DataColor Spyder24*. We followed the recommended ISO standards regarding lighting setup and capturing geometry ( $0^\circ/45^\circ$ ) under one of the standard light sources, namely D55 (DedoLight D55). Another two linear grayscale targets were also captured, namely the *Munsell Linear Grayscale (MLG)* and the *SFR/OECF Linear Grayscale (SFR)*. Both include 20+1 gray patches that are linearly spaced from black to white. The two grayscales, as well as the two color targets, differ in their finish, for instance, *Spyder24* and *SFR* both have a matt finish, in contrast to *SG* and *MLG* which both have (semi) glossy finish.

We have captured the data under the aforementioned lighting setup once as it is (i.e. no other filters or additional optical elements were introduced), and once with cross-polarization filters in place, as we mounted a circular polarization filter in front of the camera lens as well as circular polarization films in front of the used light sources.

We have shown by numbers how introducing the polarization filters contributes to an increase in the reported color difference ( $\Delta E_{00}$ ) regardless of the used and profiled color target. We have shown, as well, how there is an inevitable chroma shift occurring regardless of the state of polarization and regardless of the color target. The



(a)  $CIE LCh(Ch)$  Chroma curve of the SFR by our workflow with base-ICC (SG).



(b)  $CIE LCh(Ch)$  Chroma curve of the SFR by our workflow with base-ICC (Spyder24).

Figure 5.13.: The SFR linear grayscale target's chroma  $CIE LAB(a*b^*)$  reproduction upon applying the generated ICC profiles of the corresponding color targets indicated inside the parentheses. Ground-truth (green), polarized (red), and unpolarized (blue).

lightness color component ( $CIE LAB(L^*)$ ) reproduction proved to be highly affected by polarization resulting in an undesirable and irreversible effect on the deep levels of black/grays when a (semi) glossy target is being used (e.g. MLG) given the nature of how polarization interacts with this kind of materials where the same effect is



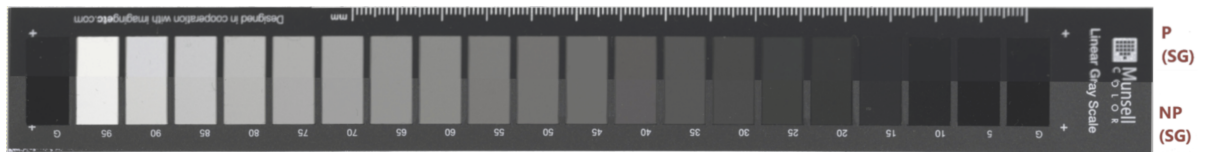


Figure 5.14.: Comparison between polarized (P) and non-polarized (NP) color-corrected grayscale using X-Rite SG ColorChecker - Munsell Linear Grayscale (MLG).

\*\*Remember that the colors of what one is looking at here depend on either the quality and the color calibration of the monitor/display that one is using to view the page on, or on the printing quality in the case of viewing a hardcopy.

not observable when using a target with a matt finish (e.g. SFR). Polarization seems to break up the linearity of a grayscale by flattening out the deep black/gray shades rendering them alike, causing a loss in information difference among them. On the other hand, when an ICC color correction profile is used that is produced using the Spyder24 (matt finish), it affects the lightness component ( $CIE_{LAB}(L^*)$ ) in a different way, in which the lightness levels of a corrected grayscale would shift upwards so that the end colors would appear rather washed-out and drab under polarization regardless of the grayscale finish (i.e. making colors prone to lose their luster).

Color neutrality reproduction, regardless of the used target for color correction and regardless of the state of polarization, does not seem to be an easy feat to achieve or guarantee so precisely. A slight, in best case scenario, but inevitable color tinge and some chroma shift are very likely to occur making the grayscale not very "gray" or neutral as supposed to be (e.g. some greenish/yellowish, blueish/reddish hut tint may be observable on some of the patches), check Figs 5.17, 5.18. Looking at the patches<sup>17</sup> with the numbers 35,40 on MLG for example, Fig.5.17(a) non-polarized –NP(SG) and NP(Sp)- they seem to have slightly reddish tone, whereas looking at the same patches in Fig.5.17(b) the patches depict slightly more of a yellowish/greenish tone. In the case of polarization like in P(SG) and P(Sp) the patches appear, relatively, brighter especially by looking at patches with the numbers 85,90,95 (on the most left-side). The patches under polarization also show a slight greenish tinge if one looks at patches with the numbers 35,40 in Fig.5.17(a). Fig.5.14 can also help in making the comparison easier to look at and visualize, as it is comprised of two halves, the upper half is polarized (P) and the lower half is non-polarized (NP). Another very noticeable observation is that the color patches under cross-polarization look crispier and more solid than their counterparts in the non-polarized version.

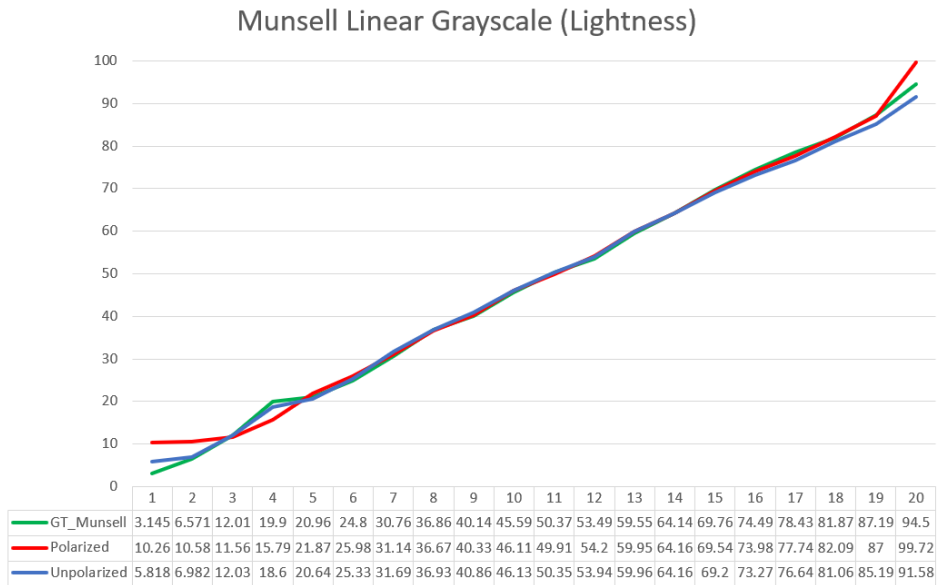
We advise to be more careful when reading color correction statistics and to take a look at the correction rather visually to assess its acceptability and suitability to the intended application beyond just accepting color difference statistics that satisfy certain quality levels. Numbers may be as low as desired, on average, however, they would not paint the full picture clearly of how the color correction would be perceived. Another point to take into consideration is polarization. It may be indispensable to certain applications to use polarization filters, however, one needs to pay more attention to what could happen to the deep black/gray levels that seem to be highly affected and lose their linearity when the surface finish interacts strongly with polarization filters (e.g. glossy surfaces), think of digitizing Rembrandt's The Night Watch painting. In addition to that, certain gray levels may transform their chroma into more greenish/cinder shades (or other shades depending on the quality of the polarization filter), one must be aware of that when rendering a scanned digital object.

The type and the quality of the polarizer in-use are also in question. Our future experiments would include the assessment of a wider set of high-quality polarization filters that are popular among professional photographers

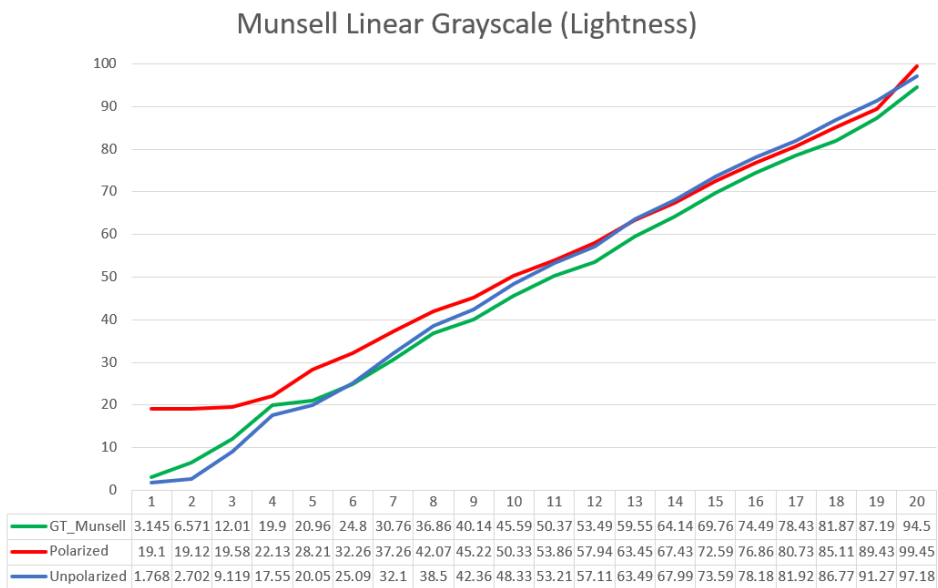
<sup>17</sup>It is important to notice that the visualization depends highly on how this document is rendered on which screen (color calibrated?), and/or how it was printed.



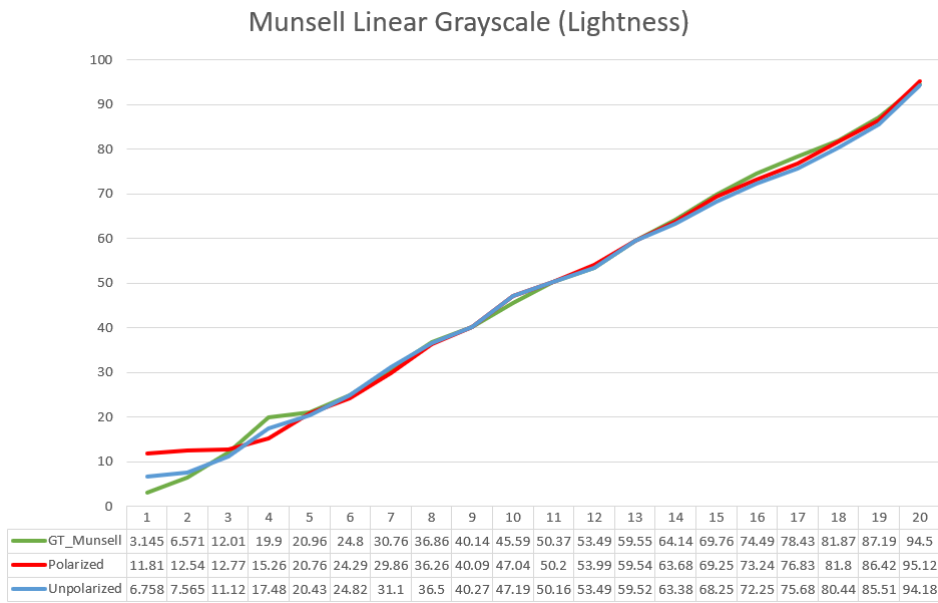
and already on the market to study the Chroma/lightness shift more systematically, while keeping in mind the desire and striving for high accuracy and fidelity when digitizing cultural heritage artifacts. In addition to our intention to carry out a more comprehensible analysis of what happens in actuality to the light source wavelengths (SPD) by investigating that using highly accurate spectral measurements, so as to understand how different types of polarization filters are responsible for having the effect on such a chroma and lightness shift that we observed under this topic.



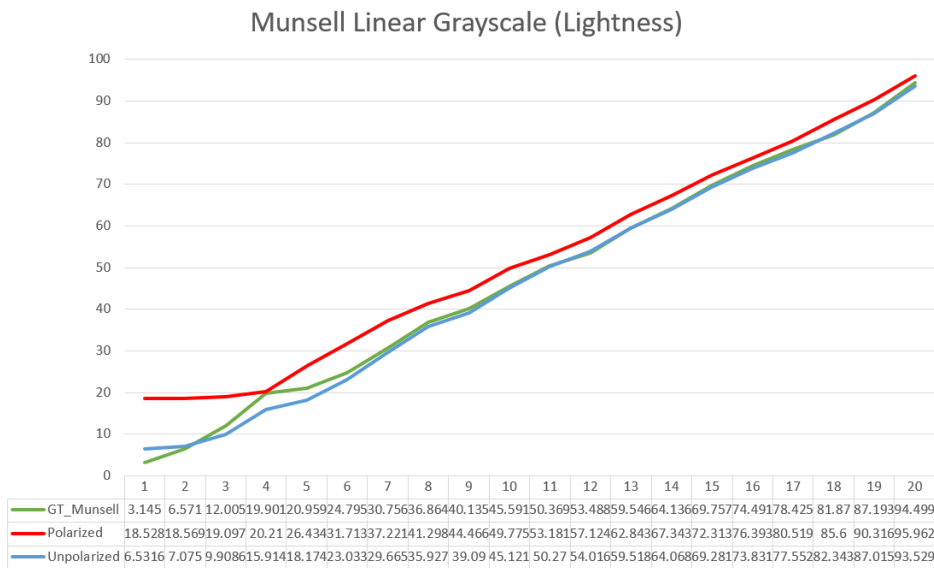
(a) MLG by BasIColor+C1 workflow with base-ICC (SG).



(b) MLG by BasIColor+C1 workflow with base-ICC (Spyder24).



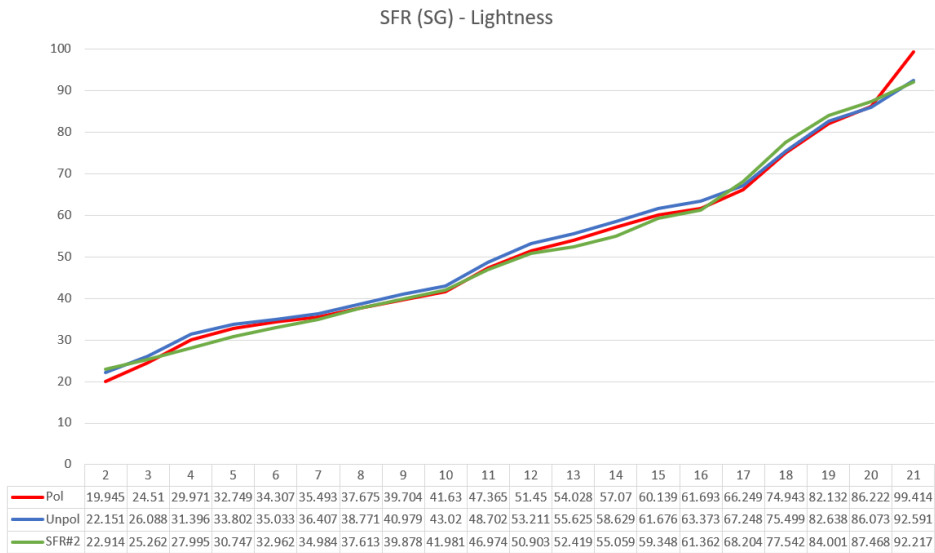
(c) MLG by our workflow with base-ICC (SG).



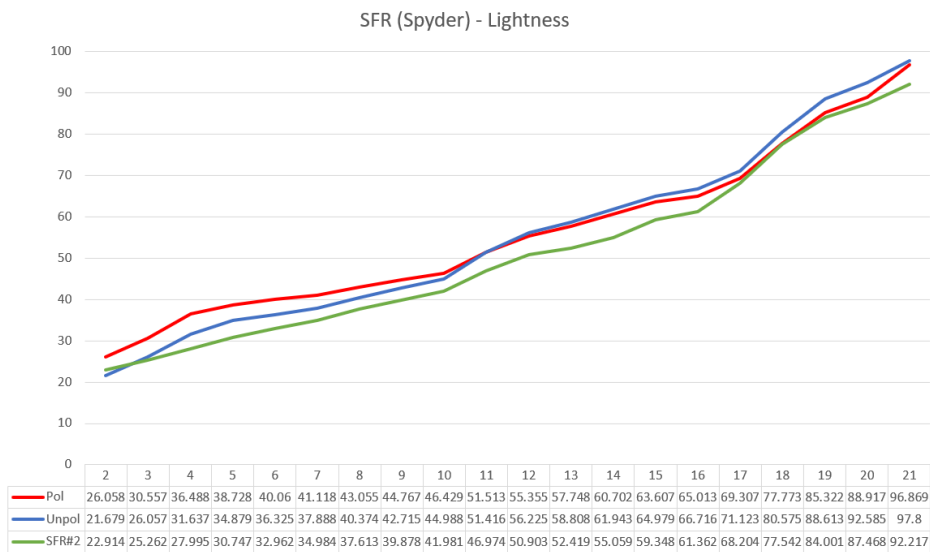
(d) MLG by our workflow with base-ICC (Spyder24).

Figure 5.15.: Munsell linear grayscale (MLG) lightness CIELAB(L\*) reproduction upon applying the generated ICC profiles of the corresponding color targets indicated inside the parentheses by the two workflows our own implementation vs. BasicColor+C1. Ground-truth (green), polarized (red) and unpolarized (blue).

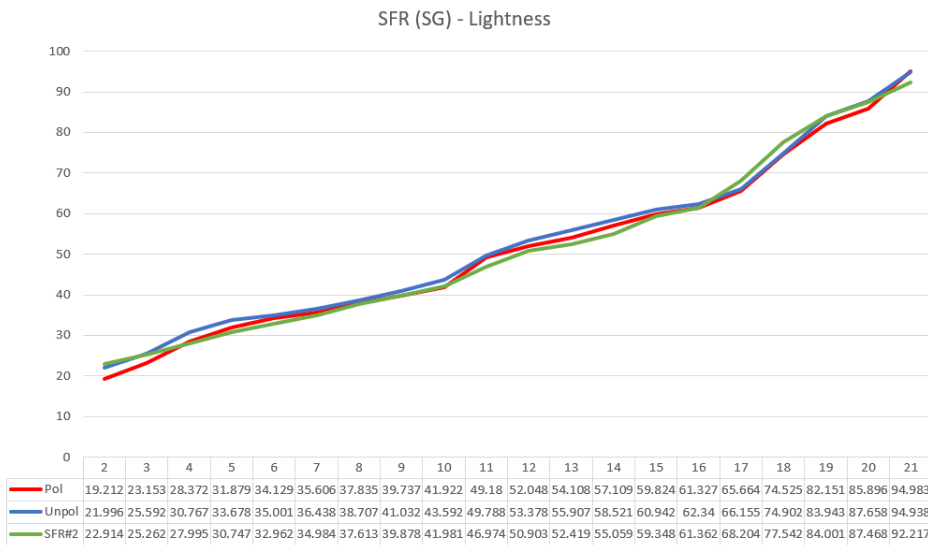
5. Effect of Cross-Polarization on RGB Imaging and Color Accuracy and Fidelity



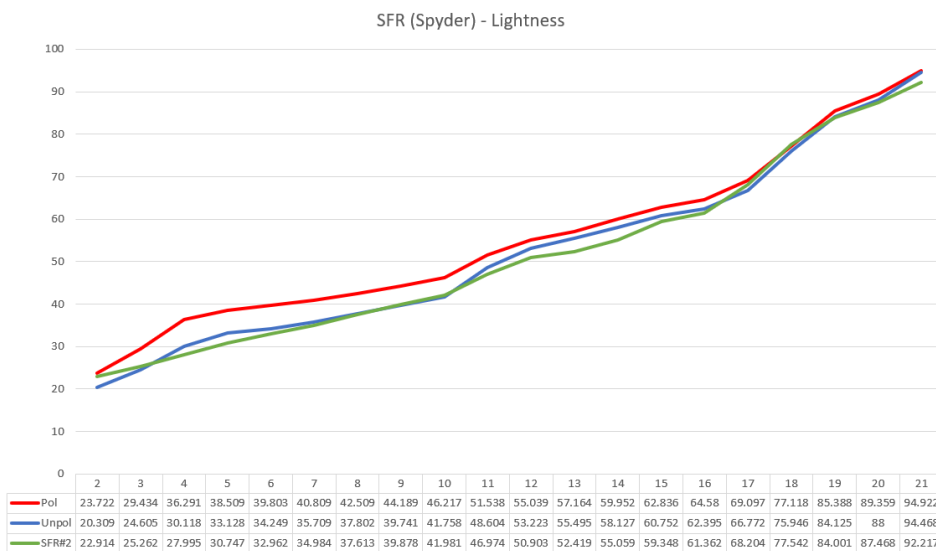
(a) SFR by BasIColor+C1 workflow with base-ICC (SG).



(b) SFR by BasIColor+C1 workflow with base-ICC (Spyder24).



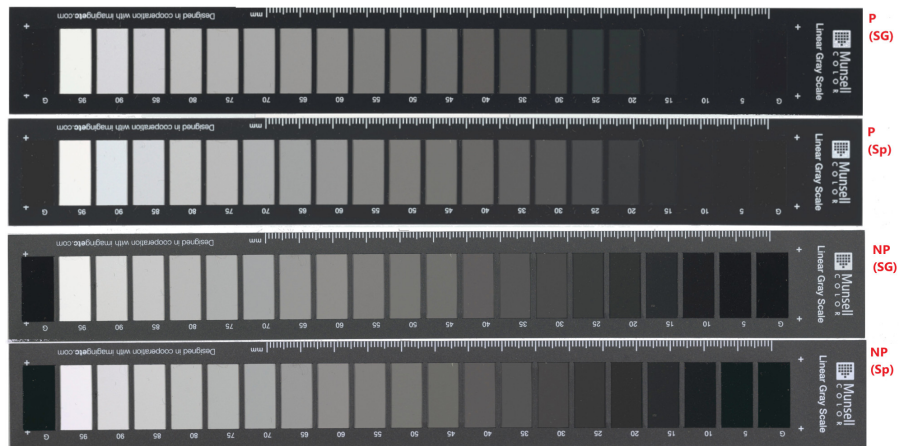
(c) SFR by our workflow with base-ICC (SG).



(d) SFR by our workflow with base-ICC (Spyder24).

Figure 5.16.: The SFR/OECF (SFR for short) lightness CIELAB(L\*) reproduction upon applying the generated ICC profiles of the corresponding color targets indicated inside the parentheses by the two workflows our own implementation vs. BasIColor+C1. Ground-truth (green), polarized (red) and unpolarized (blue).

\*\*The patch numbering starts from patch #2 for #1 is the central patch on the SFR target which is irrelevant to the linear sequence of the 20 linearly-spaced patches and hence was omitted.



(a) our pipeline

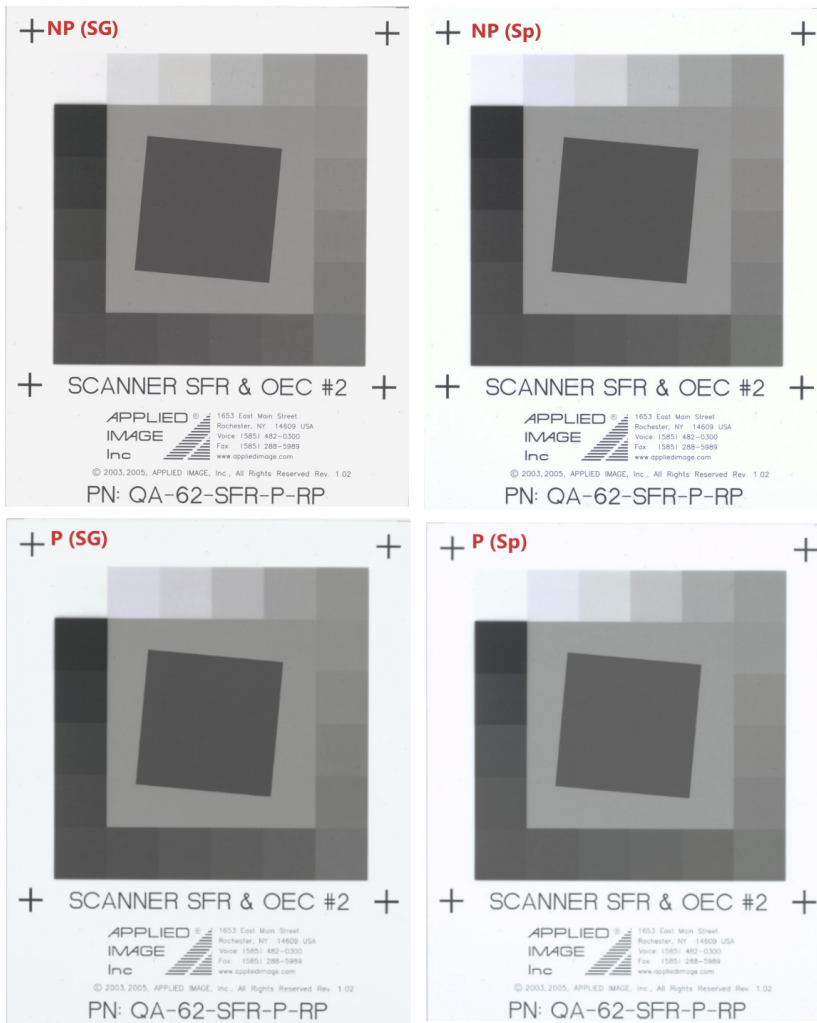
BasIColor+C1



(b) BICC

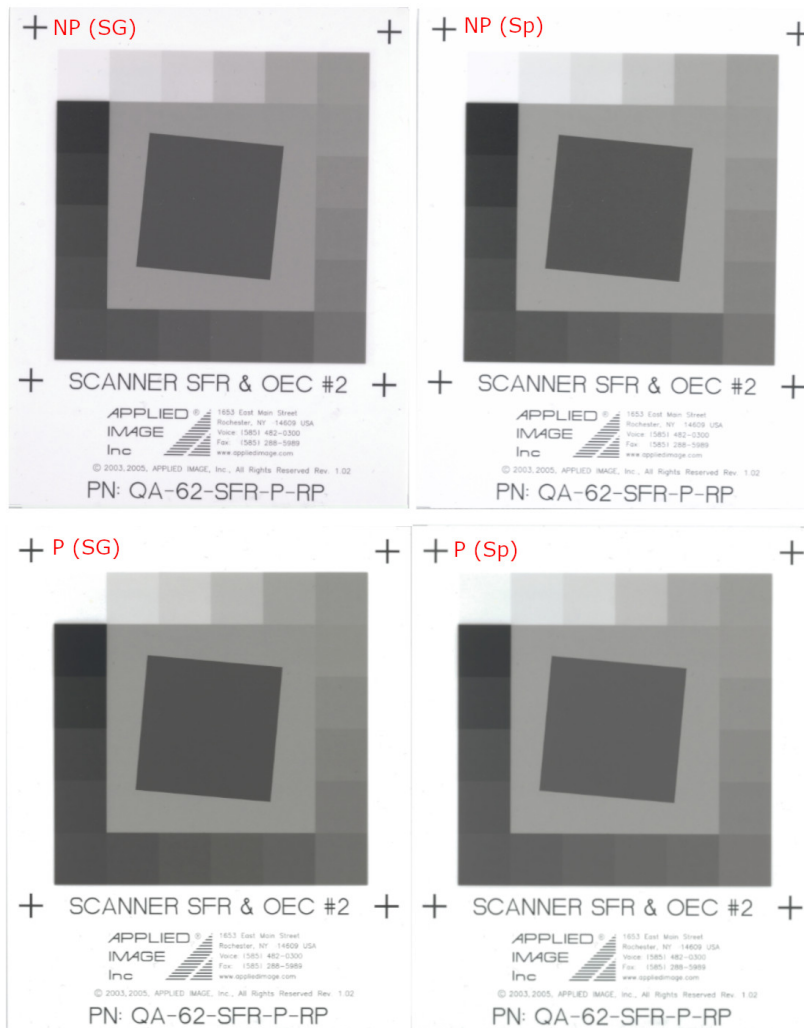
Figure 5.17.: A comparison showing the end result of profiling the Munsell Linear Grayscale (MLG) under two different lighting conditions polarized (P) and unpolarized (NP) based on X-Rite SG (SG) and Spyder24 (Sp) captured in the standard geometry  $0^\circ/45^\circ$ . Notice how under polarization some of the deep black shades are completely lost and get the same color value.

\*\*Remember that the colors of what you are looking at here depend on either the quality and the color calibration of the monitor/display that you are using to view the page on, or on the printing quality in case of viewing a hardcopy.



(a) Linear grayscale SFR target - our pipeline

BasICColor+C1

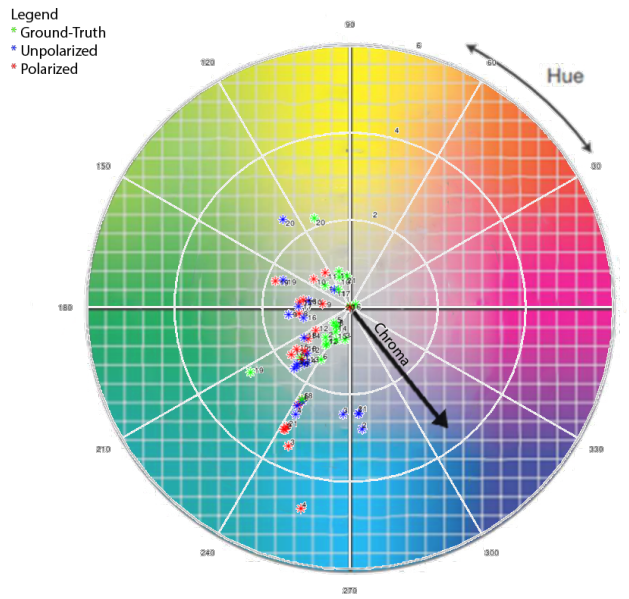


(b) Linear grayscale SFR target - BICC pipeline

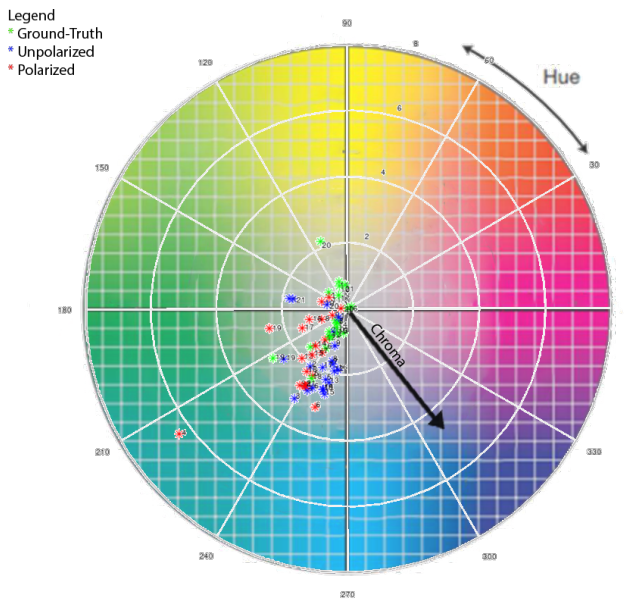
Figure 5.18.: A comparison showing the end result of profiling a the SFR/OECF linear grayscale (SFR for short) under two different lighting conditions polarized (P) and unpolarized (NP) based on X-Rite SG (SG) and Spyder24 (Sp) in the standard geometry  $0^\circ/45^\circ$ .

\*\*Remember that the colors of what you are looking at here depend on either the quality and the color calibration of the monitor/display that you are using to view the page or on the printing quality in case of viewing a hardcopy.

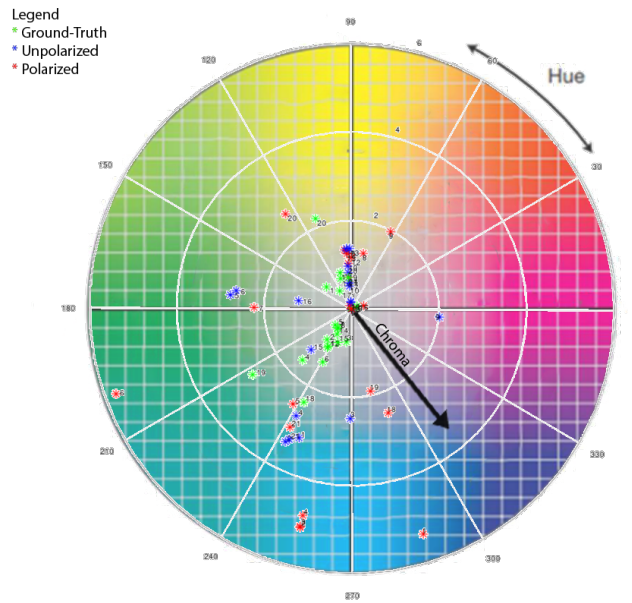




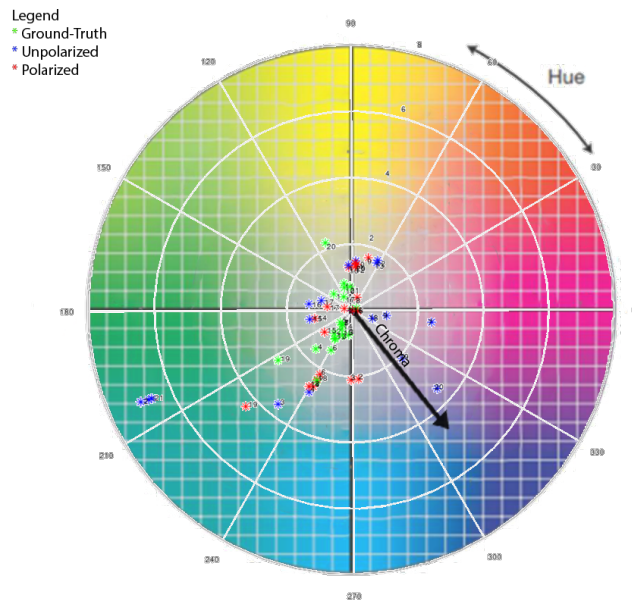
(a) *CIE LCh(Ch)* Chroma component of the MLG by BasICColor+C1 workflow with base-ICC (SG).



(b) *CIE LCh(Ch)* Chroma component of the MLG by BasICColor+C1 workflow with base-ICC (Spyder24).

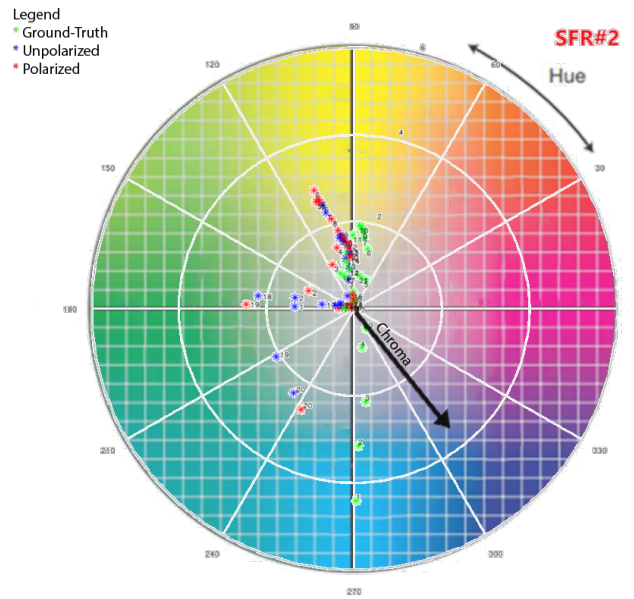


(c)  $CIELCh(Ch)$  Chroma component of the MLG by our workflow with base-ICC (SG).

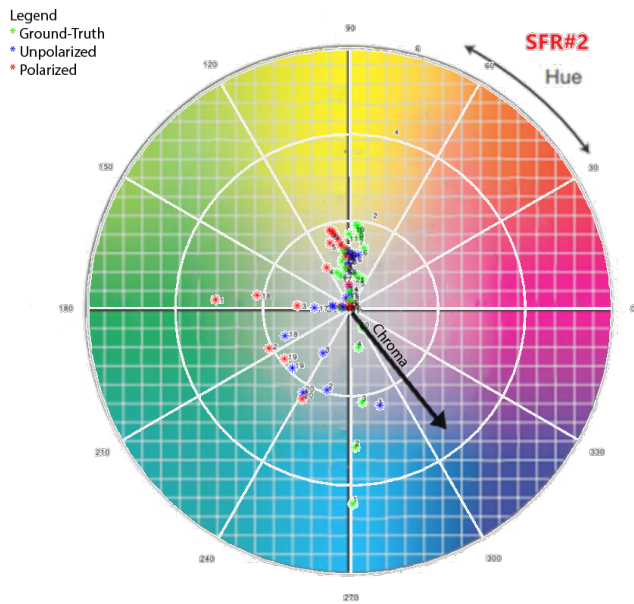


(d)  $CIELCh(Ch)$  Chroma component of the MLG by our workflow with base-ICC (Spyder24).

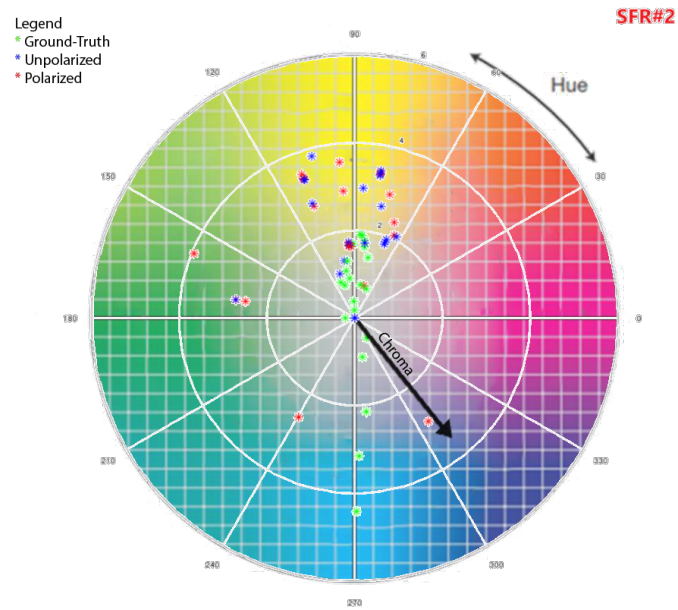
Figure 5.19.: Munsell linear grayscale (MLG) chroma CIELAB(L\*) reproduction upon applying the generated ICC profiles of the corresponding color targets indicated inside the parentheses. Ground-truth (green), polarized (red) and unpolarized (blue).



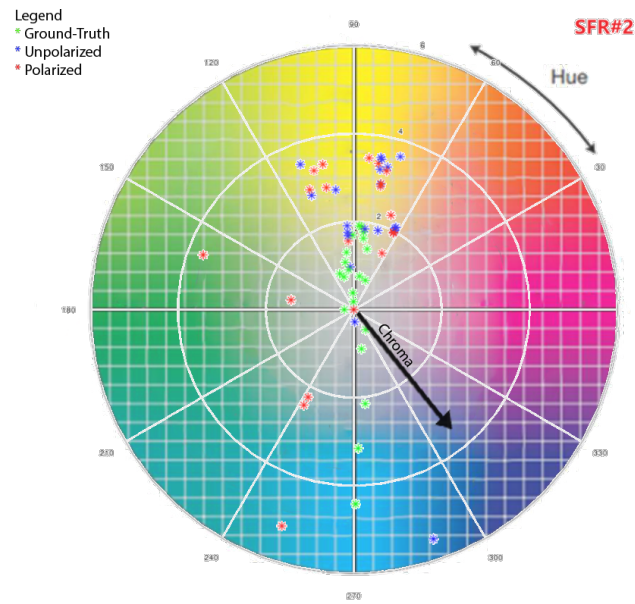
(a)  $CIE LCh(Ch)$  Chroma component of the SFR by BasICColor+C1 workflow with base-ICC (SG).



(b)  $CIE LCh(Ch)$  Chroma component of the SFR by BasICColor+C1 workflow with base-ICC (Spyder24).



(c)  $CIELCh(Ch)$  Chroma component of the SFR by our workflow with base-ICC (SG).



(d)  $CIELCh(Ch)$  Chroma component of the SFR by our workflow with base-ICC (Spyder24).

Figure 5.20.: Linear grayscale SFR target chroma CIELAB(L\*) reproduction upon applying the generated ICC profiles of the corresponding color targets indicated inside the parentheses. Ground-truth (green), polarized (red) and unpolarized (blue).

## 6. A Cross-Polarization as a Possible Cause for Color Shift in Illumination

In this chapter, we are addressing *RQ2* and talking more closely about how cross-polarization is, possibly, affecting and inflicting the light source characteristics. The common belief is that (cross-) polarization filters do not cause any shift in light wavelengths but only affect the light's intensity. Based on this assumption, a light source of a certain correlated-color temperature (CCT) should not demonstrate any shift in its CCT and hence its white-point (WP). Then, a material that would look, say, yellow under a D50 illuminant will look always the same exact yellow (i.e. same xy-Chromaticity coordinates) under this illuminant whether the light passes through polarization filters or not.

The following chapter explains in detail how in practice even the use of the highest-end circular polarization filters testifies otherwise.

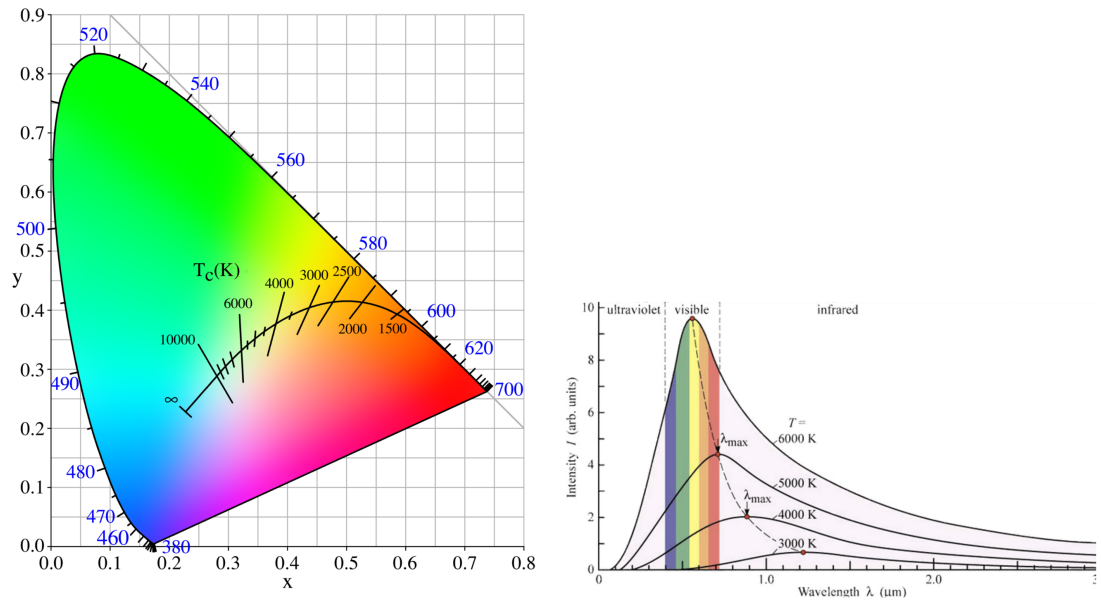
### 6.1. Introduction

Building upon the previous research topic, and after noticing how the color of certain materials has been noticeably impacted by the cross-polarization phenomenon, we have decided to trace back the problem and do further analysis. However, this time on the light source itself. If the behavior of the light source is, somehow, being impacted by the polarization filters then that would, inevitably and consequently, affect the surface color it shines onto. Polarizing the light waves, theoretically, should not cause any shift in the wavelengths along the spectrum. Polarization, as a phenomenon, affects mainly the intensity of the light, namely, halving it as only half of the light would be polarized in a certain state – in photography terminology, reduction by one *f-stop*. Artificial polarization filters would inevitably reflect a small portion of the light impinging on the filter itself, ( $\approx 2 - 10\%$ ), depending on the used technology in the filter's manufacturing process, the remaining light would then split in half as only half of it would be polarized in a certain direction, and that would account to  $\approx 46\%$  as an output on the other side of the filter in best case scenario [Hec02a].

The color a light source emits, when observed shining on a diffusing white surface, is commonly described, in the human sense, as being *cool/cold* (aka. *blueish*) or *warm* (aka. *reddish/yellowish*), which has more to do with how the (light) color would provoke certain human emotions and feelings [VM94, Vav65]. In addition, how the ambient color of a light source in an environment affects different aspects of the human behavior, as well as the psychological state and mood – this topic is beyond the scope of this work, though a curious reader may consult [BRD92] to have an insight on the topic.

This terminology of describing a light color as being *cold/warm* is closely related to what is known as the light source's *Color Correlated Temperature (CCT)* which was mentioned earlier briefly in sec.3.3.1. A light source's CCT is expressed in *Kelvin (K)* and physically corresponds to the temperatures and the colors an incandescent idealized black-body would go through when being heated up, check Fig.6.1 – We are re-referencing the figures and inserting them here for the ease of reading and access.





(a) The black-body radiation curve and the corresponding color-correlated temperatures (CCT) on xy-Chromaticity diagram. (b) The black-body radiation curves at different temperatures represented along the light spectrum.

Figure 6.1.: Black-body radiations representations.

Fig.6.1(a) shows a curved line stemming from the right corner (deep red) and moving all the way across different color regions. i.e. When the black-body's temperature increases, there is a shift in the dominant wavelength of the color it undergoes as shown in Fig.6.1(b) *Red* → *Orange* → *Yellow/Orange* → *Yellow/Green* → *Green* → *Green/Blue* → *Blue*. The curved line across the xy-Chromaticity diagram, Fig.6.1(a), shows as well intersectional lines. Any light source's CCT value that lies along one of these lines would be considered to bear the same corresponding *Kelvin* temperature value that is located directly on the main curvy line.

Keep in mind that xy-Chromaticity diagram is not perceptually uniform and it is even better to be illustrated without the background colors that fill it, as opposed to how it is commonly communicated, for two reasons. First, it omits completely the third dimension of color, namely lightness. Second, when the colors are generated to be visualized the location of the white is always static and never changing to adapt to the actual illuminant that was used to calculate these tristimulus values that would be represented on this diagram. Nevertheless, it is still a common practice to use the diagram to represent color stimuli, especially in the lighting and display industries, while keeping in mind that the representation does not tell any information regarding the color difference between any two colors represented on the diagram, nor it tells anything regarding the appearance of any color coordinates on it. It was mentioned earlier, as well, in sec.3.4 that a refined and more perceptually uniform color space was devised known as *CIE1976 u'v'*, Fig.6.2 [Ber19]. Finally, a light source *white-point (WP)* is the Chromaticity of the illuminant that is observed when illuminating a diffusing white surface, which can be expressed in *CIEXYZ* or chromaticity coordinates (*xy - Chromaticity/CIE1976 u'v'*). Table 6.1 shows the WP's of the most common illuminants, more data could be found in [Too16, CIE07, HP11].

Illuminant	CIE1931 2°		CIE1964 10°		CCT (K)
	$x_2$	$y_2$	$x_{10}$	$y_{10}$	
A	0.44757	0.40745	0.45117	0.40594	2856
D50	0.34567	0.35850	0.34773	0.35952	5003
D55	0.33242	0.34743	0.33411	0.34877	5503
D65	0.31271	0.32902	0.31382	0.33100	6504

Table 6.1.: xy-Chromaticity coordinates for 2° and 10° standard observer of few of the most common illuminants with their corresponding color-correlated temperatures.

## 6.2. The Experiment Setup

To study the effect of cross-polarization on the light source itself in terms of its CCT and WP, we have prepared the following hardware to run the experiment:

- A light source - D50 (our system's ring-light).
- Four different high-quality circular polarization filters (CPL) for the visible domain that are usually mounted on a camera lens:
  - B+W XS-Pro HTC Polfilter KSM MRC nano
  - HOYA REVO SMC CIR-PL
  - Zeiss T\* Pol-Filter
  - Marumi Fit+Slim PL
- 1x circular polarization film that is fixed in front of the light source - brandless with transmission rate  $42 \pm 2\%$  and operating range 380 – 780 nm.
- Avantes spectrometer for spectral measurements in the visible domain.
- A metallic reflective sphere to check the cross-polarization alignment/state.
- White reference / complete diffuser - Spectralon.

Fig.6.3 shows a sketch of the experiment's setup. The experiment was conducted in a completely dark room. The light source was mounted and fixed parallel to a table at a distance of nearly 30 cm and 0° angle. A white reference was fixed at an angle of nearly 45° directly below the light source. On the opposite side of the white reference, there was the probe of the spectrometer fixed at a distance of nearly 21 cm away from the white reference. A piece of a very dark cloth (black) was laid on top of the mount that held the probe as an extra measure just to eliminate any chance of any possible incoming stray light toward the probe. Directly in front of the probe, the tested CPL filters were fixed in place after making sure that they were well aligned with / rotated to match the polarization state of the polarized light. We used a metallic sphere placed next to the white reference to check when the reflections are diminishing completely from the probe angle, only then the polarization filters will be crossed with one another and ready to take the necessary measurements.

## 6.3. Objectives

The incentive behind this study was the shortage of reading materials that discuss polarization and its effects on color in real-life applications away from the basic principles behind polarization and how it works from the physics point of view. Some of the questions that have arisen and were the reason behind this work are:

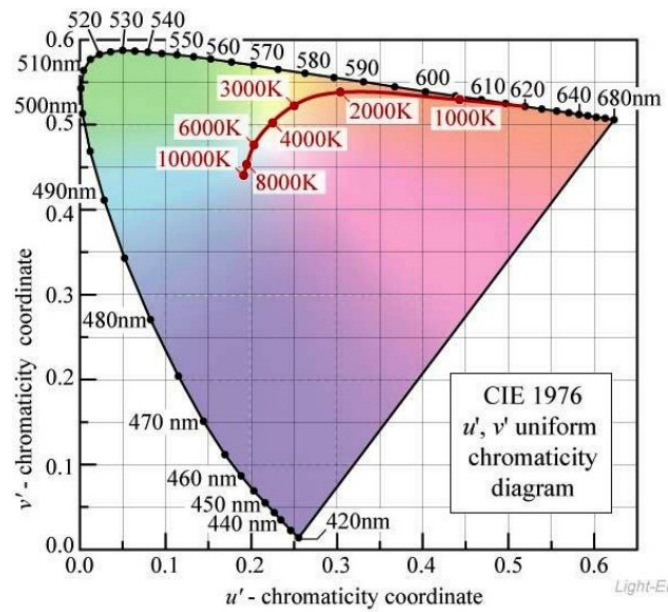


Figure 6.2.: CIE1976  $u', v'$  perceptually uniform chromaticity color space that is common to see in-use in the display industry. Source [DM12].

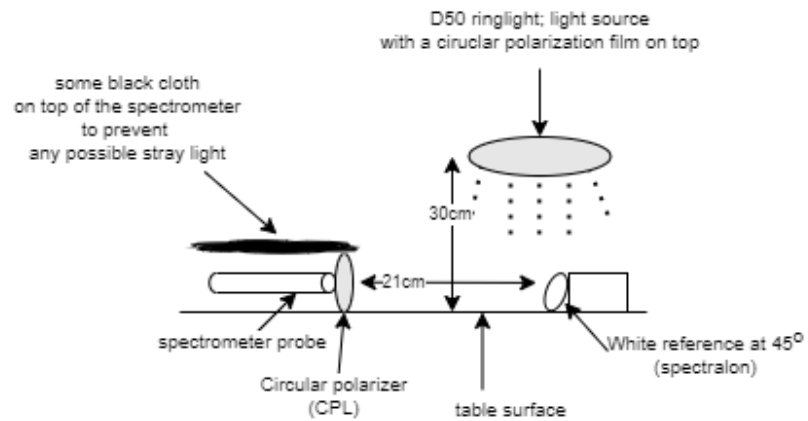


Figure 6.3.: A sketch of the experiment setup.



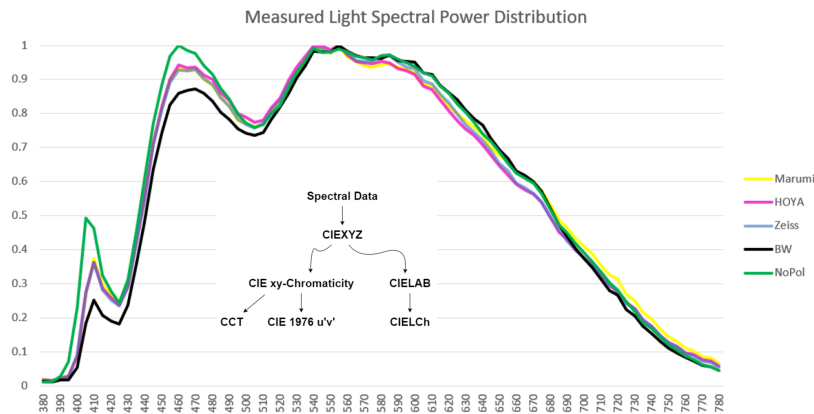


Figure 6.4.: Spectral power distribution (SPD) of the light source with and without the different polarization filters.

- Is my light source after applying cross-polarization still performing as expected in terms of its CCT, white-point, and SPD?
- How much is an imaged surface color being affected by the light cross-polarization, does it still depict/preserve its actual appearance?
- How much can I trust an imaged surface color in terms of color accuracy and fidelity when this is of high concern (e.g. digitizing and archiving museum artifacts)?

## 6.4. Methodology

### 6.4.1. Measurement - Data Acquisition

The data were captured as follows:

1. The light source was switched on in order to set the proper integration time of the spectrometer automatically. The integration time was optimized for each of the tested CPL filters individually.
2. Then, the light was switched off in order to capture a dark reference / dark spectrum that corresponds to the chosen integration time. The dark reference is to be subtracted from the measurements in the next step.
3. The light was switched on again to take the measurement and capture the light source SPD that fell directly on the white reference and has been reflected towards the probe going through the CPL on the way. The dark reference was set to be subtracted automatically from the measurements.

The above steps were repeated for each of the four CPLs we have. In addition, one more measurement was taken where all the polarization elements were removed, so that we have a reference measurement of the light's SPD itself with no interfering elements in between.

After collecting all the necessary data, the measurements were saved in a 5 nm step in the range 380 – 780 nm and normalized separately. The SPD of each measurement, Fig.6.4, then was converted into CIE XYZ<sup>1</sup> so it is

<sup>1</sup>10° standard observer was used for the conversion.

possible to derive xy-Chromaticity coordinates, as well as moving to CIELAB and CIELCh(ab) color spaces as desired.

We have also approximated and calculated the color correlated temperature (CCT) of each of the measurements based on *McCamy's* polynomial equation Eq.6.1 [McC92]. The *McCamy's* approach was chosen as it shows very minimal to negligible error in the range in which it is intended to be used in this study.

$$CCT(x,y) = -449n^3 + 3525n^2 - 6823.3n + 5520.33 \quad (6.1)$$

where  $x$  and  $y$  are the calculated chromaticity coordinates and

$$n = \frac{x - 0.3320}{y - 0.1858}$$

Moreover, a ground-truth of an actual D50 measurement was downloaded from the website of the University of Waterloo<sup>2</sup> to compare against and verify our results furthermore. The data on the website are originally from *Hunt's Measuring Colour's* book [Hun91].

## 6.5. Results and Discussion

First, it is obvious by looking at the spectral measurements, Fig.6.4, that there is a decrease, when light is being circularly cross-polarized, in certain regions along the spectrum even though the light spectrum's profile itself is not changing drastically. The decrease is very noticeable and strong in the blue and deep blue regions around 400 – 430 nm and again in the range of 450 – 500 nm. The black curve (B+W CPL filter) shows the most shift among all the other CPL filters.

To make more sense of the spectral data, we convert the data into more readable and comprehensive color spaces that can help in quantifying the color components and the color difference more easily. As it is shown in Fig.6.4, we convert the spectral data into CIE XYZ primarily, and from there we are able to move to

$CIE XYZ \rightarrow CIELAB \rightarrow CIELCh(ab)$  and

$CIE XYZ \rightarrow CIE 1931 xy - Chromaticity \rightarrow CIE 1976 u'v' \rightarrow CCT$

Table 6.2 shows the converted color values as xy-Chromaticity coordinates, CIELAB values, CIELCh(ab), and the approximated CCT. First, a simple Euclidean distance<sup>3</sup> was calculated for all the xy-Chromaticity coordinates with respect to the actual D50. Despite the fact that this information is of little weight in quantifying and measuring the difference of colors, it serves only as a primary indicator. Then, we move to observe the values in CIELAB color space, the  $L^*$  value of all the measurements accounts for 100.0 as it is the light source itself we are measuring. By looking at the  $a^*$ ,  $b^*$  we start to notice that different measurements start to show different values that are drifting away from 0.0 or neutrality as opposed to the actual D50 measurement, which shows very small  $a^*$ ,  $b^*$  values, clearly. i.e. The chroma color components  $a^*$ ,  $b^*$  are ideally supposed to be 0.0 or very close, the larger the values the less neutral the color becomes. Our tested light source without any polarization filters (*NoPol*) has, originally, some slight color tinge that originates from the used LEDs themselves, and that tinge is being accentuated and shifted away along the hue circle when the polarization filters are being introduced as the measurements testify, check Fig.6.5.

The chromaticity coordinates of the light source under polarization seem to shift along the yellow/green radial line moving towards the circumference (i.e. gaining more chroma). The  $CIELAB(b^*)$  component (blue/yellow)

---

<sup>2</sup><http://www.npsg.uwaterloo.ca/data/illuminant.php>

<sup>3</sup>Euclidean distance  $(x,y) = \sqrt{(x - \bar{x})^2 + (y - \bar{y})^2}$

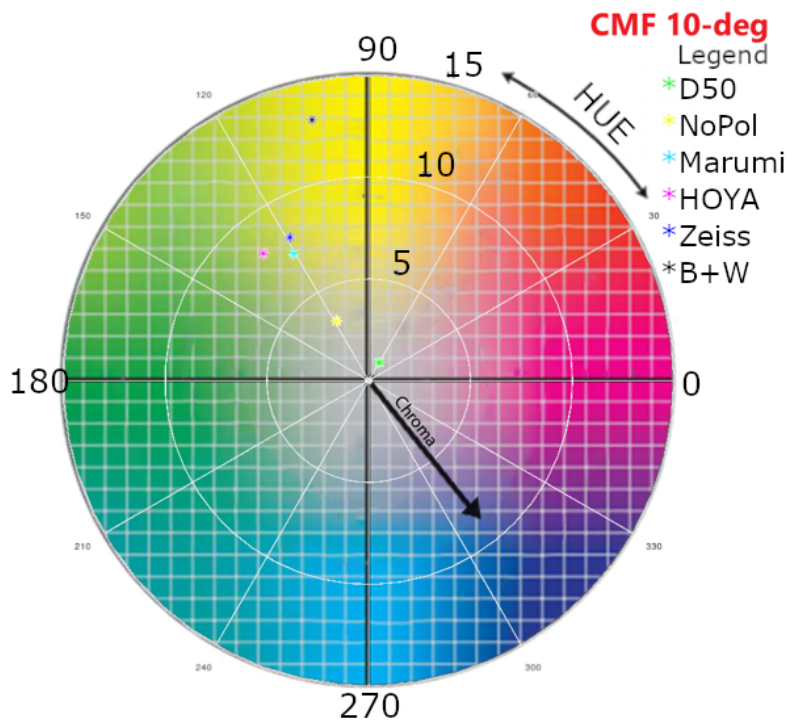


Figure 6.5.: CIELCh(ab) coordinates of the tested light source (D50) with and without polarization filters compared to an actual D50 measurement (green dot) represented on the hue circle.

## 6. A Cross-Polarization as a Possible Cause for Color Shift in Illumination

	xy-Chromaticity / Euclidean Distance to D50			CIELAB			DE00 Color Difference		LCh(ab)		Approx.
	x	y	Euc. Dist.	L*	a*	b*	to NoPol	to D50	C	h	CCT
D50	0.3477	0.3595	0.0	100.0	0.5125	0.8885	3.5274	0.0	1.0257	60.021	4931.06
NoPol	0.3480	0.3644	0.0048	100.0	-1.5851	2.9243	0.0	3.5274	3.3263	118.46	4937.57
HOYA	0.3481	0.3725	0.0129	100.0	-5.1788	6.2375	4.861	8.4314	8.1072	129.7	4958.37
Marumi*	0.3501	0.3713	0.0120	100.0	-3.6889	6.2236	3.5883	7.0922	7.2347	120.66	4887.53
Zeiss	0.3511	0.3727	0.0136	100.0	-3.87	7.0266	4.1419	7.6021	8.0218	118.84	4860.28
B+W†	0.3612	0.3809	0.0253	100.0	-2.7795	12.786	7.3421	9.9339	13.085	102.26	4576.15

Table 6.2.: Statistics of different CPL polarization filters calculated from spectral measurements and converted into xy-Chromaticity coordinates as well as into CIELAB and CIELCh(ab) color spaces based on the 10-degree standard observer data. Correlated color temperature (CCT) was also approximated using McCamy’s formula. ‘\*’ indicates the closest CPL filter to NoPol (No Polarization), while ‘†’ indicates the farthest.

seems to be a lot more affected than the  $CIELAB(a^*)$  (red/green) in most cases. In the worst case scenario, for  $B+W$  CPL filter,  $b^* \approx 12.8$  and  $a^* \approx -2.8$  which is a huge shift going in the yellow region. Whereas, the least shift, which is still very considerable and questionable anyhow, is attributed to the *Marumi* CPL filter, for which the chroma color components  $a^*b^*$  account to  $-3.7$  and  $6.2$  respectively.

	White-Point		
	X	Y	Z
D50	0.96719	1.0	0.81426
NoPol	0.95508	1.0	0.78954
Marumi	0.94304	1.0	0.75055
HOYA	0.93457	1.0	0.75038
Zeiss	0.942	1.0	0.74125
B+W	0.94823	1.0	0.67685

Table 6.3.: CIEXYZ white-point of our light source D50 (NoPol) with and without CPL cross-polarization compared to an actual D50 measurement.

SG CC #G4	X	Y	Z	L	a	b	DE00 to D50
D50	18.127	9.403	1.792	36.749	59.065	35.148	0.0
NoPol	18.067	9.3866	1.7093	36.718	59.791	35.152	0.25311
Marumi	17.967	9.356	1.6192	36.661	60.721	35.118	0.58667
HOYA	17.826	9.3038	1.6199	36.563	61.254	34.937	0.83537
Zeiss	17.974	9.3601	1.5975	36.669	60.831	35.151	0.61332
B+W	18.243	9.4711	1.4453	36.876	60.732	35.679	0.47674

Table 6.4.: Testing the red color patch (G4) of the X-Rite SG CC. The CIEXYZ coordinates were scanned spectrally under D50, the CIEXYZ coordinates are being adapted to the corresponding white-point (WP) of each of the polarization filters so that CIELAB coordinates can be calculated. DE00 to the reference D50 is provided for each case.

In terms of DE00 color difference that is mainly driven by the shift happening in the chroma components, the color difference caused by the used filters for cross-polarization ranges from nearly 3.6 to 7.3 for the minimum and the maximum difference, which correspond to *Marumi* and *B+W* respectively when compared to the ground-truth, which is our light source **NoPol** (with No Polarization).

We have provided in the table, as well, the DE00 color difference to the actual D50 measurement, in which we notice that our ring-light that is indeed a D50, because of the technology in its LEDs, is causing a color difference of nearly 3.5, because of the shift in the chroma color components  $|a^*, b^*| > 1.0$ .

All this shift in the chroma components has a non-negligible effect on the light source's CCT after all. Looking at the approximated CCT values in Table 6.2 we see clearly how it starts to diverge from the ground-truth *NoPol*  $\approx 4940K \rightarrow$  *Marumi*  $\approx 4890 K \rightarrow$  *B+W*  $\approx 4580 K$  which is a shift of nearly 360 K in the worst case scenario. This change in CCT would have an inevitable consequence on the final look of the corrected colors when these circular polarization filters are to be used on an imaging system (e.g. a camera). The color correction model assumes a certain white-point in which *CIEXYZ* values need to be (D50 in our case), remember Eq.3.8, whereas these values are prone to shift when CPL polarization filters are in action.

Table 6.3 shows the shifted WP for each of the tested CPL polarization filters. It is clear that some CPL filters are diverging quite much from the original D50 values before polarization. For instance, *B+W* has the most shift, especially its *CIEXYZ(Z)* component, from the actual D50 or even from our D50 ring-light before polarization  $0.79 \rightarrow 0.677$ . Our D50 ring-light diverges, as well, from a natural D50 moving from  $0.814 \rightarrow 0.79$  in its *CIEXYZ(Z)* component. Table 6.4 shows *CIEXYZ* and *CIELAB* coordinates of the red patch on the X-Rite SG CC (G4). The color target has been scanned, beforehand, spectrally using *Barbieri Spectro LFP qb* with a specified D50 as a light source. Then, based on the WPs in Table 6.3 the initial D50 *CIEXYZ* coordinates were adapted to the corresponding WP and then transformed into *CIELAB* color space. Finally, the color difference  $\Delta E00$  is calculated between each row and the reference D50 measurement. Table 6.5 shows the same thing done on the other two primary color patches (Green; F4 and Blue; E4), for brevity we have omitted *CIEXYZ* values from the table.

Tables 6.4 and 6.5 show how colors, technically, would appear when a camera looks at them through a certain CPL filter with cross-polarization, depending on how the white-point is shifted, because of the cross-polarization and based on the characteristics of the used CPL filters color appearance changes (i.e. *CIELAB* values). Some colors like the blue (patch *E4*) suffers, for instance, under *B+W* CPL filter greatly causing a major shift that accounts to  $\Delta E00 \approx 3.5$ .

Spectrally speaking, polarization filters seem to have a major problem in the blue region of the light spectrum and that is obvious from Fig.6.4. Even after a complete adaptation to the new WP induced by the corresponding CPL polarization filter, a non-negligible color difference (DE00) can still be observed mainly for the blue colors (e.g. patch *E4*) ranging from  $1.4 \rightarrow 3.5$  depending of the brand and the technology used for manufacturing (e.g. coating layers and the finish). Polarization filters do account for at least double the error of  $\Delta E00$  compared to without it (**NoPol**) in the best-case scenario.

Fig.6.6(a) and 6.6(b) illustrate the shift of the light source's white-point (D50), when cross-polarization is being used, of different brands of the highest quality CPL filters available on the market. The WPs are represented on the *xy-Chromaticity diagram* and on the *CIE 1976  $u'v'$  color space diagram* respectively. The latter is considered to be more perceptually uniform than the former. In the worst-case scenario, the shift is drifting away very noticeably from the 5000 K inter-sectional line more towards the 4500 K line. The *CIE 1976  $u'v'$  coordinates* are provided in Table 6.6.

SG CC #E4	L	a	b	DE00 to D50
D50	22.387	8.8847	-55.209	0.0
NoPol	22.27	7.8672	-55.341	0.72777
Marumi	22.146	6.7296	-55.464	1.5272
HOYA	22.169	6.8794	-55.41	1.4089
Zeiss	22.111	6.4147	-55.505	1.7494
B+W	21.832	3.9365	-55.865	3.4911
SG CC #F4	L	a	b	DE00 to D50
D50	51.93	-35.004	37.487	0.0
NoPol	51.977	-34.988	37.392	0.059373
Marumi	52.037	-35.044	37.274	0.14205
HOYA	52.066	-35.361	37.294	0.23891
Zeiss	52.044	-34.987	37.239	0.14961
B+W	52.052	-34.106	36.931	0.36118

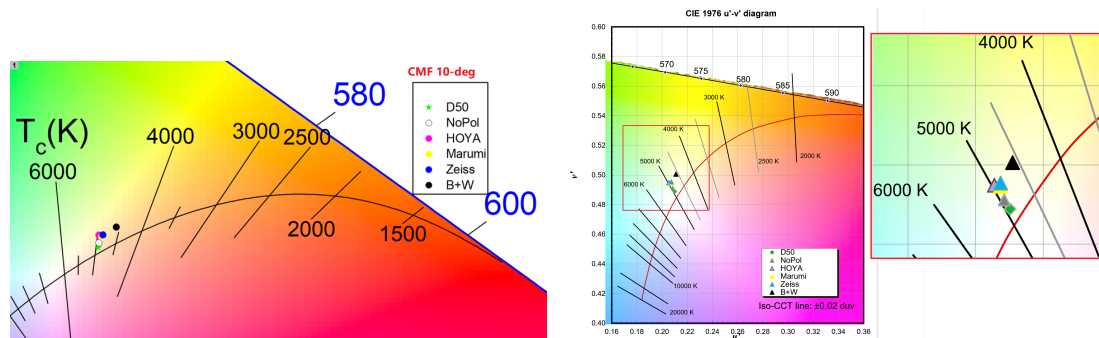
Table 6.5.: Testing color patches (E4; Blue and F4; Green) of the X-Rite SG CC. The CIEXYZ coordinates were scanned spectrally under D50, the CIEXYZ coordinates are being adapted to the corresponding white-point (WP) of each of the polarization filters so that CIELAB coordinates can be calculated afterwards. DE00 to the reference D50 is provided for each case.

Source	$u'$	$v'$
D50	0.2101	0.4889
NoPol	0.2085	0.4912
HOYA	0.2056	0.4949
Marumi	0.2073	0.4946
Zeiss	0.2074	0.4954
B+W	0.2110	0.5006

Table 6.6.: CIE1976  $u'v'$  coordinates of the light source's WP (D50) with and without cross-polarization.

## 6.6. Conclusion

Despite all this shift happening to the light source's WP and being influenced by high chroma values, it is quite imperceptible to the naked eye to notice when looking directly at the light source itself or at its reflection off a white surface (e.g. a complete diffuser; Spectralon), mainly because of the process of chromatic adaptation the human eye automatically undergoes (in analogy to camera white-balancing). It is hard to tell towards which color / chroma tinge the light source is shifting when being cross-polarized using different CPL filters as this chroma tinge is, technically, hiding behind the light source intensity component / full brightness ( $CIELAB(L^*)$ ) and it is only possible to see its effect only when the light source is being shone on a certain color surface (e.g. illuminating a color target) so its inflicted SPD starts to interact with a surface color spectral reflectance. Only then, the effect of this cross-polarization and the shift in the light source's original WP would be more perceptible, as a consequence, befalling different color surfaces, remember the effect of cross-polarization (CPL filters) that was described earlier in the first research topic, in Chapter 5, on RGB imaging.



(a) Light source (D50) white-point illustrated on  $xy$ - (b) Light source (D50) white-point illustrated on  $u'v'$  CIE1976 Chromaticity diagram. perceptually uniform space.

Figure 6.6.: The shift of the light source (D50) white-point caused by cross-polarization when different CPL brands are used. Calculations are based on the spectral measurements.

It seems as if the coating layers used to manufacture these kinds of CPL filters are, primarily, responsible for the chroma shift happening in calculating the light source's WP *CIELAB/CIELCh* coordinates. (Cross-) polarization as a phenomenon, per se, should not introduce any wavelength shift or change in the profile of the light SPD except for the intensity, which usually is halved. However, looking at the light's SPD with and without cross-polarization, even though at first glance the SPD profile looks to follow the same trend, one notices that certain regions along the visible domain of the spectrum are being affected differently and the SPD curve does not preserve its exact shape when different CPL filters are introduced, which is apparent by looking at the region between  $\approx 400 - 500\text{nm}$  in Fig.6.4. Hence, a color surface reflectance with a dominant wavelength in the blue region would be more affected than other colors with dominant wavelengths in other parts of the spectrum. Even after a full adaptation to the new WP, a noticeable color difference,  $\Delta E_{00}$ , is at least doubling when compared to the light source without polarization altogether, based on the calculation on few different color patches *CIEXYZ* values as seen in Table 6.4 and Table 6.5.

The chroma gain happening in the light source's WP when different CPL filters are used in a cross-polarization manner accounts for at least  $\Delta E \approx 3.6 \rightarrow 7.3$  compared to the original light source's WP without cross-polarization. The color difference is mainly due to the changes happening in the chroma color components *CIELAB(ab)*. In terms of CCT, the change accounts for CCT moving from  $\approx 4940\text{ K} \rightarrow 4890\text{ K} \rightarrow 4580\text{ K}$ , which is a change of nearly  $360\text{ K}$  in the worst-case scenario.

It is highly recommended to avoid (CPL) polarization filters altogether, whenever possible, when color accuracy and fidelity are sought and of high importance to the imaging application (e.g. museum artifacts digitization). However, to certain technology, applications, and setups (CPL) polarization filters may be indispensable, hence we advise minimizing the influence and the impact of the chosen filters by understanding how much color shift such filters may introduce and what colors the most affected are. We advise understanding and analyzing -if possible- systematically the behavior of the chosen (CPL) filters and having a good understanding of the compromise one is making when setting up an imaging system with (cross) polarization filters in place.





# 7. Color Calibration Based on Mosaic Stitching of a Color Target as an Alternative to a Single-Shot Approach

In this chapter, we are addressing *RQ3*, in which we propose a new and unconventional way of color calibration so as to overcome the challenges of scanning highly reflective surfaces, and/or the challenges that come with the use of lenses with small field-of-view (FOV), and/or the challenges that come with the use of non-standard illumination and scanning geometry (i.e. other than the recommended standards  $0^\circ/45^\circ$ ). The following proposed method shows a very high accuracy comparable to – or even at some points better than- the standard method in terms of color accuracy. In addition, it paves the way toward 3D color calibration, which is still a very challenging and little-researched problem in the field.

## 7.1. Introduction

We have mentioned earlier that the recommended geometry for proper acquisition of a color target, according to the ISO standards, is  $0^\circ/45^\circ$  relative between an imaging system, an imaged surface, and the light setup [ISO17]. However, what if the color target does not fit fully inside the imaging system's field of view (FOV), such as having a camera with a Macro lens at a close range where the FOV is quite small and would require, usually, a smaller color target? Smaller color targets are, unfortunately, manufactured only with fewer color patches normally (e.g. X-Rite Nano  $24 \times 40mm$  comes with 24 patches, ColorGuage Micro Target  $35 \times 41mm$  comes with 30 patches) compared to the size of richer color targets with more patches (e.g. X-Rite SG CC  $21.6 \times 27.9cm$  with 140 patches, NGT  $19 \times 15cm$  with 130 patches).

Obviously, more color patches are more desirable than just a few as that will have a non-negligible effect on the color correction model and the end result of the color calibration process. More colors would allow better representation and more accurate interpolation, which would, consequently, allow for better and more precise coverage of the used color gamut as opposed to using fewer patches.

### 7.1.1. The Problem

The ISO standards, and any other recommendations in the field of color calibration, assume a color target to fit fully inside a camera's FOV, let alone the geometry between the camera, the light source, and the target. i.e. capturing a color target for color calibration in a single shot with optimal  $0^\circ/45^\circ$  geometry. However, in certain applications, all the aforementioned requirements may not be possible to fulfill. For example, (a) due to the technical design of an imaging system [Cul23] (see Fig.7.1), in which the light source and the optical system share the same plane rather than having  $45^\circ$  angle relative to one another, and/or (b) due to the high-quality scan requirement, in which as much details as possible are to be captured with the help of a Macro lens at a close

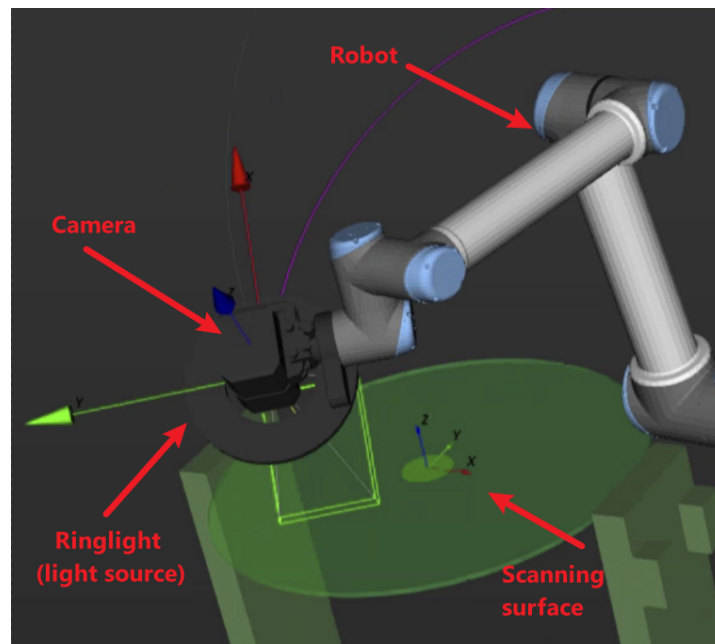


Figure 7.1.: CultArm3D system's design – Acquisition mode.

range (i.e. smaller FOV), in addition to the desire of using the best possible color target for the color calibration and correction processes –which comes usually with more color patches and only in large sizes.

Using a Macro lens comes with a few challenges though. One of them is the small size of the camera's FOV, which does not help much to fit a large color target (e.g. X-Rite SG CC or NGT) when better color calibration and color rendition are sought for high-quality scans (e.g. digitizing museum artifacts in high details, small crafted reliefs,... etc.). Another challenge is the geometric distortion any Macro lens suffers from.

We have prepared the following experiment and tested the following approach of scanning at a tilted angle rather than orthogonally, then running homography to re-project the captured images in a certain/corrected perspective, and finally stitching in a mosaic-fashion the captured data to form a complete ortho-image from the scanned parts of a color target, as if the whole color target was captured rather in a single shot and from an orthogonal view.

## 7.2. Stitching Approach

The most abundant example of a practical stitching algorithm is panoramic images that most of the current smartphones are capable of creating on the fly. A stitching algorithm aims to merge a sequence of images, of a scene, taken separately –because the whole scene does not fit into the camera's FOV all at once- into one complete image better known as a *mosaic image* (also referred to as the "*stitched image*").

The sequence of the images must have an overlapping area shared between one another defining the starting and the ending regions of each image with its neighboring images in the sequence so that the merge looks seamless and free of undesirable artifacts.

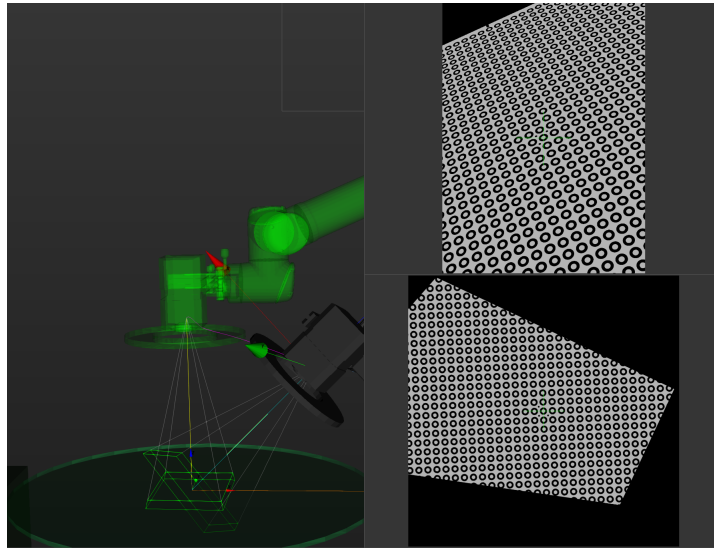


Figure 7.2.: Left side - virtual camera (in green) vs. real camera (in black). Top right - captured image by the real camera. Bottom right - rectified image as if it were taken from the pose of the virtual camera

A stitched image may suffer from various artifacts though such as *edge vignetting*, *non-sharp/out-of-focus regions in the image away from the image's center*, *visible seam-lines along the stitched edges*, and *a sudden change in brightness along the stitching line (aka. intensity shift)* [CK99, SS97, ZLPW06]. These kinds of artifacts would make the final stitched image look unnatural, let alone the distortion the image data undergoes both in terms of geometry and photometry (color information).

Our stitching procedure consists of the following main steps:

1. Image acquisition
2. Image rectification
3. Image merging

The camera captures many images of a certain color target by moving across the color target at a pre-defined angle as it would be described later in the **Methodology** section, which results in different camera poses for each of the captured images. The rectified images are assumed to share the same camera pose though. Therefore, the captured images are not registered based on their features, but rather they are rectified based on a common virtual camera pose, check Fig.7.2. That means, all captured images are projected onto a common image plane, that is of a virtual camera. i.e. As if all the images were taken by the camera from the same pose, the pose of the virtual camera. All the rectified images are, then, merged in a mosaic-fashion to form what is known as the "*stitched image*" while applying some masking and blending techniques to keep the final image as sharp and as clean as possible, which would be explained next.

### 7.2.1. 2D Planar Image Rectification

In computer vision, a *plane-induced homography* maps a set of points from one image to another only when these points, from the two images, share the same real-world plane [HZ03].

A homography is a linear transformation (i.e. a  $3 \times 3$  matrix transformation with 8 degrees of freedom) in which one image plane  $P$  can be moved to another image plane  $\hat{P}$  using the following transformation as shown in Eq.7.1.

$$\hat{P} = HP : H = \begin{bmatrix} h_{11} & h_{12} & h_{13} \\ h_{21} & h_{22} & h_{23} \\ h_{31} & h_{32} & h_{33} \end{bmatrix} \quad (7.1)$$

During the process of moving one image plane to another, a mapping from one image plane to the real-world plane is taking place, check Eq.7.2, where the scene's points, taken from a real-world 2D plane  $X, Y$  (assuming  $Z = 0$ ), are being transformed into the image plane  $u, v$ . The mapping from the 3D world to the 2D image can, hence, be also inverted as shown in Eq. 7.3.

$$\begin{bmatrix} u \\ v \\ 1 \end{bmatrix} = \Pi \begin{bmatrix} X \\ Y \\ Z \\ 1 \end{bmatrix} = [\pi_1 \ \pi_2 \ \pi_3 \ \pi_4] \begin{bmatrix} X \\ Y \\ 0 \\ 1 \end{bmatrix} = [\pi_1 \ \pi_2 \ \pi_4] \begin{bmatrix} X \\ Y \\ 1 \end{bmatrix} \quad (7.2)$$

$$\begin{bmatrix} u \\ v \\ 1 \end{bmatrix} = H \begin{bmatrix} X \\ Y \\ 1 \end{bmatrix} \Leftrightarrow \begin{bmatrix} X \\ Y \\ 1 \end{bmatrix} = H^{-1} \begin{bmatrix} u \\ v \\ 1 \end{bmatrix} \quad (7.3)$$

After the transformation from the real camera image plane to the real-world plane, now it is possible to map it once again onto the virtual camera image plane. The homography transforming from the real to the virtual image plane is given by Eq.7.4

$$H_{real \rightarrow virtual} = K_{virtual} \left( R - \frac{t n^T}{d} \right) K_{real}^{-1} \quad (7.4)$$

The intrinsic matrix  $K$ , Eq.7.5, is determined using the calibrated horizontal and vertical focal lengths in pixels  $f_u, f_v$  and the principal points  $c_u, c_v$ . The intrinsic parameters of the virtual camera need to be adapted to the increased size of the stitched image.

$$K = \begin{bmatrix} f_u & 0 & c_u \\ 0 & f_v & c_v \\ 0 & 0 & 1 \end{bmatrix} \quad (7.5)$$

The transformation from the measured real camera pose  $T_{real \rightarrow world}$  to the defined virtual camera pose  $T_{virtual \rightarrow world}$  is given by Eq.7.6:

$$T_{real \rightarrow virtual} = T_{virtual \rightarrow world}^{-1} T_{real \rightarrow world} = \begin{bmatrix} R & t \\ 0 & 1 \end{bmatrix} \quad (7.6)$$

Where  $t$  is the translation vector and  $R$  is the rotational matrix. The plane's equation with the plane's normal  $n$  given in the real camera coordinates and with the distance  $d$  from the real camera to the plane is written as in Eq.7.7:

$$n^T t_{real \rightarrow world} + d = 0 \quad (7.7)$$

It is necessary to keep in mind, that in order to run these transformations successfully, a camera calibration for the intrinsic and extrinsic parameters is, essentially, required. So, given the known distortion parameters as

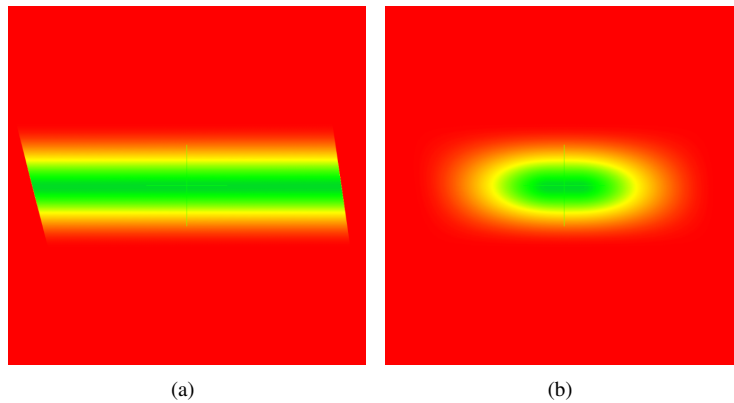


Figure 7.3.:  
(a) A depth-of-field (DOF) mask, (b) DOF mask with vignetting.

a result of the camera calibration, all the captured images would be corrected, subsequently, for any radial and tangential distortion. Images are, then, rectified when being transformed into the stitched image.

### 7.2.2. Depth of Field Masking and Vignetting

The non-sharp regions of the rectified images are masked out based on the depth of field (DOF), a volume projected onto the captured plane [vBTS\*22]. The DOF volume is a slice of the pyramidal FOV volume that lies between the near and the far planes. The mask is not binary since the sharpness decreases, rather, gradually. Check Fig.7.3, in which there are two masks, rectangular (a) and radial (b), where the dark green represents the very sharp focused part of the DOF, whereas the more the color changes toward yellow the less sharp it becomes. The radial mask exhibits the vignetting effect as well (i.e. gradual changes occur all along the edges).

The masked images are blended together into one stitched image using a weighted average method. The weighted average is the weighted sum of the images normalized by the sum of the weights. The weight of each pixel depends on its proximity to the center of the image. The farther a pixel is from the image center, the less it is weighted (vignetting effect).

## 7.3. Methodology

### 7.3.1. Technical Design

The technical nature of high-resolution scans imposes on us the use of a Macro lens sometimes. In addition to the technical design of our scanning system, which imposes yet another constraint regarding the geometry of the light in relation to the imaging system's optical axis. The system uses a light source directly attached to the camera lens' body, better known as a ring-light due to its design as shown earlier in Fig.7.1.

The ring-light is a ring varying in diameter with respect to the used lens, it has an opening in the middle where the camera lens fits in and where the polarization filter is to be mounted. The ring-light consists of tiny LEDs

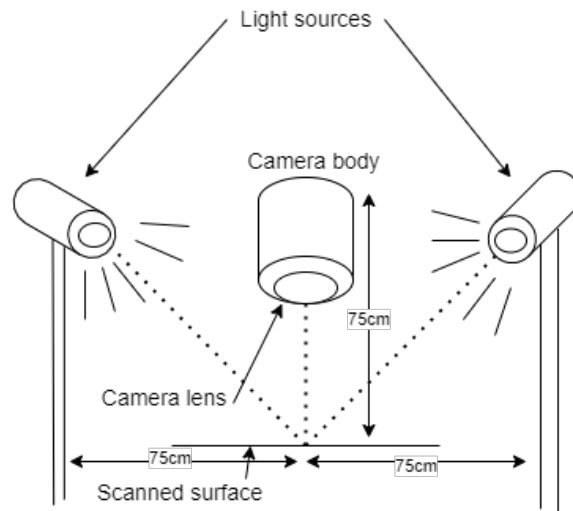


Figure 7.4.: Setup#1 to define a reference anchor measurements for color calibration and metric calculations.

fixed next to each other covering the whole surface area of the ring-light. The color correlated temperature (CCT) of the used LEDs is D50 [AHTR\*23] (Discussed under the research topic in Ch.6).

Because of the geometry between the ring-light and the imaging system, a set of polarization filters was necessary to deploy so as to cut out any direct and undesirable reflections and specularities that could obscure the photographed object. One circular polarization film is fixed on top of the ring-light directly (on top of the LEDs), and one circular polarization filter is fixed in front of the lens to create a complete cross-polarization effect [Hec02a, Shu62]. Cross-polarization has a non-negligible effect on the process of color calibration and hence on the accuracy of color, both in terms of the lightness and the chroma components depending on the scanned material [AHTR\*22] (Research paper in Ch.5).

A camera is fixed at the end-effector of a robotic arm. Finally, there is also a scanning table, better known as a turn-table, for it can be controlled by our software for rotational movement, on top of which the scanned object is to be placed and positioned.

### 7.3.2. Experiment

First, setup #1 Fig.7.4, we have prepared an anchor point to use as a reference and to compare against that complies more with the recommended ISO standards [ISO17] in terms of the light source (D50) and the scanning geometry  $0^\circ/45^\circ$  with no polarization filters. We have chosen the exposure parameters (aperture, shutter speed, and ISO number) based on a gray patch that has a  $CIELAB(L^*) \approx 65$ . Two external light sources were mounted on both sides of the scanning table and tilted nearly  $45^\circ$  towards the scanned target. Two color targets were selected for this experiment, namely X-Rite SG CC (#140 color patches) and NGT<sup>1</sup> v1.0 (#130 color patches).

Next, in setup #2 we removed the external light sources and mounted the ring-light on the camera lens returning the system to its default design, in which it usually operates, with all of the corresponding polarization filters in place. Look back at Fig.7.1.

<sup>1</sup>NGT: Next Generation Target. Available via <https://www.avianrochester.com/nextgentarget.php>

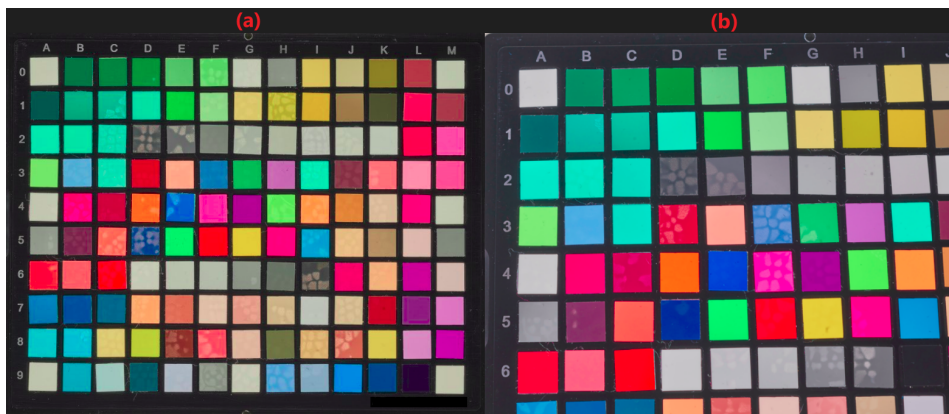


Figure 7.5.: The reflections NGT shows despite the cross-polarization setup by (left:a) a perpendicular scan  $0^\circ/90^\circ$  and (right:b) a  $0^\circ/75^\circ$  geometry. Reflections seem to be inevitable due to the strict geometry the ring-light and the camera has in relation to one another.

The NGT v.1.0 color target has a very reflective and shiny finish, which makes it with an orthogonal acquisition geometry with our setup ( $0^\circ/0^\circ$ ), even when it fits completely in the camera's FOV, impossible to scan cleanly in full even with a perfect cross-polarization fixed in place, also if the camera/ring-light were to be tilted at an angle (i.e. when the light shines directly towards the target at a perpendicular angle  $90^\circ$ , one can clearly see the reflections of some of the ring-light's LEDs), check Fig.7.5 – On the other hand, it is completely possible to scan X-Rite SG CC with the same setup with the help of cross-polarization eliminating by that all possible reflections completely.

For that reason, it is necessary for our system, whether we are using a normal 72mm lens or a 100mm Macro lens, to find another alternative to be able to scan the NGT color target rather cleanly and in a way that still guarantees color accuracy according to the ISO standards' level "A".

A stitching approach comes in very handy in this situation. By taking multiple images at a certain angle ( $45^\circ < \theta < 90^\circ$ ) so as to create one final image (mosaic) that contains the whole color target, while performing perspective correction to produce an ortho-image at the end. However, a couple of questions arise here:

- What about the color accuracy of such an approach?
- How much will the color calibration process be impacted?
- Would the color calibration result be any comparable to the standard approach  $0^\circ/45^\circ$ ?
- How viable is the resultant color correction to put in use?

We have decided, at this stage, to run extensive tests on a normal 72mm lens first before moving to the Macro setup as the problem of the reflections NGT-v1.0 color target depicts – when being scanned perpendicularly with our system, which is what we are trying to solve primarily- is independent of the lens type anyway, and the findings can easily be extended.

So to summarize the experiment's setup hardware:

- A PhaseOne iXG 100MP camera body with 72mm lens.
- Two external light sources with D50 CCT.
- A ring-light full of LEDs with D50 CCT - attachable to the camera lens.



- Brandless circular polarization film for the visible domain 380 – 780 nm - to be fixed in front of the ring-light.
- A Circular polarization filter (Marumi) for the visible domain 380 – 780 nm - to be fixed in front of the camera lens.
- An NGT v1.0 and an X-Rite SG CC color target<sup>2</sup>.

### 7.3.3. Data Acquisition

The camera white-balance was set first with the help of a neutral gray patch, and the exposure settings (aperture, shutter speed, and ISO number) were chosen based on a neutral gray patch, as well, that has  $CIELAB(L^*) \approx 65$  for both setups. The aperture was fixed to  $f/11$  and the ISO number to 100 always. In setup#2, the exposure was chosen so that the gray patch has  $CIELAB(L^*) \approx 65$  at an angle of  $65^\circ$ , for it turned out, heuristically, it yielded the best results while moving the camera across a color target while scanning it.

For data acquisition in setup #2, the robot was instructed to tilt at varying angles  $45^\circ \leq \theta < 90^\circ$  so as to capture the needed data for evaluation. Despite the fact that the NGT color target still shows some reflections if the angle is not steep enough, look at Fig.7.5.

At each angle, the algorithm will plan and decide the number of images required to capture based on the overlapping factor and the scanned surface diameter. Images were saved in their raw format (IIQ) to be converted later into 16-bit TIFF using COPE conversion engine that belongs to *CaptureOne*<sup>3</sup> software with no alteration that would inflict the raw data, to the most possible extent. The following parameters were used during the conversion process:

- Gamma: linear scientific curve.
- Input ICC: no color correction.
- Output ICC: ProPhoto RGB.
- Output format: 16-bit TIFF.

We chose to export the 16-bit TIFF and move from the camera ICC profile into a more standardized output ICC profile *ProPhoto RGB* rather than keeping only the camera profile embedded as the guidelines in [CHg17] says because the experiment implementation expects an Image in ProPhoto RGB color space. *ProPhoto RGB* preserves the original RGB color information and is more adequate to carry out the necessary color transformations related to the color calibration procedure [SGW00]. *ProPhoto RGB* fulfills as well the recommendations described by the ISO standards as a large color gamut larger than the calibration target itself [ISO17].

The exported TIFFs were stitched together after running homography and the perspective correction that were explained previously. The final mosaic stitched image was saved back in 16-bit TIFF with a ProPhoto RGB color profile embedded. At this stage, the image is ready for profiling.

The RGB values will be extracted out of each of the color patches for creating the corresponding ICC profile using *ArgyllCMS*<sup>4</sup>. Then, the resultant ICC profile (the color correction) will be applied to the TIFF image so we have a color-corrected image of the color target, Fig.7.6. We will, then, convert it into JPEG format while embedding the *ProPhoto RGB* as an output ICC profile. The image is now ready for the color evaluation and assessment by extracting the color values once again -after correction- and moving them from ProPhoto RGB into CIELAB color space using the appropriate formulae and the necessary transformations, check [Kan06b, Bru23], check the appendix A.4. An overview of the workflow is illustrated in Fig.7.7.

---

<sup>2</sup>Ground-truth CIELAB values were measured spectrally beforehand using a Barbieri spectrophotometer LFP qb for each.

<sup>3</sup><https://www.captureone.com>

<sup>4</sup><https://www.argyllcms.com>



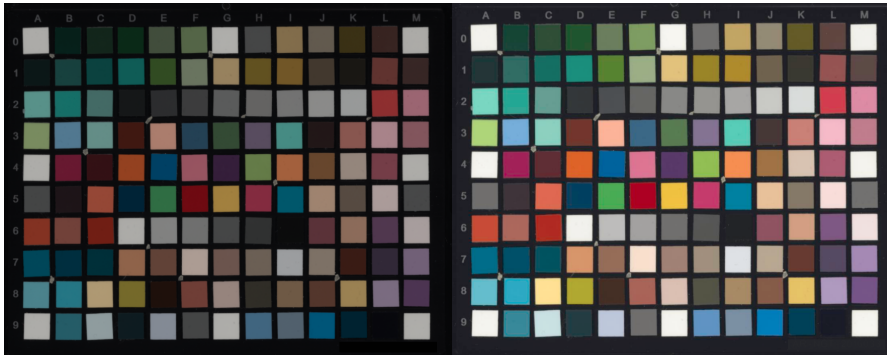


Figure 7.6.: Example of the end-mosaic stitched color target (NGT v1.0). Left: Gamma linear and before color correction. Right: After a successful color correction [Avg(DE00) = 1.23 and Max(DE00) = 4.15].

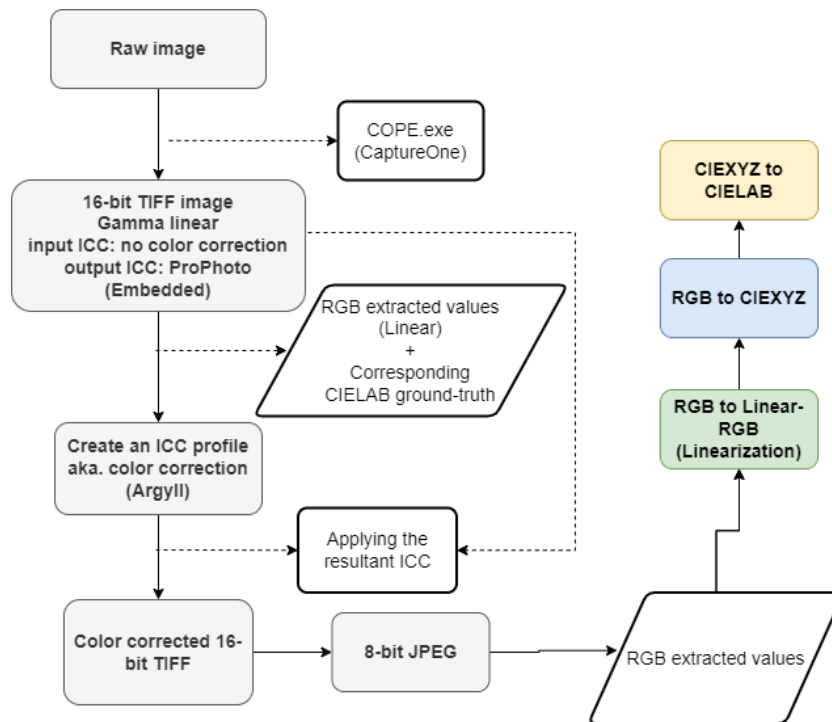


Figure 7.7.: An illustration of the steps of converting and moving color data from the raw format up, creating a color correction model, until the color correction takes place. Colors are, then, converted into CIELAB color space for calculating the color difference (DE00) after the color correction process has taken place.

## 7. Color Calibration Based on Mosaic Stitching of a Color Target as an Alternative to a Single-Shot Approach

NGT v1.0	ISO (A)	Angle/Overlap						65°/60	* 65°/50	* 65°/30	* 45°/60	† Single Shot 90°
		85°/60	85°/50	85°/30	75°/60	75°/50	75°/30					
DE00	mean ( $\leq 4$ )	1.08	1.06	1.19	1.17	1.18	1.19	1.12	1.12	1.12	1.23	1.04
	max ( $\leq 10$ )	4.35	4.45	4.51	4.06	4.28	4.28	4.17	4.18	4.31	4.15	4.05
RMS Noise	max ( $\leq 1.6$ )	1.43	1.49	1.77	1.49	1.5	1.57	1.01	0.98	1.01	0.72	0.4
WB DE(ab)	mean	1.11	0.99	1.06	1.2	1.22	1.23	1.06	1.1	1.08	1.18	1.12
	max ( $\leq 3$ )	3	1.73	2.88	2.67	2.69	2.75	1.9	1.9	1.9	1.9	2.87
TRC(L*)	min(-2)	-3.94	-5.05	-4.26	-3.18	-3.35	-3.48	-2.05	-1.82	-1.98	-1.49	-0.82
	max(+2)	1.73	0.78	1.31	1.44	2.27	2.27	1.33	1.46	1.41	1.46	0.43
Gain Mod.	min(0.7)	0.69	0.69	0.72	0.75	0.7	0.71	0.82	0.83	0.82	0.85	0.96
	max(1.3)	1.12	1.1	1.12	1.3	1.21	1.22	1.16	1.18	1.17	1.1	1.07

Table 7.1.: NGT v1.0 statistics of the stitched and perspective-corrected color target at different angles and with different overlap percentage ( $Angle^\circ/Overlap\%$ ) compared to the standard profiling (indicated by '†') that adheres more to ISO recommendations  $0^\circ/45^\circ$ . Columns marked with '\*' indicate the measurements that satisfy ISO level 'A' for color evaluation.

SG CC	ISO (A)	Angle/Overlap				† Single Shot 90°
		* 65°/60	* 65°/50	* 75°/60	* 85°/60	
DE00	mean ( $\leq 4$ )	1.03	1.03	0.95	0.99	1.05
	max ( $\leq 10$ )	4.44	4.29	4.25	4.15	4.31
RMS Noise	max ( $\leq 1.6$ )	0.48	0.49	0.41	0.34	1.27
WB DE(ab)	mean	0.93	1.02	0.74	0.99	0.86
	max ( $\leq 3$ )	2.06	2.83	2.21	3.12	2.29
TRC(L*)	min(-2)	-0.71	-0.71	-0.44	-0.75	-4.23
	max(+2)	1.01	1.07	0.79	0.6	0.87
Gain Mod.	min(0.7)	0.88	0.88	0.94	0.93	0.98
	max(1.3)	1.05	1.05	1.09	1.03	1.30

Table 7.2.: X-Rite SG CC statistics of the stitched and perspective-corrected color target at different angles and with different overlap percentage ( $Angle^\circ/Overlap\%$ ) compared to standard profiling (indicated by '†') that adheres more to ISO recommendations  $0^\circ/45^\circ$ . Columns marked with '\*' indicate the measurements that satisfy ISO level 'A' for color evaluation.

## 7.4. Result

Tables 7.1 & 7.2 show the statistics of the tested color targets after scanning at varying angles and with different overlapping factors/percentages, perspective correction, stitching, color profiling, and finally color correction. The header reads ( $Angle^\circ/overlap\%$ ). The tables show 5 different metrics to assess and evaluate the color correction process according to the ISO standards level "A" for photography and archiving systems [ISO20].

- DE00: color difference  $\Delta E_{2000}$ .
- RMS Noise: Root Mean Square Noise of a grayscale.
- WB DE(ab): White-Balance chroma difference of a grayscale.
- TRC(L\*): Tone Response Curve measured for the CIELAB(L\*) values of a grayscale.
- Gain Mod.: Gain Modulation describes the variation in the CIELAB(L\*) slope of the TRC(L\*).

The last column in both tables with the label "Single Shot" (indicated by †) is the statistics against which all the other measurements are to be compared and benchmarked. "Single Shot", setup #1, measurements were captured in complete accordance with the ISO standards, i.e. external light sources were mounted at nearly 45° angle relative to the scanned surface (0°), a camera was mounted orthogonal to the scanned surface with no polarization elements at all as shown earlier in Fig.7.4. Measurements that are indicated by "\*" are those that satisfy all the aforementioned ISO standards metrics in the table and fall within the ISO standards level "A", apart from the single shot.

In Tables 7.3 & 7.4, we are showing the statistics of testing the resultant ICC color correction on a different set of colors (different color target), different from the one was used for creating the color correction model. It shows the viability of putting the resultant ICC color correction profile in use for a different scan under the same conditions. More insights to follow next.

	Stitched Targets	NGT v.1 ICC		SG CC ICC		ISO (B)
	ISO (A)	NGT v.1	SG	SG	NGT v.1	
DE00	mean ( $\leq 4$ )	1.32	2.95	1.09	2.93	mean ( $\leq 5$ )
	max ( $\leq 10$ )	4.24	7.95	5.09	7.5	max ( $\leq 15$ )
RMS Noise	max ( $\leq 1.6$ )	1.07	3.11	0.52	2.82	max ( $\leq 2$ )
WB DE(ab)	mean	1.17	1.6	0.99	1.48	max ( $\leq 4$ )
	max ( $\leq 3$ )	1.88	5.48	3.16	5.39	
TRC(L*)	min(-2)	-2.76	0.8	-0.71	-6.2	min(-3)
	max(+2)	1.49	6.94	1.38	-0.21	max(+3)
Gain Mod.	min(0.7)	0.81	0.91	0.9	0.68	min(0.6)
	max(1.3)	1.14	1.19	1.11	1.16	max(1.4)

Table 7.3.: Extra tests and validation. Scanning both color targets (NGT v.1 and X-Rite SG CC) under the same conditions, then stitching both of them and creating an ICC color correction profile for both, and finally testing each of the created ICC profiles on the other color target as shown in the table.

## 7.5. Discussion

It is evident that even when a color target has to be stitched, homographed, and mosaicked from multiple images to form one image with an orthogonal view (Fig.7.6), it is still possible to fulfill the ISO standards level "A" in terms of color accuracy reproduction. However, one needs to pay attention to other metrics other than just looking at the color difference (DE00) mean and max values. For instance, looking at Table 7.1, for the NGT target, one notices an increase in the *RMS Noise* when the angle gets closer to 90° moving from 0.72 at 45°/60 up to 1.49 at 85°/60 (noise is nearly doubled). The White balance chroma difference also undergoes a noticeable change from a max value of 1.9 at 45°/60, 65°/50 and 65°/30 to 3.0 at 85°/60. The tone response curve (TRC) gets worse and worse the closer the angle to 90°, as well, which is reflected in the gain modulation<sup>5</sup> especially in the min value that is deviating farther away from 1.0. X-Rite SG CC shows less significant changes, though, in comparison to the NGT v1.0 target when varying the angle.

<sup>5</sup>Gain modulation value should be ideally 1.0 for all gray patches.

	Single Shot	NGT v.1 ICC		SG CC ICC		ISO (B)
	ISO (A)	NGT v.1	SG	SG	NGT v.1	
DE00	mean ( $\leq 4$ )	1.04	2.25	0.92	2.27	mean ( $\leq 5$ )
	max ( $\leq 10$ )	3.97	6.22	3.43	6.68	max ( $\leq 15$ )
RMS Noise	max ( $\leq 1.6$ )	0.38	0.81	1.52	1.06	max ( $\leq 2$ )
WB DE(ab)	mean	1.13	0.72	0.61	1.09	max ( $\leq 4$ )
	max ( $\leq 3$ )	2.87	1.32	1.41	1.6	
TRC(L*)	min(-2)	-0.64	-1.27	-4.95	-2.69	min(-3)
	max(+2)	0.44	1.19	1.22	1.1	max(+3)
Gain Mod.	min(0.7)	0.94	0.98	0.99	0.82	min(0.6)
	max(1.3)	1.06	1.08	1.3	1.29	max(1.4)

Table 7.4.: Extra tests and validation under standard geometry  $0^\circ/45^\circ$ . Scanning both color targets (NGT v.1 and X-Rite SG CC) under the same conditions, then creating an ICC color correction profile for both and testing each of the created ICC profiles on the other color target as shown in the table.

It is worth noticing that, even the used anchor point "*Single Shot*" -for this experiment- that is more conforming with the ISO standards with respect to the geometry, the capturing and profiling procedures, it is still challenging to completely fulfill all the specified metrics within the defined thresholds and limits. For instance, for the X-Rite SG CC the value  $\min(TRC(L^*)) \approx 4.2$  is quite out of the defined limit for the ISO standards level "A". One of the grayscale patches, namely *J6* with a reference value of  $CIELAB(L^*) \approx 89$  is being mapped, while profiling, into  $CIELAB(L^*) \approx 93^6$  –even using another ICC profiling software for proof-checking, a similar error shows up, however, for a different gray patch this time (i.e. Using *BasICColor input* to create an ICC profile, it would map the patch *E5* a little bit higher throwing it also outside the ISO standards level "A" tolerance threshold  $E5 : 96 \rightarrow 98.5$ ). On the other hand, no such problem would occur when we use our approach of scanning, stitching, and profiling a mosaicked image of the SG color target.

Looking at the NGT "*Single Shot*", it shows a noticeable chroma difference (measuring neutrality), in *WB – DE(ab)*, of 2.87. While if the NGT is to be scanned at an angle and stitched it shows better neutrality that amounts to only 1.9 for the measurements that fall within the ISO level "A" limits.

Our approach of stitching and profiling proves to deliver better color correction statistics that are closer to the ISO recommendations for the highest level (level "A"), especially for a challenging color target such as the NGT color target that requires very careful lighting setup and scanning geometry. Otherwise, it is impossible to scan cleanly without undesirable shiny reflections.

Tables 7.3 and 7.4 show the results of different sets of tests and validation that have been conducted for both approaches *Single Shot vs. our stitching mosaic approach*.

Table 7.3 shows the results for our stitching approach illustrating its viability of using the resultant color-correction on another scan under the same conditions. After capturing both targets -NGT v.1.0 and X-Rite SG CC- using the aforementioned and described method -of taking multiple images of the intended color target and then stitching them together in a mosaic fashion to form one complete image of the scanned color target- each of the color targets was used to produce a color-correction ICC profile (training data). Then, the resultant ICC

<sup>6</sup>Different experimental data with lower exposure settings –lower than recommended- showed more conformant statistics with the ISO standards level "A" where all the metrics are within the defined tolerance

color-correction profiles would be applied and validated on the other stitched color target (testing data). i.e. The ICC color-correction profile created using the NGT target would be validated on the X-Rite SG CC target and vice versa. In Table 7.4 the recommended standard approach was followed using a "single shot" with a geometry  $0^\circ/45^\circ$  to create and validate the ICC color-correction profiles.

The two Tables 7.3 and 7.4 show very similar trends and almost very comparable results. By looking, for instance, at the color difference  $DE_{00}$  our stitching approach shows a slight increase in the mean and max error, where the mean is moving up to  $\approx 3.0$  and the max up to nearly  $\approx 7.5 - 8.00$ , whereas for the single-shot approach the error for the mean( $DE_{00}$ ) is moving up to  $\approx 2.25$  and the max up to  $\approx 6.5$ .

The more noticeable change is affecting rather the grayscale patches, which are more sensitive to light fall-off and direction. For instance,  $\max(TRC)$  goes up to nearly  $\approx 7.0$  when correcting the stitched SG CC target using the ICC profile of the stitched NGT v.1.0 target, and that is caused by the dark patches of the grayscale like (J5) being mapped/corrected to have  $CIELAB(L^*) \approx 10.0$  while its reference value measures to  $CIELAB(L^*) \approx 17.0$  resulting in  $\Delta L^* \approx 7.0$ . The neutrality of the grayscale patches is also affected when correcting one stitched target using the other and that is apparent by observing the chroma components  $DE(ab)$  that moves up to  $\approx 5.5$ . Keep in mind also the effect of using cross-polarization filters on colors that was discussed in Ch.5.

Keep in mind that, the grayscale patches are very sensitive to the light direction, fall-off, and distribution. In addition to the fact that using a stitching approach (composing a color target out of multiple and different images with different light fall-offs) can be challenging regarding choosing the parts that need to be stitched, and choosing the appropriate algorithm for averaging for example. It has been also proven while experimenting that, the NGT v.1.0 target is less challenging and less tricky than the X-Rite SG CC target while scanning and profiling, especially when it comes to their grayscale accuracy reproduction, and that could be due to many factors, one of them is the nature of their texture and the finish the target depicts. In addition to the distribution of these patches across each of the targets and hence the light fall distribution.

## 7.6. Conclusion

Taking multiple images at an angle different from  $90^\circ$  of a color target and then correcting for their different perspectives, and then stitching only the sharp and clear parts of them together to form one mosaic clean image with an orthogonal view, that is to be used for color profiling, can, with careful attention, pass ISO level "A" (i.e. the highest) in terms of color reproduction and accuracy.

The NGT color target (v.1.0) has a very reflective finish that makes it impossible to scan in an orthogonal manner when the light source and the imaging system share the same plane, even with perfect cross-polarization in place, the target still shows undesirable and visible reflections. Hence, scanning such kind of a color target (material) by capturing multiple images at a certain angle  $45^\circ \leq \theta < 90^\circ$  and stitching the clean parts only into one mosaicked image seems to be a very practical solution that yields very comparable results (in some cases even better) to that if the target were to be scanned and profiled in accordance with the ISO standards recommendations (i.e. Single shot with  $0^\circ/45^\circ$  geometry) as the statistics above can testify.

Our proposed stitching approach shows that the resultant ICC color-correction profile is very viable to use for color correction as it was shown in Table 7.3. However, it is advised to pay extra care and attention if the scanned material/object is composed of mostly gray shades, which could be more sensitive to light fall-off. In addition to the care that needs to be taken while using polarization filters anyway.

Furthermore, Our stitching and calibration approach produces very similar and comparable outcomes to the usual reconstructed 3D surface/texture, for the proposed stitching approach resembles the mosaicking technique, used in photogrammetry and other image-based 3D reconstruction software, for texturing 3D models. This makes

our approach very promising for color-correcting 3D objects that is still an area of research and is considered very challenging so far to run color correction accurately on 3D surface textures due to the (arbitrary) geometry of the objects usually and how usually fixed lighting setups would interact with the object's curvature and illuminate it in an uneven way.

Our system and technique of scanning uses a ring light attached to a moving camera and extracts only the sharp and well-lit parts from each captured image, thus ensuring comparable lighting conditions across all the extracted image parts during the whole scan of a 2D/3D object. As a result, we are able to compose at the end a homogeneous mosaic texture featuring an overall even light distribution that makes color-correcting for a texture of a 3D model more applicable.

## 8. Conclusions and Future Work

Light polarization is a widely known phenomenon that has many applications as seen in Ch.1.1 ranging from dentistry, HDR imaging, forensics, rocks and minerals digitization to cultural heritage artifacts photography and virtual museums. In spite of the wide range of its applications, all the existing research in the literature addresses only the benefits of using polarization filters in photographing and scanning objects, while they overlook one very important element of imaging and that is **color**. Several researchers mention, indeed, the process of color calibration while using polarization filters and report back the color difference of their color correction model in terms of  $\Delta E00$ , which is usually within the acceptable limits and seems to be quite low. However, they fail to make the distinction and the comparison between the colors' behavior and the  $\Delta E00$  **before** and **after** using polarization filters shedding the light on how much deviation, possibly, colors undergo when they go through polarization filters. Hence, they fail to address whether polarization filters have a non-negligible impact on color reproduction itself or not, both in terms of chroma and lightness.

We have taken it upon ourselves, in this work, to investigate and understand the impact of polarization filters on colors, primarily on grayscales, so as to answer vital questions that are of great concern in any attempt for faithful and accurate digitization and imaging such as in the cultural heritage sector, among others. We have started by asking ourselves fundamental questions as presented earlier in Ch.1.2 like:

- How much, if at all, the color components -chroma and lightness- are affected and influenced by polarization filters?
- Is the light source affected, if at all, by polarization filters? if so, in which way and how much?

We explored the first question, which is the backbone of **RQ1**, in Ch.5 and showed by graphs and in numbers how cross-polarization filters have a big impact on grayscale reproduction in a negative way both in terms of Chroma/neutrality, lightness, and linearity. We showed how cross-polarization could be the reason behind losing certain shades (black shades), making those color data irretrievable, which is the main reason behind breaking the linearity of a linear grayscale ( $CIELAB(L^*) \approx 5 \rightarrow 95$ ). We showed, as well, how cross-polarization causes a shift in the *lightness* color component in a way that would make the overall perception of the colors look less lustrous and more washed-out. Finally, we showed how cross-polarization adds a certain tinge to neutral colors (grayscale) causing a few patches to look more reddish or greenish. The impact of cross-polarization was studied on two different materials, matt and (semi-) glossy, and we showed that most of the aforementioned problems are affecting both but in different ways. Of course, all the analysis was carried out after running color calibration on the data using two different color targets with two different finishes, matt, and semi-glossy obviously.

The inspection and the color analysis of polarized colors showed that despite having a low  $\Delta E00$  color difference upon color calibration, visually some colors look quite different from their original counterparts (i.e. without polarization). The knowledge of this chapter is of utmost importance to any work that involves and aims for faithful surface color acquisition and reproduction, such as in the cultural heritage sector, for example.

The findings have proved to contradict and refute the common misconception that polarization filters do not alter colors or affect them in any negative way, and such filters only make colors look more saturated and stretch their dynamic range while lowering the light intensity no more.

Then in Ch.6, answering **RQ2**, we investigated the influence and the impact of cross-polarization filters on the light source itself, and how possibly that would alter the light's behavior, if at all, in terms of color and its white-point (WP), which is directly related to and expressed as the light's color-correlated temperature (CCT). The widely accepted assumption, even among professionals and some experts, is that polarization filters only force the light to oscillate in a certain direction and block any non-conforming oscillations. Consequently, reducing the light intensity only, which is fundamentally true. However, our findings have shown clearly in numbers how the light source's CCT/WP is impacted, as well, and shifted depending on the quality of the polarization filter in use. Our statistics showed how the light source's chroma components *CIELAB(ab)* start to diverge from their neutrality, and they undergo rather a big change that amounts to  $\Delta E \approx 7.3$  in worst case scenario and to  $\Delta E \approx 3.5$  in the best case, which should not be neglected at all, as this will have a direct influence on how surface colors would be rendered under such kind of light after all. The corresponding change in the light source's CCT amounts to  $\approx 360 K$  in the worst-case scenario, shifting the light source from being  $D50 = 5000 \rightarrow 4576$ . As a result, more attention and awareness to how polarization filters change a light source's *CIELAB* values, hence affecting its CCT/WP, must be paid. When we talked to some of the representatives of the big brands in the industry manufacturing polarization filters, they assured us that polarization filters would not alter the light source's CCT/WP in any way and should not have any negative impact on shifting colors as these kinds of filters are wavelength-invariant. However, the statistics and our experiments on several polarization filters did not agree with them, unfortunately, and tell another story. So we wish that the manufacturers take it upon themselves to produce rather more neutral polarization filters that align better with their claims and to help with the strive toward accurate color acquisitions in critical applications and photography for which the use of polarization filters is indispensable and crucial.

In Ch.7, answering **RQ3**, we came across two problems. One is that, certain surfaces are hard to capture with our lighting setup ( $0^\circ/0^\circ$ ; camera/light) and impossible to cut off reflections using only cross-polarization filters due to the surface finish that is highly reflective. Two, trying to address and push toward 3D color calibration and standardization as it is something still very challenging, not standardized, and not addressed enough in the literature. To solve both problems, we came up with a novel technique for running the color calibration process based on mosaic stitching instead of a single-shot calibration (the standard way). We proved in our experiment by presenting the data and the statistics that using our new technique we are able to fulfill the highest *ISO* level (level A) in terms of color accuracy for cultural heritage digitization and photography according to *ISO 19264-1* [ISO20]. Our proposed technique is based on choosing only the clearest and the perfectly well-lit part of each image we capture and then stitching it with its neighboring parts from other images until we have a full representation of the object intended to scan, in a similar fashion to the construction of a *UV*/texture map for 3D models. Using our technique, it is guaranteed that every single part of this mosaic image has the same light intensity and is evenly illuminated as the rest of the image regardless of the curvature of the scanned object (2D/3D), paving the way toward the possibility to ensure, as well, that the surface color representation of a 3D *UV*/texture map is homogeneous, and it represents the actual colors of the real object. Our proposed method was very welcomed by the Society of Cultural Heritage and Imaging as it has received good attention with the eyes looking forward to establishing rigid foundations for the problem of 3D color calibration, hoping that this is the first milestone down the road.

All of the analysis and the data capturing that helped in conducting this body of research would not be possible without the design and the successful implementation of a fully functional color management system, as well as the "exposure algorithm" we developed that is capable of assisting in determining and proposing adequate camera exposure parameters for best data acquisition while taking the camera and the lighting conditions into account. Answering **RQ4** and building a color management system from the ground up was an essential part of the development of the whole system that runs *CultArm3D* technology, so that the image data, especially regarding color, are processed and controlled fully by the *CultArm3D* software from the moment the data capture



---

happens, going through the image raw data processing, creating a color correction profile, applying and validating this color correction model, up to the final stage of saving a color corrected image in the intended format and color space (e.g. 8-bit sRGB JPEG) that are ready for further processing like 3D photogrammetry in order to build a 3D digital model. The color management pipeline helps as well in the preparation of the color data in the proper format for the later step, which is 3D printing taking into account how the 3D printer would expect the data to be (encoded in a certain color space) and then prints accordingly. Otherwise, the printed colors and the quality would not match what one intends to print, hence failing the whole concept behind the technology *CultArm3D*. The 3D printing step is a whole research on its own and beyond the scope of this research, though it will be described briefly next.

The aim of this research was to, first, implement a functional color management system and integrate it with the *CultArm3D* software. Second, to understand the influence and the impact of using (cross-) polarization filters on color accuracy and color calibration when scanning objects. Last but not least, to be able to 3D print an actual replica of any scanned object with high color fidelity and accuracy. So at the end of this research, we ran a few primary tests regarding 3D printing with very successful and promising results. We scanned a 2.5D painting and managed to 3D print it using *Stratasys J826*, which was newly acquired by Fraunhofer IGD. With the help of the 3D Printing Technology department at Fraunhofer IGD, we analyzed and understood the behavior of the 3D printer first, so we were able at the end to achieve a high printing color accuracy. An example of the tested object with the 3D printed replicas can be seen in Fig.8.1. In the figure, one sees the original 2.5D painting (top), and two 3D printed and color-calibrated replicas with (bottom-left) and without (bottom-right) polarization. The very first impression upon having a glance, it is clear how colors get more saturated when polarization filters are in use (bottom-left).

In Fig.8.2 we zoom in on one part of the painting in order to understand the differences between all three cases. Looking at the blue areas that are highlighted by the numbers (1) and (2), we notice how the cyan color (1) in the original painting looks dull and muddy while in both scanning techniques, with and without polarization, the cyan color gets much lighter in its tone and yet moreover in the polarization case the color gets brighter. The dark blue under number (2) in the original is very dark and deep. Whereas in the unpolarized case, it has a brighter tone color of blue, while in the polarized case, it is quite dark and almost getting on the verge of being navy blue especially because of the high contrast the polarization filters are causing between the cyan blue and dark blue (contrast effect). Now, if we look at area number (3), originally the color is supposed to look like muddy dark red, which is almost replicated quite well in the unpolarized case. Whereas in the polarized case, despite being also muddy dark red it appears to be slightly brighter in comparison, which is giving a different feel to the color (also the brightness in neighboring colors plays a role in how a certain color in the vicinity would be perceived). Finally, we are looking at the green color next to area number (4) for which the original green looks bright on its right side and dark and muddy on the rest of it. In the unpolarized case, it looks adequately dark green while losing the brightness on the right side of it. Whereas in the polarized case, the green is getting brighter in tone overall – look as well to the green stroke next to area number (3) and notice how the green is brighter in the polarized case.

Overall, the problem with polarization originates from the fact that it affects the contrast between colors drastically - stretching the dynamic range-. Hence, it gives rather an artificial feel to the overall experience when colors are being looked at. It drags down dark colors to make them much darker, in this case the dark blue for instance. Whereas it adds quite unbalanced lightness to light colors while pushing their chroma making them appear too saturated and too bright, just like what happened to the cyan color and the red color in the discussed painting above. In the unpolarized case, the harmony between the color tones is better preserved despite some changes in some color tones, but that is very likely due to the 3D printer capability rather than to the actual scan. However, delving into the details is not within the scope of this dissertation and is left for future work.



Figure 8.1.: Top: Original 2.5D painting. Bottom-left: 3D print of the original painting using cross-polarization scanning technique. Bottom-right: 3D print of the original painting using standard scanning geometry  $0^\circ/45^\circ$ . All scans were color calibrated and corrected in *sRGB* color space

---

The observations above, on how polarization is affecting colors, are basically a confirmation of the findings of this body of research that polarization filters have a non-negligible effect on both color components, lightness  $CIELAB(L^*)$  and the chroma  $CIELAB(a^*b^*)$ .

Finally, one must keep in mind that 3D printers usually have a limited and small color gamut, as they usually operate and print exclusively in  $sRGB$  color space, which is the smallest color gamut out there, and many colors may be out of reach. Using  $sRGB$  to render such painting or any other would, inevitably, shift some colors that would exist and be rendered perfectly better in either *Adobe or ProPhoto RGB*, while they would have to shift around and accommodate the availability of such color shades or find the closest in  $sRGB$ , which would cause such colors to appear, possibly, brighter and less Chromatic in their tones (getting closer to the center of the xy-Chromaticity diagram). In addition to the nature of the used materials for printing that must not be forgotten and removed from the equation.

In the end, we were left with some open questions and a new research quest to explore regarding 3D replication, color accuracy print, and how polarization filters may affect the quality of a 3D print. The challenge in 3D printing is twofold: first, the color gamut of the printer itself and the restrictions it imposes on the available range of colors to use and the type of material. Second, how the  $UV$ /texture map would be, best, sliced and printed so that the surface color at all points is a very close match to the original under any arbitrary or specific illumination condition.

We hope that these findings will help people and researchers better understand how polarization filters impact surface colors, light, and the process of color calibration. We hope, as well, that our research will lay the foundations for the standardization of 3D color calibration, opening the door to solving one of the big challenges in color science and digitization.

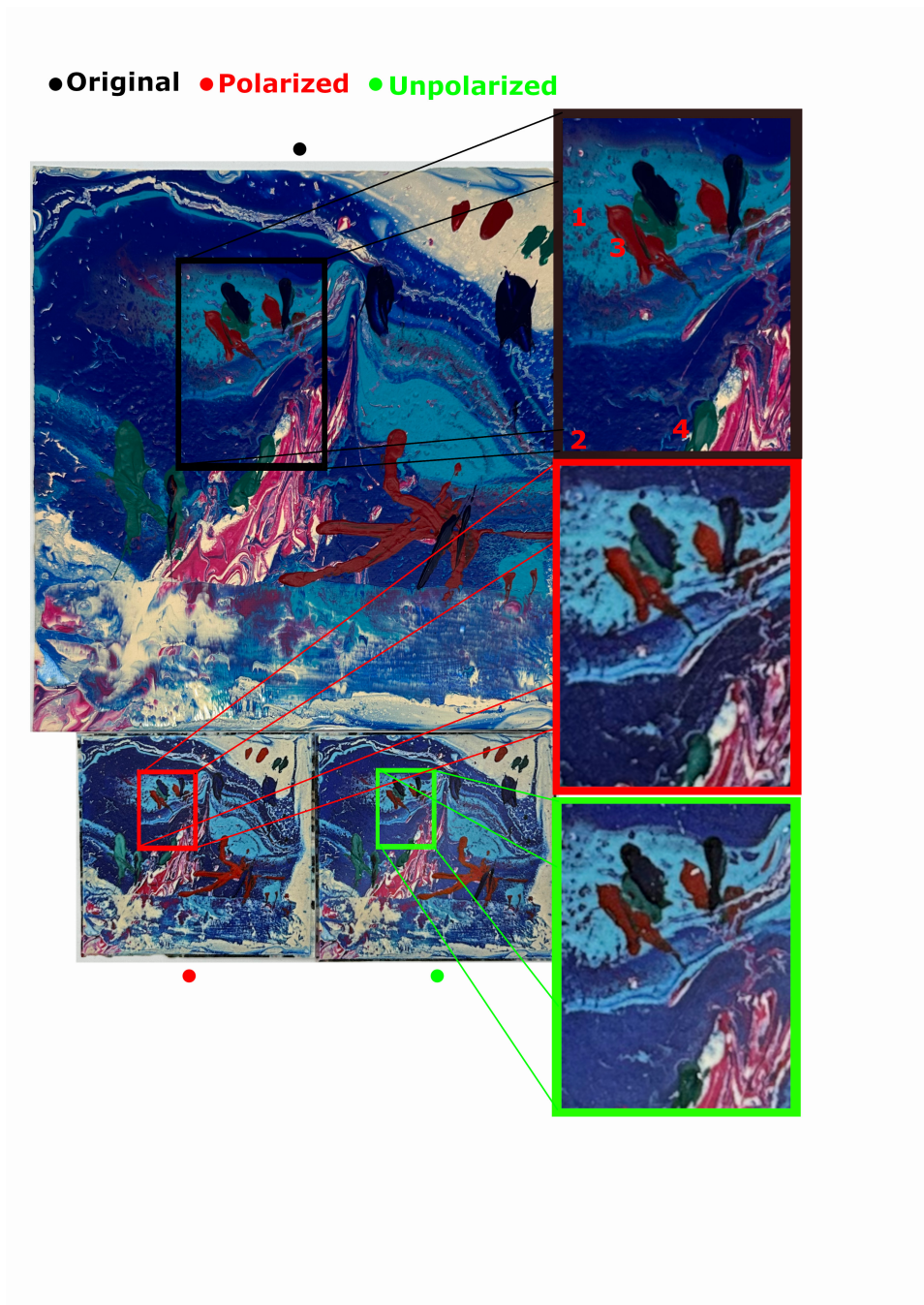


Figure 8.2.: zoom in on 3 2.5D paintings. Top is the original, and the two on the bottom are 3D-printed replicas, left is polarized, right is unpolarized.

# A. Appendix

## A.1. CIEDE00 - Color Difference

Here is the set of formulae that describes how to calculate the color difference DE2000 ( $\Delta E00$ ). This metric was used in this research to quantify and calculate the color difference between any two colors that are in CIELAB color space.

$$\Delta E00 = \sqrt{l^2 + r^2 + k^2 + R_T r k} \quad (\text{A.1})$$

Where:

$$t = \frac{\Delta L'}{K_L S_L}, \quad r = \frac{\Delta C'}{K_C S_C}, \quad k = \frac{\Delta H'}{K_H S_H} \quad (\text{A.2})$$

$$\Delta L' = L'_1 - L'_2 \quad (\text{lightness difference}),$$

$$\Delta C' = C'_1 - C'_2 \quad (\text{Chroma difference}),$$

$$\Delta H' = 2\sqrt{C'_1 C'_2} \sin(d),$$

$$d = \frac{\Delta h'}{2}$$

$$h' = \begin{cases} 0 & b^* = a' = 0 \\ \tan^{-1}\left(\frac{b^*}{a'}\right) & \text{otherwise} \end{cases}$$

$$\Delta h' = \begin{cases} 0 & C'_1 C'_2 = 0, \text{ otherwise} \\ h'_1 - h'_2 & |h'_1 - h'_2| \leq 180 \\ (h'_1 - h'_2) - 360 & (h'_1 - h'_2) > 180 \\ (h'_1 - h'_2) + 360 & (h'_1 - h'_2) < -180 \end{cases}$$

$$\bar{h}' = \begin{cases} h'_1 + h'_2 & C'_1 C'_2 = 0, \text{ otherwise} \\ \frac{h'_1 + h'_2}{2} & |h'_1 - h'_2| \leq 180 \\ \frac{h'_1 + h'_2 + 360}{2} & |h'_1 - h'_2| > 180; (h'_1 + h'_2 < 360) \\ \frac{h'_1 + h'_2 - 360}{2} & |h'_1 - h'_2| > 180; (h'_1 + h'_2 \geq 360) \end{cases}$$

$$a' = (1 + G)a^*,$$

$$G = 0.5 \left( 1 - \sqrt{\frac{C_{ab}^{*7}}{C_{ab}^{*7} + 25^7}} \right),$$

$$C_{ab}^* = \sqrt{(a^*)^2 + (b^*)^2},$$

$$\bar{C}_{ab}^* = \frac{C_{ab,1}^* + C_{ab,2}^*}{2},$$

$$C' = \sqrt{(a')^2 + (b')^2}$$

$$S_C = 1 + 0.045\bar{C}',$$

$$S_L = 1 + \frac{0.015(\bar{L}' - 50)^2}{\sqrt{20 + (\bar{L}' - 50)^2}},$$

$$\bar{L}' = \frac{L_1^* + L_2^*}{2},$$

$$S_H = 1 + 0.015\bar{C}'T,$$

$$T = 1 - 0.17\cos(\bar{h}' - 30)$$

$$+ 0.24\cos(2\bar{h}')$$

$$+ 0.32\cos(3\bar{h}' + 6)$$

$$- 0.20\cos(4\bar{h}' - 63)$$

$$\begin{aligned}R_T &= -\sin(2\Delta\theta)R_C, \\R_C &= 2\sqrt{\frac{\bar{C}^7}{\bar{C}^7 + 25^7}}, \\ \Delta\theta &= 30 \exp\left(-\left[\frac{\bar{h} - 275}{25}\right]^2\right)\end{aligned}$$

## A.2. COPE - Command Line Executable

The following screen shot, Fig.A.1, shows the list of commands available to use through *COPE.exe* raw image conversion engine made available by *CaptureOne™*. We have used *COPE.exe* to convert the raw images captured by *PhaseOne* camera into *16-bit TIFF* formats. The converted images, in this research, must be minimally processed so to keep the original captured data intact as much as possible. Here is an example of the used command:

```
COPE.exe input_raw_image_IIQ output_decoded_image
-outputformat=tif
-bits=16
-filmcurve="PhaseOneIXG100MP-Linear Scientific.fcrv"
-inputprofile="Phase One Effects - No color correction.icm"
-outputprofile="ProPhoto.icm"
```

```
D:\PhaseOne\COPE>COPE.exe -help
COPE version 10.1.2.7
Usage :
COPE <input[,inputDir] | inputDir> <output[,outputDir] | outputDir> [options...]

o : required value
[] : optional value
| : alternative value
n : integer number
f : floating point number

Options :
Name                Default      Range          Notes
[-outputprofile=<file>]    embed
[-outputformat=<value>]  tif          'jpg', 'tif', 'j2k', 'jxr', 'dng', 'png', 'psd', 'jpg80', 'lcc'
[-jgquality=<n>]          100 (max)    0 to 100
[-tifcompression=<value>] none         'none', 'lzw' or 'zip'
[-resolution=<n>]        300         ?
[-resolutionunit=<value>] inch         'inch' or 'cm'
[-bits=<n>]               8           8 or 16
[-lccskipDustRemoval=<n>] 0           0 or 1          Changes how LCCs are created. Skips dust removal which is a slow process
[-lccTechnicalCamera=<n>] 0           0 or 1          Changes how LCCs are created. Includes analysis for technical wideangles
[-inputprofile=<file>]    Camera specific
[-filmcurve=<file>]      Camera specific
[-scale=<f>]             1           0.1 to 2.5
[-orientation=<n>]       0           steps of 90
[-rotation=<f>]          0.0        0.0 to 360.0
[-keilvin=<f>]           as shot     800.0 to 14000.0
[-tint=<f>]              as shot     -50.0 to 50.0
[-exposure=<f>]          0.0        -2.5 to 2.5
[-brightness=<f>]       0.0        -50.0 to 50.0
[-contrast=<f>]         0.0        -50.0 to 50.0
[-saturation=<f>]       0.0        -100.0 to 100.0
[-levelHighlight=<f>]   1.0        0.0 to 1.0
[-levelShadow=<f>]     0.0        0.0 to 1.0
[-levelHighlightG=<f>]  1.0        0.0 to 1.0
[-levelShadowG=<f>]    0.0        0.0 to 1.0
[-levelHighlightB=<f>]  1.0        0.0 to 1.0
[-levelShadowB=<f>]   0.0        0.0 to 1.0
[-levelHighlightR=<f>]  1.0        0.0 to 1.0
[-levelShadowR=<f>]   0.0        0.0 to 1.0
[-targetHighlight=<f>]  1.0        0.0 to 1.0
[-targetShadow=<f>]    0.0        0.0 to 1.0
[-midtoneR=<f>]        0.0        0.0 to 1.0
[-midtoneG=<f>]        0.0        0.0 to 1.0
[-midtoneB=<f>]        0.0        0.0 to 1.0
[-midtone=<f>]         0.0        0.0 to 1.0
[-highlightRecovery=<f>] 0.0        0.0 to 100.0
[-shadowRecovery=<f>]  0.0        0.0 to 100.0
[-clarity=<f>]         0.0        0.0 to 100.0
[-CNRAmount=<f>]        Camera specific 0 to 100
[-noiseReductionAmount=<f>] Camera specific 0 to 100
[-SurfaceSmoothnessAmount=<f>] Camera specific 0 to 100
[-CleanLongExposureAmount=<f>] Camera specific 0 to 100
[-USMAmount=<f>]        Camera specific 0 to 1000
[-USMRadius=<f>]        Camera specific 0.2 to 2.5
[-USMThreshold=<f>]    Camera specific 0 to 12
[-moireAmount=<f>]     0.0        0.0 to 100.0
[-moireRadius=<n>]     8           0 to 80
[-lcc=<file>]          none
[-style=<file>]         none
[-ignoreSettingsFile=<n>] 0           0 or 1          Will not attempt to use the input image's settings file
[-writeSettingsFile=<n>] 0           0 or 1          Will write a settings file that Capture One can open. An existing settings file will be overwritten
[-defaultTingine=<n>]    9           6, 7, 8 or 9   Value will be used if there are no settings for the image to create default variant.
[-enableOpenCL=<n>]    0           0 or 1          Allows usage of OpenCL pipeline if possible
[-hotfolder=<n>]        0           0 or 1          Scan input folder and process images, that come there instantly
[-hotfolderProcessed=<folder>] Processed
[-hotfolderPollRate=<n>] 500        0 to 3000     Hotfolder-polling interval in milliseconds
```

Figure A.1.: COPE raw converter engine list of commands for converting PhaseOne IIQ raw images



## A.3. Argyll - ICC Profiler

*Argyll* is called through *colprof.exe* and used to create *ICC* color correction profiles after collecting and arranging the necessary data. *Argyll* requires the ground-truth of the measured data (colors) in *CIELAB* color space as well as the corresponding percentage of the *RGB* camera response to those colors. *Argyll* offers several possibilities to create a color correction model, for example based on gamma curves, matrix-based or a look-up table (*LUT*). Here is an example of how we used *Argyll* in this research, the chosen parameters heuristically proved to yield the best results:

```
colprof.exe -V -Z a -qh -al -R -ua -bh
```

where:

- V: for verbose.
- Za: for intent absolute colometric.
- qh: for quality high.
- al: for algorithm based on *CIELAB* *cLUT*.
- R: for some restrictions on the white, black and primary values to be more compatible.
- ua: for forcing absolute intent for input profiles.
- bh: for high quality *B2A* table.

```

i:\cuba\hatten\Argyll_V2.1.2\bin\colprof.exe
Create ICC profile, Version 2.1.2
Author: Graeme W. Gill, licensed under the AGPL Version 3
Diagnostic: Too few arguments, got 0 expect at least 1
usage: colprof.exe [-options] infile
-v          Verbose mode
-A manufacturer Manufacturer description string
-M model    Model description string
-D description Profile Description string (Default "infile")
-C copyright Copyright string
-Z tmb      Attributes: Transparency, Matte, Negative, BlackAndWhite
-Z pmsa     Default intent: Perceptual, Rel. Colorimetric, Saturation, Abs. Colorimetric
-q lnhu     Quality - Low, Medium (def), High, Ultra
-b [lnhu]   Low quality B2A table - or specific B2A quality or none for input device
-ni        Don't create input (Device) shaper curves
-np        Don't create input (Device) grid position curves
-no        Don't create output (PCS) shaper curves
-nc        Don't put the input .t13 data in the profile
-k zhr     Black ink generation target: z = zero K,
           h = 0.5 K, x = max K, r = ramp K (def.)
-k p stpo  enpo enle shape
           stle: K level at White 0.0 - 1.0
           stpo: start point of transition Wh 0.0 - Bk 1.0
           enpo: End point of transition Wh 0.0 - Bk 1.0
           enle: K level at Black 0.0 - 1.0
           shape: 1.0 = straight, 0.0-1.0 concave, 1.0-2.0 convex
-k parameters Same as 'k', but target is K locus rather than K value itself
-l klimit  override total ink limit, 0 = 400% (default from .t13)
-l klimit  override black ink limit, 0 = 100% (default from .t13)
-a lxygms65 Algorithm type override
           l = Lab cLUT (def.), x = XYZ cLUT,
           X = display XYZ cLUT + matrix, Y = display XYZ cLUT + debug matrix
           g = gamma-matrix, s = shaper-matrix, m = matrix only,
           G = single gamma-matrix, S = single shaper-matrix
-u         If input profile, auto scale WP to allow extrapolation
-ua       If input profile, force absolute intent
-uc       If input profile, clip cLUT values above WP
-V scale  If input profile, scale media white point by scale
-R        Restrict white = 1.0, black and primaries to be ev0
-v demphas Degree of dark region cLUT grid emphasis 1.0-4.0 (default 1.00 = none)
-f [illum] Use Fluorescent whitening Agent compensation [opt. simulated inst. illum.:
           Mb, M1, M2, A, C, D50 (def.), D50M2, D65, F5, F8, F10 or file.sp]
-i illum  Choose illuminant for computation of CIE XYZ from spectral data & FMA:
           A, C, D50 (def.), D50M2, D65, F5, F8, F10 or file.sp
-o observ  Choose CIE Observer for spectral data:
           1931_2 (def.), 1964_10, 2012_2, 2012_10, S88 1955_2, shaw, 28V 1978_2, or file.cnf
-f avgdev Average deviation of device-instrument readings as a percentage (default 0.500)
-s src.icm|cperc Apply gamut mapping to output profile perceptual B2A table
-c viewcond set input viewing conditions for output profile CIECAM02 gamut mapping,
           either an enumerated choice, or a parameter
-d viewcond set output viewing conditions for output profile CIECAM02 gamut mapping
           either an enumerated choice, or a parameter
           Also sets out of gamut clipping CW space,
           either an enumerated choice, or a series of parameters:value changes
-pp       Practical Reflection Print (ISO-3664 P2)
-pc       Critical print evaluation environment (ISO-3664 P1)
-pe       Print evaluation environment (CIE 136-1995)
-pm       Print evaluation with partial Mid-tone adaptation
-mb       Bright monitor in bright work environment
-mt       Monitor in typical work environment
-md       Monitor in darkened work environment
-jm       Projector in dim environment
-jd       Projector in dark environment
-tv       Television/Film Studio
-pcd      Photo CD - original scene outdoors
-ob       Original scene - Bright Outdoors
-cx       Cut Sheet Transparencies on a viewing box
-P        Create gamut gammap_p.wrl and gammap_s.wrl diagnostics
-o outputfile Override the default output filename.
-i infile   Base name for input.t13/output.icm file

```

Figure A.2.: Argyll list of commands



## A.4. ProPhoto RGB to CIELAB Formulae

To move from any RGB color space into *CIELAB* first we must remove the gamma encoding from the original RGB data, in other words do gamma decoding / inverting gamma and linearizing the RGB data. The RGB values must first be normalized in the range  $[0.0 - 1.0]$ .

For ProPhoto RGB for instance:

$$v = V^\gamma \quad \exists \gamma = 1.8 \quad (\text{A.3})$$

$$v = \begin{cases} V/12.92 & \text{if } V \leq 0.04045 \\ ((V + 0.055)/1.055)^{2.4} & \text{otherwise} \end{cases} \quad (\text{A.4})$$

Then to move the linear RGB to *CIEXYZ*:

$$\begin{bmatrix} X \\ Y \\ Z \end{bmatrix} = M \begin{bmatrix} R_{lin} \\ G_{lin} \\ B_{lin} \end{bmatrix} \quad (\text{A.5})$$

Where the matrix  $M$  for ProPhoto RGB for D50 is:

$$M = \begin{bmatrix} 0.7976749 & 0.1351917 & 0.0313534 \\ 0.2880402 & 0.7118741 & 0.0000857 \\ 0.0000000 & 0.0000000 & 0.8252100 \end{bmatrix} \quad (\text{A.6})$$

After moving to *CIEXYZ*, now it is possible to move to *CIELAB* as following:

$$L = 116f_y - 16 \quad (\text{A.7})$$

$$a = 500(f_x - f_y) \quad (\text{A.8})$$

$$b = 200(f_y - f_z) \quad (\text{A.9})$$

where  $f \in \{f_x, f_y, f_z\}$ ,  $u \in \{x_r, y_r, z_r\}$  and  $U \in \{X, Y, Z\}$ :

$$f = \begin{cases} \sqrt[3]{u} & \exists u > \varepsilon \\ \frac{ku+16}{116} & \text{otherwise} \end{cases} \quad (\text{A.10})$$

given that:  $\varepsilon = \frac{216}{24389}$ ,  $k = \frac{24389}{27}$

$$u = \frac{U}{U_r} \quad (\text{A.11})$$

where subscript *indicates to the values of reference white*  $[X_r, Y_r, Z_r]$ .



# Bibliography

- [ABB\*21] APOPEI A., BUZGAR N., BUZATU A., MAFTEI A., APOSTOAE L.: Digital 3d models of minerals and rocks in a nutshell: Enhancing scientific, learning, and cultural heritage environments in geosciences by using cross-polarized light photogrammetry. *Carpathian Journal of Earth and Environmental Sciences* 16 (02 2021), 237–249. 2
- [AF15] ANZAGIRA L., FOSSUM E. R.: Color filter array patterns for small-pixel image sensors with substantial cross talk. *J. Opt. Soc. Am. A* 32, 1 (Jan 2015), 28–34. 57
- [AHTR\*22] ABU HAILA T., TAUSCH R., RITZ M., SANTOS P., FELLNER D.: Effect of Polarization on RGB Imaging and Color Accuracy/Fidelity. In *CIC30 IST (2022)*, IST. 106
- [AHTR\*23] ABU HAILA T., TAUSCH R., RITZ M., SANTOS P., FELLNER D.: A Cross-Polarization as a Possible Cause for Color Shift in Illumination. In *EI2023 IST (2023)*, IST. 106
- [AJR99] ANGUS J. ROBERTSON K. J. T.: Cross-polarized photography in the study of enamel defects in dental paediatrics. *Journal of Audiovisual Media in Medicine* 22, 2 (1999), 63–70. PMID: 10628000. 2
- [AMCS96] ANDERSON M., MOTTA R., CHANDRASEKAR S., STOKES M.: Proposal for a standard default color space for the internet—srgb. In *Color and imaging conference (1996)*, vol. 1996, Society for Imaging Science and Technology, pp. 238–245. 30, 31, 35
- [AR20a] ANGHELUTA L., RADVAN R.: 3d digitization of translucent materials in cultural heritage objects: a comparative study between laser scanning and photogrammetry. *Romanian Journal of Physics* 65 (10 2020), 1. 3
- [AR20b] ANGHELUTA L., RADVAN R.: 3d digitization of translucent materials in cultural heritage objects: a comparative study between laser scanning and photogrammetry. *Romanian Journal of Physics* 65 (10 2020), 1. 3
- [Bal03] BALASUBRAMANIAN R.: Device characterization. In *Digital Color Imaging Handbook*, Sharma G., (Ed.). CRC Press, 2003. 30, 68
- [Bay76] BAYER B. E.: Color Imaging Array, US Patent 3,971,065, July 1976. 57
- [Ber19] BERNS R. S.: *Billmeyer and Saltzman's PRINCIPLES OF COLOR TECHNOLOGY*. Wiley and Sons Inc., 2019. 18, 28, 32, 90
- [BRD92] BARON R., REA M., DANIELS S.: Effects of indoor lighting (illuminance and spectral distribution) on the performance of cognitive tasks and interpersonal behaviors: The potential mediating role of positive affect. *Motivation and Emotion* 16, 1 (1992), 1–33. 89
- [Bru23] Bruce Lindbloom - Color formulae and transformations. <http://www.brucelindbloom.com/>, 2023. Accessed: 2023-02-16. 108
- [CHg17] *Color Reproduction Guide For Cultural Heritage*. Tech. rep., Digital Transitions, 2017. 108
- [CIE01] *Improvement to Industrial Colour-Difference Evaluation*. Tech. Rep. 142-2001, CIE (International Commission on Illumination), 2001. 64, 65

- [CIE07] In *Colorimetry Understanding the CIE system*, Schanda J., (Ed.). Wiley and Sons Inc., 2007. 35, 90
- [CK99] CHEN C.-Y., KLETTE R.: *Computer Analysis of Images and Patterns*. Springer Berlin Heidelberg, Berlin, Heidelberg, 1999, ch. Image Stitching — Comparisons and New Techniques, pp. 615–622. 103
- [CMDC13] CAMPISI P., MAIORANA E., DEBATTISTA K., CHALMERS A.: High dynamic range media watermarking issues and challenges. In *21st European Signal Processing Conference (EUSIPCO 2013)* (2013), pp. 1–5. 32
- [Cul23] Verus Digital. <https://verus.digital>, 2023. Accessed: 2023-02-16. 1, 101
- [DM12] DRUZIK J., MICHALSKI S. W.: *Guidelines for Selecting Solid-State Lighting for Museums*. Los Angeles: Getty Conservation Institute; Ottawa: Canadian Conservation Institute, 2012. 92
- [Edw11] EDWARDS N.: Cross-polarisation, making it practical. *Journal of Visual Communication in Medicine* 34, 4 (2011), 165–172. 2
- [GGB\*16] GURREA J., GURREA M., BRUGUERA A., SAMPAIO C. S., JANAL M., BONFANTE E., COELHO P. G., HIRATA R.: Evaluation of dental shade guide variability using cross-polarized photography. *International Journal of Periodontics & Restorative Dentistry* 36, 5 (2016). 2
- [GPY10] GRUEV V., PERKINS R., YORK T.: Ccd polarization imaging sensor with aluminum nanowire optical filters. *Opt. Express* 18, 18 (Aug 2010), 19087–19094. 2
- [Han18] HANLON K.: Cross-polarised and parallel-polarised light: Viewing and photography for examination and documentation of biological materials in medicine and forensics. *Journal of Visual Communication in Medicine* 41 (01 2018), 1–6. 2
- [Hec02a] HECHT E.: *Optics*. Addison Wesley, 2002, ch. Polarization. 1, 11, 13, 89, 106
- [Hec02b] HECHT E.: *Optics*. Addison Wesley, 2002. 25
- [HP11] HUNT R. W. G., POINTER M. R.: *Measuring Colour*, fourth ed. Wiley IS&T, 2011. 25, 64, 90
- [Hun91] HUNT R.: *Measuring Colour 2nd Edition*. Ellis Horwood Limited, 1991. 94
- [HZ03] HARTLEY R., ZISSERMAN A.: *Multiple view geometry in computer vision*. Cambridge university press, 2003. 103
- [ISO17] *ISO/TR 19263-1; Best Practices for digital image capture of cultural heritage material*. Tech. rep., ISO (International Organization for Standardization), 2017. 1, 43, 45, 49, 53, 55, 58, 101, 106, 108
- [ISO20] *ISO/TR 19264-1; Photography — Archiving systems — Imaging systems quality analysis — Part 1: Reflective originals*. Tech. rep., ISO (International Organization for Standardization), 2020. 1, 65, 68, 110, 116
- [JMW\*64] JUDD D. B., MACADAM D. L., WYSZECKI G., BUDDE H. W., CONDIT H. R., HENDERSON S. T., SIMONDS J. L.: Spectral distribution of typical daylight as a function of correlated color temperature. *J. Opt. Soc. Am.* 54, 8 (Aug 1964), 1031–1040. 35
- [Kan06a] KANG H. R.: *Computational Color Technology*. SPIE, 2006. 38
- [Kan06b] KANG H. R.: *Computational Color Technology*. SPIE—The International Society for Optical Engineering, 2006, ch. 5-6. 108
- [KG10] KRISS M. A., GREEN, P. (ED.): *Color Management : Understanding and Using ICC Profiles*. The Wiley - IS&T Series in Imaging Science and Technology, 2010. 43, 61, 62
- [Koe10] KOENDERINK J.: *Color for the Sciences*. The MIT Press, 2010. 9

- 
- [LCR01] LUO M. R., CUI G., RIGG B.: The development of the cie 2000 colour-difference formula: Ciede2000. *Color Research & Application* 26, 5 (2001), 340–350. 64, 65
- [LP05] LUKAC R., PLATANIOTIS K.: Color filter arrays: design and performance analysis. *IEEE Transactions on Consumer Electronics* 51, 4 (2005), 1260–1267. 57
- [LYENPE06] LIN S.-S., YEMELYANOV K. M., EDWARD N. PUGH J., ENGHETA N.: Polarization-based and specular-reflection-based noncontact latent fingerprint imaging and lifting. *J. Opt. Soc. Am. A* 23, 9 (Sep 2006), 2137–2153. 2
- [McC92] MCCAMY C. S.: Correlated color temperature as an explicit function of chromaticity coordinates. *Color Research & Application* 17, 2 (1992), 142–144. 94
- [Mor03] MOROVIC J.: Gamut mapping. In *Digital Color Imaging Handbook*, Sharma G., (Ed.). CRC Press, 2003. 62
- [New04] NEWTON I.: *Opticks: or, A Treatise of the Reflexions, Refractions, Inflexions and Colours of Light*. 1704. 9
- [NN11] NEITZ J., NEITZ M.: The genetics of normal and defective color vision. *Vision research* 51, 7 (2011), 633–651. 10
- [Pal01] PALUM R. J.: Image sampling with the bayer color filter array. In *Image Processing, Image Quality, Image Capture Systems Conference* (2001). 57
- [RIM02] ANSI/I3A IT10.7466-2002 - Photography - Electronic Still Picture Imaging - Reference Input Medium Metric RGB Color Encoding (RIMM-RGB), 2002. 30
- [ROAG08] REINHARD ERIK A. A. K. E., OGUZ AKYÜZ A., GARRETT J.: *Color imaging fundamentals and applications*. A. K. Peters Ltd., 2008. 19, 20, 25, 30, 35
- [Row20] ROWLANDS D. A.: Color conversion matrices in digital cameras: a tutorial. *Optical Engineering* 59, 11 (2020), 110801. 29, 30
- [SBS99] SÜSSTRUNK S., BUCKLEY R., SWEN S.: Standard RGB Color Spaces. vol. in Proc. IS&T 7th Color and Imaging Conf., pp. 127–134. 31
- [SGW00] SPAULDING K., GIORGIANNI E., WOOLFE G.: Reference input/output medium metric rgb color encodings. pp. 155–163. 58, 60, 64, 108
- [Sha18] SHARMA A.: *Understanding Color Management*. Wiley & Sons Ltd., 2018. 43, 62
- [Shu62] SHURCLIFF W. A.: *polarized light production and use*. Harvard University Press, 1962. 1, 11, 13, 106
- [SNS06] SHWARTZ S., NAMER E., SCHECHNER Y.: Blind haze separation. In *2006 IEEE Computer Society Conference on Computer Vision and Pattern Recognition (CVPR'06)* (2006), vol. 2, pp. 1984–1991. 2
- [Son18] Polarsens Sony. <https://www.sony-semicon.com/en/technology/industry/polarsens.html>, 2018. Accessed: 2023-06-14. 2
- [SS97] SZELISKI R., SHUM H.-Y.: Creating Full View Panoramic Image Mosaics and Environment Maps. In *Proceedings of the 24th Annual Conference on Computer Graphics and Interactive Techniques* (USA, 1997), SIGGRAPH '97, ACM Press/Addison-Wesley Publishing Co., p. 251–258. 103
- [Sus12] SUSAN HAGEN: The mind's eye. [https://www.rochester.edu/pr/Review/V74N4/0402\\_brainscience.html](https://www.rochester.edu/pr/Review/V74N4/0402_brainscience.html), 2012. Online; accessed 11 January 2023. 13

- [SWD05] SHARMA G., WU W., DALAL E. N.: The ciede2000 color-difference formula: Implementation notes, supplementary test data, and mathematical observations. *Color Research & Application* 30, 1 (2005), 21–30. [64](#), [65](#)
- [TMMIE11] TOQUE J. A., MURAYAMA Y., MATSUMOTO Y., IDE-EKTESSABI A.: Polarized light scanning for cultural heritage investigation. In *Computer Vision and Image Analysis of Art II* (2011), Stork D. G., Coddington J., Bentkowska-Kafel A., (Eds.), vol. 7869, International Society for Optics and Photonics, SPIE, p. 78690N. [3](#)
- [Too16] TOOMS M. S.: *colour reproduction in electronic imaging systems: photography, television, cinematography*. WILEY, 2016. [34](#), [35](#), [64](#), [90](#)
- [TS09] TREIBITZ T., SCHECHNER Y. Y.: Active polarization descattering. *IEEE Transactions on Pattern Analysis and Machine Intelligence* 31, 3 (2009), 385–399. [2](#)
- [TVG17] TOSCANI M., VALSECCHI M., GEGENFURTNER K. R.: Lightness perception for matte and glossy complex shapes. *Vision research* 131 (2017), 82–95. [9](#)
- [Vav65] VAVILOV S.: *The human eye and the sun "hot" and "color" light*. Pergamon Press Ltd., 1965. [89](#)
- [vBTS\*22] VON BUELOW M., TAUSCH R., SCHURIG M., KNAUTHE V., WIRTH T., GUTHE S., SANTOS P., FELLNER D. W.: Depth-of-Field Segmentation for Near-lossless Image Compression and 3D Reconstruction. *Journal on Computing and Cultural Heritage (JOCCH)* 15, 3 (2022), 1–16. [105](#)
- [VM94] VALDEZ P., MEHRABIAN A.: Effects of color on emotions. *Journal of Experimental Psychology: General* 123, 4 (1994), 394–409. [89](#)
- [WR05] WU H., RAO K.: *Digital Video Image Quality and Perceptual Coding*. Signal Processing and Communications. Taylor & Francis, 2005. [32](#), [33](#)
- [WZH\*20] WU X., ZHANG H., HU X., SHAKERI M., FAN C., TING J.: Hdr reconstruction based on the polarization camera. *IEEE Robotics and Automation Letters* 5, 4 (2020), 5113–5119. [2](#)
- [ZLPW06] ZOMET A., LEVIN A., PELEG S., WEISS Y.: Seamless image stitching by minimizing false edges. *IEEE Transactions on Image Processing* 15, 4 (2006), 969–977. [103](#)

# A. Publications and Talks

The thesis is based on the following publications:

## A.1. Publications

1. **Tarek Abu Haila**, Reimar Tausch, Martin Ritz, Pedro Santos, Dieter W. Fellner, "*A cross-polarization as a possible cause for color shift in illumination*" in Electronic Imaging, 2023, pp 192-1 - 192-5, <https://doi.org/10.2352/EI.2023.35.15.COLOR-192>
2. **Tarek Abu Haila**, Reimar Tausch, Martin Ritz, Pedro Santos, Dieter Fellner, "*Effect of Polarization on RGB Imaging and Color Accuracy/Fidelity*" in Color and Imaging Conference, 2022, pp 165 - 175, <https://doi.org/10.2352/CIC.2022.30.1.30>
3. **Tarek Abu Haila**, Felix Schneider, Reimar Tausch, Martin Ritz, Pedro Santos, Dieter Fellner, "*Color Calibration Based on Mosaic Stitching of a Color Target as an Alternative to a Single-Shot Approach*" in Archiving Conference, 2023.





## B. Curriculum Vitae

Google-Scholar account:

[https://scholar.google.com/citations?user=-p\\_aSXkAAAAJ&hl=en](https://scholar.google.com/citations?user=-p_aSXkAAAAJ&hl=en)

### Personal Data

Name Tarek Abu Haila  
Birth date & place 15.Jun.1992, Damascus.  
Nationality Syrian.

### Education

Jun.2020 – May.2023 Ph.D. Marie Sklodowska-Curie Early-Stage Researcher at Fraunhofer IGD / TU Darmstadt.  
Sep.2017 – Sep.2019 M.Sc. Color Science (Computational Colour and Spectral Imaging) - Erasmus Mundus+ Programme: Jean-Monnet University (UJM; part of Lyon University), Granada University (UGR), University of Eastern Finland (UEF) and Norwegian University of Science and Technology (NTNU).  
Sep.2010 – Sep.2015 B.Sc. Informatics Engineering - Arab International University (AIU). Damascus, Syria

### Work Experience

Jun.2020 – May.2023 PhD Researcher  
Fraunhofer IGD (CultArm3D aka. Verus Digital) / Technical University of Darmstadt (TU), Germany.  
Focus: Camera cross-polarization effect on colors.  
Oct.2021 – Jan.2022 Visiting Researcher  
Vienna University of Technology (TU), Rendering and Modelling group.  
Focus: Material rendering using Adobe Substance 3D Designer.  
Jan.2020 – Apr.2020 Intern  
SeeTrue Technologies Oy, Joensuu, Finland.  
Focus: Eye tracking, CUDA GPU, Python and deep learning.

## B. Curriculum Vitae

---

- Sep.2018 – Dec.2018 Teacher Assistant  
University of Eastern Finland.  
Focus: Lab teaching, MatLab, computer vision.
- Sep.2013 – Sep.2015 Math Teacher  
Al-Ihsan intermediate school, Damascus, Syria.  
Focus: Teaching math classes for the 7th and 8th grades including homework and exams.
- Jun.2012 – Sep.2012 Programming private teacher  
Damascus, Syria.  
Focus: Linux OS, Python and C#.
- 2005 – 2012 Freelancer - Technical support  
Damascus, Syria.  
Focus: Hardware and software solutions, installation and administration of Windows and Linux OS, Network.

### Languages

- Arabic: Mother tongue.  
English: Professional fluency.  
German: Professional interaction.  
Spanish: Intermediate (B1 level).

### Personal Interests

- Photography  
Reading (Psychology, Philosophy, non-fiction, classic literature)  
Music (Guitar playing - Flamenco)